AN *IN VITRO* EVALUATION OF SELENIUM INCORPORATED GUAR GUM NANOPARTICLES AGAINST ISCHEMIA REPERFUSION IN H9c2 CARDIOMYOBLAST

Thesis submitted to
Cochin University of Science and Technology
in partial fulfilment of the requirements for the degree of

Doctor of Philosophy
in
Biochemistry
under the faculty of science

By

SOUMYA R.S
(Reg. No. 4154)

Under the supervision of

Dr. K. G. RAGHU

Agroprocessing and Natural Products Division
Council of Scientific and Industrial Research–National Institute for Interdisciplinary Science and Technology (CSIR-NIIST)
Thiruvananthapuram – 695 019, Kerala, India.

JANUARY 2015

DECLARATION

I hereby declare that the thesis entitled *"***AN *IN VITRO* EVALUATION OF SELENIUM INCORPORATED GUAR GUM NANOPARTICLES AGAINST ISCHEMIA REPERFUSION IN H9c2 CARDIOMYOBLAST***"* embodies the results of investigations carried out by me at Agroprocessing and Natural Products Division of Council of Scientific and Industrial Research - National Institute for Interdisciplinary Science and Technology (CSIR-NIIST), Thiruvananthapuram as a full time research scholar under the supervision of Dr. K. G. Raghu and the same has not been submitted elsewhere for any other degree.

In keeping with the general practice of reporting scientific observations, due acknowledgement has been made wherever the work described is based on the findings of other investigators.

Soumya R.S

Thiruvananthapuram
January, 2015

COUNCIL OF SCIENTIFIC & INDUSTRIAL RESEARCH
NATIONAL INSTITUTE FOR INTERDISCIPLINARY SCIENCE & TECHNOLOGY
GOVERNMENT OF INDIA
Thiruvananthapuram-695 019, Kerala, India

Telephone: 91-471-2515486
Fax: 91-471-2491712

Dr. K. G. Raghu
Principal Scientist
Agroprocessing and Natural Products Division

CERTIFICATE

*This is to certify that the work embodied in the thesis entitled "***AN *IN VITRO* EVALUATION OF SELENIUM INCORPORATED GUAR GUM NANOPARTICLES AGAINST ISCHEMIA REPERFUSION IN H9c2 CARDIOMYOBLAST***" has been carried out by Ms. Soumya R.S**, under my supervision and guidance at Agroprocessing and Natural Products Division of Council of Scientific and Industrial Research-National Institute for Interdisciplinary Science and Technology (CSIR-NIIST), Thiruvananthapuram in partial fulfilment of the requirements for the award of degree of Doctor of Philosophy in Biochemistry under Faculty of Science, Cochin University of Science and Technology, Kochi, Kerala, India and the same has not been submitted elsewhere for any other degree. All the relevant corrections, modifications and recommendations suggested by the audience and the doctoral committee members during the pre-synopsis seminar of **Ms. Soumya R.S** has been incorporated in the thesis.*

K. G. Raghu
(Thesis Supervisor)

Thiruvananthapuram,
January, 2015

e-mail: raghukgopal2009@gmail.com; raghukgopal@rediffmail.com

..... TO MY FAMILY

ACKNOWLEDGEMENTS

It is with immense pleasure that I express my deep sense of gratitude to my research supervisor Dr. K. G. Raghu for suggesting the research topic and his guidance, encouragement and constant support throughout my research.

I wish to thank Dr. Suresh Das and Dr. B. C. Pai, present and former Directors, NIIST, Trivandrum, for providing necessary facilities for carrying out the work.

I would like to express my gratitude to Dr. A. Sundaresan, Head, Agroprocessing and Natural Products Division and Mr. M. M. Sreekumar, Chief Scientist, Agroprocessing and Natural Products Division, CSIR-NIIST for their support and encouragement extended to my work.

I wish to extend my sincere thanks to Dr. S. Priya, Smt. M. V. Reshma, Dr. P. Nisha, Dr. Jayamurthy, Dr. B. S. Dileep Kumar, and Mr. D. R. Soban Kumar for their help in my work. All the former and present members of Agroprocessing and Natural Products Division have been extremely helpful and co-operative and I am thankful to one and all for their kind gesture.

I am obliged to Dr. T. Emilia Abraham, Dr. Swapan Kumar Gosh and Dr. T. P. D. Rajan, Senior Scientist, Material Science and Technology Division (Convener, NIIST-CUSAT Research Council) for all their help and support.

I express my sincere thanks to Dr. C. S. Paulose, Professor, Dept. of Biotechnology Cochin University of Science and Technology for his care and support as an external expert in Doctoral Committee.

I would like to express my gratitude to Mr. Adarsh N, Mr.Anees, Mrs. Smitha, Mr. Peer Mohammad, Mr. Robert Philip, Mr. Kiran and Mr. Guruswamy for characterization studies.

I gratefully acknowledge the help and support received from, Mr. Prathapan A, Mr. Salin Raj, Ms. Vineetha V. P, Ms. Anusree S. S, Ms. Nisha V. M, Ms. Priyanka A, Ms. Priya Rani, Dr. Vandana Sankar, Ms. Riya Mariam Philip, Ms. Antu K. Antony, Ms. Reshma P.L, Ms. Shyni., Ms. Kavitha, Ms. Preetha, Ms. Saranya, Ms. Shilpa, Ms. Indu Sasidharan, Ms. Shamla L, Mr. Arun K. B, Ms. Dhanya R, Ms. Shyama H. P, Mr. Ajayan, Mr. Pratheesh S. Nair, Dr. Mahesh S. Krishna, Dr. Nishanth Kumar, Dr. Venu Narayan, Dr. Sangeetha K etc. and all other friends of Agroprocessing and Natural products division.

I would like to express my gratitude to all the members of library, administrative, academic programme committee and technical staff of NIIST for their help and support.

I extent my sincere thanks to my seniors and all friends in other divisions of NIIST for their help and support.

I express my sincere gratitude to all my teachers for their care and support.

I am also indebted to Indian Council of Medical Research for financial assistance in the form of research fellowship.

I owe my deep sense of gratitude and regard to my mother, my father, my husband, my daughter and my brother for their prayers, affection, encouragements, inspiration, patience and support which smoothly paved my path towards the successful completion of the research work.

Finally, I humbly bow before the almighty God for showering his blessings upon me and giving me the strength, wisdom and luck to reach this important milestone in my academic life.

Soumya R.S.

ABBREVIATIONS

CVD	:	Cardiovascular diseases
PLGA	:	Poly-(d, l-lactic-co-glycolic acid)
tPA	:	Tissue plasminogen activator
CHD	:	Coronary heart disease
ATP	:	Adenosine triphosphate
I/R	:	Ischemia reperfusion
ROS	:	Reactive oxygen species
mPTP	:	Mitochondrial permeability transition pore
$O_2^{\cdot -}$	:	Superoxide anion
H_2O_2	:	Hydrogen peroxide
$OH^{\cdot}$	:	Hydroxyl radical
$^1O_2$	:	Singlet oxygen
XO	:	Xanthine oxidase
NADPH	:	Reduced nicotinamide adenine dinucleotide phosphate oxidases
SOD	:	Superoxide dismutase
GPx	:	Glutathione peroxidase
GSH	:	Glutathione
GG	:	Guar gum
LDL	:	Low density lipoprotein
Se	:	Selenium
TrxR	:	Thioredoxin reductase
Sec	:	Selenocysteine
H_2O_2	:	Hydrogen peroxide
GGN	:	Guar gum nanoparticle
SGG	:	Selenium incorporated guar gum nanoparticles
H_2O_2	:	Hydrogen peroxide
TEM	:	Transmission electron microscopy
XRD	:	X-ray diffraction
ATCC	:	American Type Culture Collection
$\Delta\Psi m$	:	Mitochondrial transmembrane potential
PMS	:	Phenazine methosulfate
NBT	:	Nitro blue tetrazolium

TBA	:	Thiobarbituric acid
TCA	:	Trichloroacetic acid
DMSO	:	Dimethyl sulfoxide
MTT	:	3-(4, 5-dimethylthiazol- 2-yl)-2,5-diphenyl tetrazolium bromide)
TPP	:	Sodium tripolyphosphate
DMSO	:	Dimethyl sulfoxide
DCFH-DA	:	2', 7' dichlorodihydrofluorescein diacetate
AO	:	Acridine orange
EtBr	:	Ethidium bromide
JC-1	:	5, 5', 6, 6'-tetrachloro-1, 1', 3, 3'tetraethylbenzimidazolylcarbocyanine iodide
DAPI	:	4', 6-diamidino-2-phenylindole
AA	:	Ascorbic acid
Tris-HCl	:	Tris hydroxymethyl aminomethane hydrochloride
EDTA	:	Ethylene diamine tetraacetic acid
DMEM	:	Dulbecco's modified Eagle's medium
FBS	:	Foetal bovine serum
PCS	:	Photon correlation spectroscopy
$FeCl_3$	:	Ferric chloride
TRP	:	Total reducing power
MGG	:	Macro guar gum
PDI	:	Polydispersity index
NaCl	:	Sodium chloride
KCl	:	Potassium chloride
$MgSO_4$	:	Magnesium sulphate
HEPES	:	4-(2-hydroxyethyl)-1-piperazineethanesulfonic acid
LDH	:	Lactate dehydrogenase
DTNB	:	5,5'dithio-*bis*-2-(nitrobenzoic acid)
TNB	:	5-thio-2-nitrobenzoic acid
MES	:	2-(*N*-morpholino) ethanesulfonic acid
DTT	:	dithiothreitol
ABTS	:	2, 2'- Azino-di-[3-ethylbenzthiazoline sulphonate]
HRP	:	Horse radish peroxidise

DNPH	:	2, 4-Dinitrophenylhydrazine
Nrf2	:	Nuclear factor E_2-related factor 2
ANSA	:	1-amino 2-naphthol 4-sulphonic acid
MDA	:	Malondialdehyde
ETC	:	Electron transport chain
mCa^{2+}	:	Mitochondrial calcium
HIF-1 α	:	Hypoxia inducible factor-1 alpha
ANP	:	Atrial natriuretic peptide
DCPIP	:	Dichlorophenolindophenol
KCN	:	Potassium cyanide
DAB	:	3, 3′-diaminobenzidine
HSP 60	:	Heat shock protein 60
GAPDH	:	Glyceraldehyde 3 phosphate dehydrogenase
TBST	:	Tris buffered saline-tween 20
PVDF	:	Polyvinylidene difluoride
TNF-α	:	Tumor necrosis factor
IL-6	:	Interleukin-6
NF-kB	:	Nuclear factor kappa B
IL-2	:	Interleukin-2
MCP-1	:	Monocyte chemoattractant protein-1
INF-γ	:	Interferon-γ
TNNI3K	:	Serine/threonine-protein kinase
ERK	:	Extracellular signal-regulated kinases
IGF-1	:	Insulin like growth factor 1
TGF-β	:	Transforming growth factor-beta
nm	:	Nanometer
g	:	Gram
Kg	:	Kilogram
°C	:	Degree celcius
%	:	Percentage
mg	:	Milligram
µg	:	Microgram
ml	:	Millilitre
µl	:	Microlitre

nM	:	Nanomole
min	:	Minute
M	:	Molar
ng	:	Nanogram
IC_{50}	:	Median inhibition concentration
v/v	:	Volume by volume
h	:	Hour
BSA	:	Bovine serum albumin

CONTENTS

List of Tables

List of Figures

Chapter 1

Introduction

1.1. Nanoparticles

Nanoscience is one of the key technologies of the 21st century and has become an important area of research in biomedical sciences. Nanoparticles differ significantly from powdered particles or bulk materials due to its size-related properties (Buzea *et al* 2007). Nanoparticles are sized between 1 to 100 nanometers and in the area of drug delivery, relatively large [~10-200 nm] nanoparticles may be needed for loading a sufficient amount of drug onto the nanoparticles (Jong and Borm 2008). In drug delivery, carrier can be either engineered particles or the drug itself at nanoscale can be used (Cascone *et al* 2002; Baran *et al* 2002; Duncan 2003; Kipp 2004). Carriers are prepared from a variety of materials such as protein, polysaccharide and synthetic polymers. Nanoparticles deliver a wide range of drugs such as hydrophilic and hydrophobic drugs, proteins, vaccines and biological macromolecules to target areas of the body like lymphatic system, brain, arterial walls, lungs, liver and spleen for sustained periods of time (Hans and Lowman 2002). The selection of matrix materials is dependent on many factors like size of nanoparticles required, inherent properties of the drug, degree of biodegradability, biocompatibility, toxicity and surface characteristics such as charge and permeability (Mohanraj and Chen 2006). The advantages of nanoparticle as drug carriers are their high stability and improved oral bioavailability, reduced toxicity with increase in drug efficacy, high carrier capacity and site specific delivery (Athar and Das 2013).

The importance of the novel uses of nanoparticle in medical biology is due to their very high surface to volume ratio. For example, a nanoparticle of 6 nm diameter will have 35% of its atoms at their surface and therefore possesses exceptionally greater interfacial reactivity. The important and unique features of nanoparticles are their surface to mass ratio which is much larger than that of micro and macro sized particles. This facilitates catalytic promotion of reactions as well as their ability to adsorb and carry other compounds. Depending on the

presence of reactants and adsorbing compounds, the surface of the nanoparticles can be easily modified. Figure 1.1. represents different types of nanoparticles (Abilash 2010).

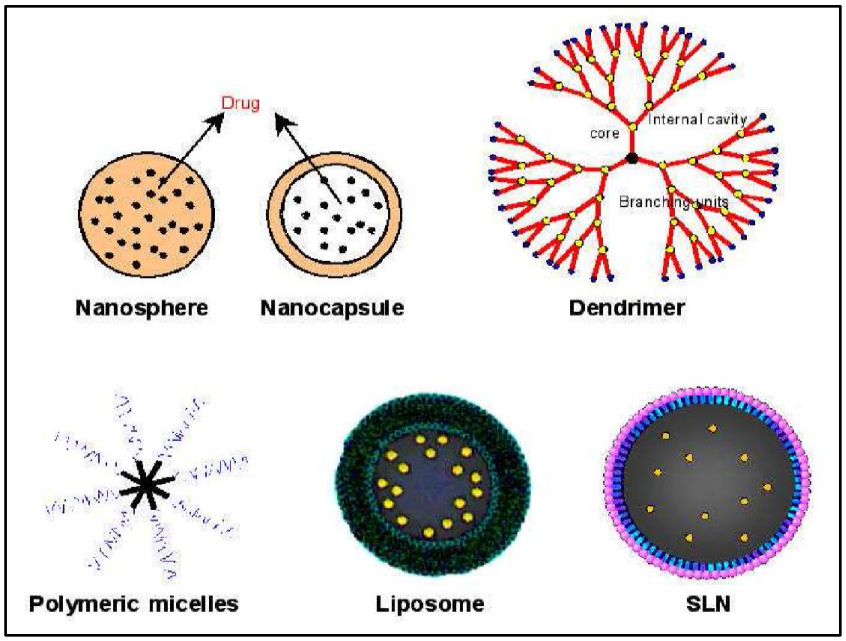

Figure 1. 1. Types of nanoparticles (Abilash, 2010 with permission).

Among the natural polymers polysaccharides are found to be the most promising sources for the synthesis of nanoparticles. Polysaccharides are polymeric carbohydrate structures, formed of repeating units (either mono or disaccharides) attached together by glycosidic bonds. These structures are often linear, but contain various degrees of branching. In nature, polysaccharides have various resources like algal (alginate), plant (pectin and guar gum), microbial (dextran and xanthan gum) and animal origin (chitosan and chondroitin) (Carballoa *et al* 2010). Due to their wide range of molecular weight and chemical composition they offer a great variety of structure and property. Biological activity of polysaccharide depends on its molecular structure including sugar units, glycosidic bonds of sugar chains, the type and degree of polymerization of branches, flexibility and configuration of chains. In drug delivery, polysaccharides have been used to generate coatings, films, controlled release matrices, hydrogels and nanoparticles. Polysaccharide possess many positive characteristics like cost effectiveness, availability, low toxicity, biocompatibility,

biodegradability, colloidal stability (because of the hydrophilicity of polysaccharide chains) and specific interactions with biological systems (Sinha and Kumria 2001; Baldwin and Kiick 2010). Moreover, the presence of hydrophilic groups in their structure such as hydroxyl, carboxyl and amino groups enhance bioadhesion with biological tissues like epithelia and mucous membranes forming non-covalent bonds and is a useful strategy to improve bioavailability of drugs included in drug delivery systems (Lee *et al* 2000). All of these qualities have led to the growing use of polysaccharides in drug delivery systems. Some of the commonly preferred methods for preparing nanoparticles from biodegradable polymers include solvent evaporation (Song *et al* 1995), monomer polymerisation (Harmia *et al* 1986), nanoprecipitation (Molpeceres *et al* 1996) and the salting out procedure (Allemann *et al* 1993). The nanoprecipitation method developed by Fessi *et al* (1989) represents an easy and reproducible technique and has been used widely for preparing nanoparticles (Behera *et al* 2012). In this study nanoprecipitation method was employed for preparing nanoparticles. Nanoprecipitation method is very simple and straightforward method with reproducibility. Three components are needed to perform nanoprecipitation process: the polymer, the polymer solvent and the non-solvent of the polymer. To produce nanoparticles, the polymer solution is mixed with the non-solvent. Nanoparticles are instantaneously formed during the fast diffusion of the polymer solution in the nonsolvent. This technique has been mainly applied for polysaccharide derivatives (Hornig and Heinze 2008).

1.2. Nanoparticles in cardiovascular diseases

Various nanoparticles based drug delivery systems have been and being developed for the treatment of cancer, cardiovascular diseases (CVD) and other conditions. These have different functionalities like (i) size (ii) shape and (iii) surface functionalization. One of the major foci of the application of nanotechnology for cardiovascular research has been the directed imaging and therapy of atherosclerosis, restenosis and cardiovascular conditions.

Nanotechnology offers advantages for the treatment of CVD mainly in four areas like:

i. Targeted therapeutics: delivering drugs where they are needed.

ii. Tissue engineering: building new tissues to replace defective valves, damaged

heart muscle, clogged blood vessels, etc.

iii. Molecular imaging: using imaging agents that identify disease more specifically.

iv. Biosensors and diagnostics: improved diagnostic devices for the laboratory and implantable sensors to detect problems inside the body (Arayne *et al* 2007).

For the treatment of CVD pharmaceutical nanoparticles have gained great importance. Several research groups are interested in targeting endothelial-selective delivery of therapeutic agents which is a useful tool for modifying vascular function in various CVD (Spragg *et al* 1997). There are reports on the development of novel nanoparticulate drug delivery system that mimics platelets binding to the injured vessel wall under physiological flow conditions (Kona *et a*l 2012). Glycoprotein Ib was chosen as the targeting ligand and it is conjugated to nanoparticles. Dexamethasone-loaded biodegradable poly-(d, l-lactic-co-glycolic acid) (PLGA) nanoparticles were formulated using a standard emulsion method. This increases the cellular uptake of nanoparticles as well as controlled release of the model drug to the required site (Kona *et a*l 2012).

The polysaccharide part of nanoparticles may play diverse roles in cardiovascular disease management. For example, it increases the therapeutic effect, facilitate controlled release, provide recognition functions, framework for chemical modifications in order to enable functionalization with target ligands. For reducing intimal hyperplasia controlled release of heparin *via* polysaccharide nanoparticles were used. Heparin was encapsulated into poly (DL lactidecoglycolide) (pLGA) spheres sequestered in an alginate gel. Heparin releasing gels were able to inhibit the proliferation of bovine vascular smooth muscle cells in tissue culture. In addition, heparin controlled release from gels reduced intimal hyperplasia in animal models of vascular disease (Edelmana *et al* 2000). Polysaccharide based nanoparticles were investigated for fibrinolytic drug delivery in the treatment of thrombolysis. Studies reported that poly (lactic-co-glycolic acid) nanoparticles loaded with tissue plasminogen activator (tPA) and coated with chitosan were designed for thrombolysis. Thrombolysis process using such nanoparticles could be enhanced by photomechanical drug delivery (Medeiros *et al* 2012).

Fucoidan is a branched polysaccharide sulfate ester with l-fucose 4-sulfate building blocks that is recognized by P selectin and L selectin. Fucoidan based systems were used for the molecular imaging of activated platelets. P selectin binding by radiolabled ^{99m}Tc fucoidan was detected *in vivo* by scintigraphy in a rat model of platelet rich arterial thrombi as well as in a myocardial ischemia reperfusion (I/R) model. The reported results verified the potential of fucoidan as an efficient imaging agent in cardiovascular pathologies (Rouzet *et al* 2011). In another study, fucoidan was conjugated to ultra small paramagnetic iron oxide coated with carboxylmethyl dextran was used in accurately detecting the thrombus in a rat model of an expanding aneurysm (Suzuki *et al* 2011). Taking into account clinical application of polysaccharide based nanoparticles was limited to plaque macrophage imaging using dextran coated iron oxides. As a reference, iron dose should remain 2.6 mg iron/kg body weight for human oncological MRI (Will *et al* 2006). Sinerem (Guerbet) is the only commercial polysaccharide based nanoparticle tested in clinical trials for managing atherothrombotic disease. Meanwhile, the study of polysaccharide based nanosystems in animal models as molecular imaging tools and targetable drug delivery systems holds great promise in extending current knowledge of therapy/imaging limits as well as of the pathological mechanisms involved in atherothrombotic diseases.

1.3. Current status of cardiovascular disease

CVD comprising coronary heart disease (CHD) and cerebrovascular diseases are currently the leading cause of death globally, accounting for 21.9% of total deaths, and are projected to increase to 26.3% by 2030 (WHO 2008). The Global Burden of Diseases (GBD) study reported the estimated mortality from CHD in India is 1.6 million in the year 2000. A total of nearly 64 million cases of CVD are likely in the year 2015, of which nearly 61 million would be CHD cases (the remaining would include stroke, rheumatic heart disease and congenital heart diseases). Epidemiological studies show a sizeable burden of CHD in adult rural (3–5%) and urban (7–10%) populations. Thus of the 30 million patients with CHD in India, there would be 14 million are in urban and 16 million in rural areas. In India about 50% of CHD related deaths occur in people younger than 70 year compared with only 22% in the West. Extrapolation of these numbers estimates the burden of CHD in India to be more

than 32 million patients (WHO 2008).

1.4. Pathophysiology of cardiovascular disease

The cardiovascular system comprises of heart (Figure.1.2.a) and blood vessels for circulating blood throughout the body for delivering oxygen and nutrients to the tissues and removing carbon dioxide and waste products. CVDs include coronary or ischemic heart disease, cerebrovascular disease, stroke, peripheral vascular disease, chronic heart failure, and congenital heart disease. In most CVDs presence of asymptomatic atherosclerosis starts from early days and progresses with age. During atherosclerosis the lipid filled fibrous plaques accumulates on the inner surface of coronary artery and these plaques are composed of cholesterol rich fatty deposit, collagen, other proteins and excess smooth muscles. These plaques leads to the thickening of the arterial wall block the flow of blood and cause the starving of heart to oxygen and other vital nutrients leading to ischemia (Figure.1.2.b). This condition causes muscle cramp like chest pain called angina.

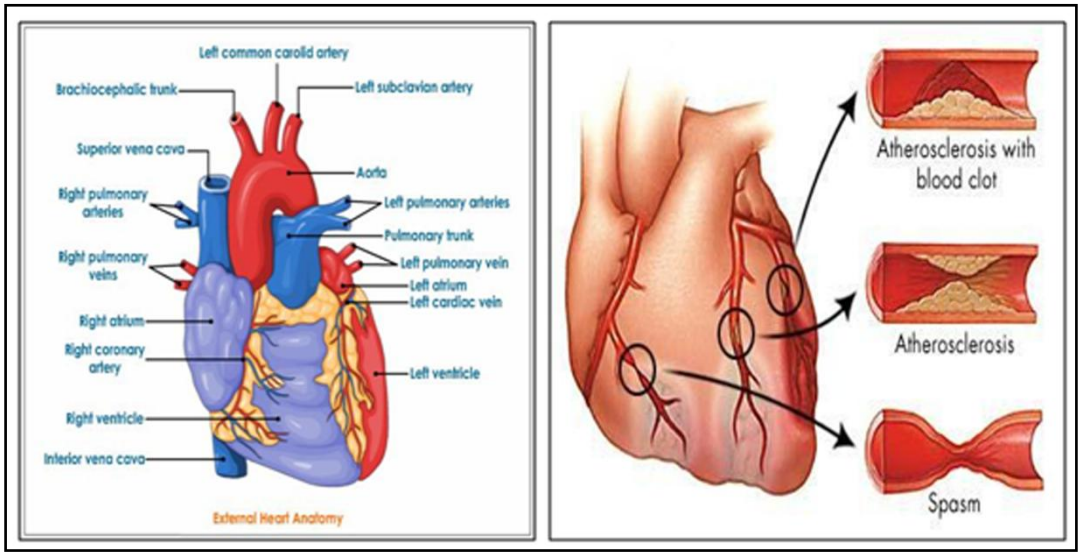

Figure 1. 2. (a) Structure of heart (b) Blockage of coronary artery.

1.5. Ischemic heart disease

Ischemic heart disease occurs when there is an imbalance between oxygen supply and demand. The decrease of oxygen input into the myocardium leads to myocardial dysfunction which will lead to decrease in adenosine triphosphate (ATP) production (Bopassa 2012) resulting in metabolic and functional disruption (Anselmi *et al* 2004).

Prolonged ischemia causes the accumulation of lactate which leads to reduction in pH .The decrease in intracellular pH along with accumulation of NADH, lactate, proton, succinate and alanine inhibits ATP production *via* inhibition of enzymes like pyruvate dehydrogenases, pyruvate fructokinase and glyceraldehyde phosphate dehydrogenase as well as inhibition of malate aspartate shuttle and citric acid cycle. This reduces contractile function and ionic homeostasis. Under circumstances of energy depletion the cytosol and mitochondria of myocardial cells are loaded with calcium (Ca^{2+}) and sodium (Na^{+}). During ischemia the intracellular concentration of Ca^{2+} increases resulting in acidosis with the decrease of Na^{+}/ H^{+}- ATPase and Ca^{2+}-ATPase activity. The intracellular concentration of potassium (K^{+}) also decreases due to the inhibition of Na^{+}-K^{+} ATPase (Mozaffari *et al* 2013). Alteration in the ratio of K^{+} concentration leads to change in membrane potential and thus leads to arrhythmias. One of the most well-known intracellular messenger molecules is Ca^{2+} and plays an essential role in signal transduction pathways (Clapham 1995). Loss of Ca^{2+} homeostasis leads to activation of proteases, lipases, nucleases, nitric oxide synthases, protein kinases and eventual cell death (Hoyt *et al* 1998; Clapham 1995).

1.6. Reperfusion

The most effective management for ischemic myocardium is reperfusion. Early reperfusion ensures tissue survival whereas late reperfusion damages previously ischemic tissues. I/R in the myocardium generate both irreversible injury marked by apoptotic and necrotic tissue and also reversible injury manifested by contractile dysfunction. During reperfusion intracellular and mitochondrial events such as Ca^{2+} overload, inadequate synthesis of ATP, loss of membrane phospholipids, low production of nitric oxide and oxidative stress by reactive oxygen species (ROS) leads to reperfusion injury (Figure.1.3) (Crompton *et al* 1999; Kutala *et al* 2007; Ladilov *et al* 2003; Piper *et al* 2004). As concentration of ATP increases, it will also leads to reperfusion injury leading to hypercontracture of cardiomyocytes membrane disruption and subsequently necrosis (Piper *et al* 2004; Piper *et al* 2006). A low pH, oxidative stress and Ca^{2+} overload leads to the opening of mitochondrial permeability transition pore opening (mPTP) which is a large conductance pore in the inner mitochondrial membrane which permits the communication

between cytoplasm and mitochondrial matrix (Ruiz-Meana *et al* 2007; Di Lisa and Bernardi 2009; Heusch *et al* 2010; Boengler *et al* 2011; Di Lisa *et al* 2011; Hunter *et al* 1976). In normal condition the pore is rapidly closed (Di Lisa *et al* 2009; Bernardi *et al* 2006). Opening of the pore have a number of detrimental effects leading to cell death. In fact the importance of mPTP closure as a target for mitochondrial protection has been described in several studies (Griffiths and Halestrap 1993; Hausenloy *et al* 2003; Javadov *et al* 2003; Shanmuganathan *et al* 2005).

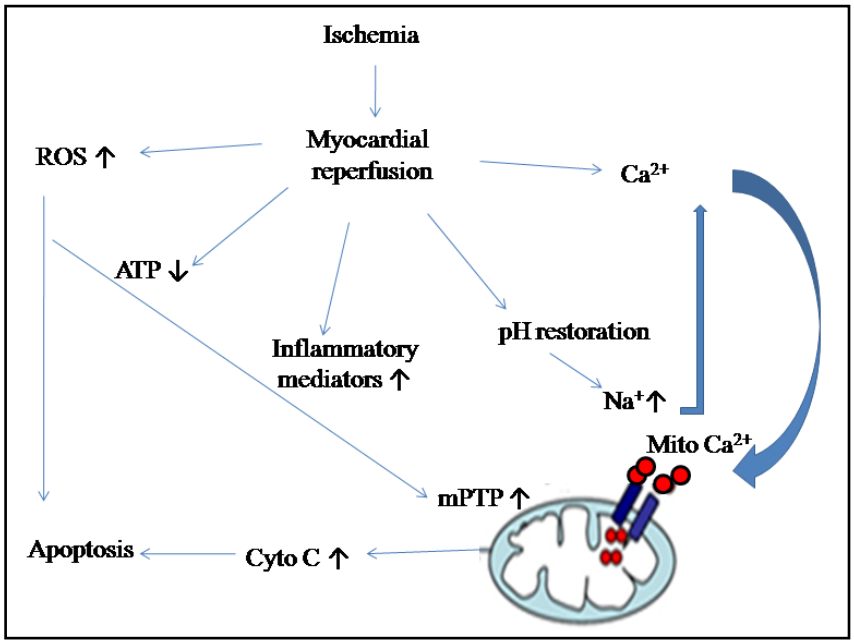

Figure 1. 3. Factors contributing to I/R.

1.7. Free radicals

Plenty of disorders in humans including atherosclerosis, arthritis, central nervous system injury, gastritis, cancer, AIDS and macular degeneration are due to the generation of surplus reactive free radicals (Kumpulainen and Salonen 1999). A free radical is any species that contains one or more unpaired electrons. One electron reduction or oxidation of molecules creates unpaired electrons leading to the generation of free radicals. In the myocardium the reduction of oxygen to water proceeds by two pathways. The major site for reactive oxygen species (ROS) production is mitochondrial respiratory chain. In normal condition about 97% of oxygen consumed at terminal electron acceptor at complex 1V.

Roughly about 3% of consumed oxygen is reduced by electrons that have leaked from electron transport chain i.e., superoxide anions ($O_2^{\cdot -}$), hydrogen peroxide (H_2O_2), hydroxyl radical ($OH^{\cdot}$), and singlet oxygen ($^1O_2$). These are activated oxygen species and are collectively known as reactive oxygen species. Potential sources of ROS include xanthine oxidase (XO), reduced nicotinamide adenine dinucleotide phosphate (NADPH) oxidases, lipoxygenase, cytochrome P-450, nitric oxide synthases, peroxidases and other hemoproteins (Mebazaa *et al* 2008). All these enzymes system are present in the three major cardiac cell types: cardiac myocytes, fibroblasts, and endothelial cells.

1.8. Antioxidants

Low levels of oxygen radicals and oxidants are normally formed within the cells and play an important role in cellular homeostasis, mitosis, swelling, differentiation and signaling. The damaging effects of ROS are reduced by antioxidants in normal physiological conditions. A series of defence mechanisms has developed on exposure to free radicals from a variety of sources. Defence mechanisms against free radical induced oxidative stress involve: (i) preventative mechanisms, (ii) repair mechanisms, (iii) physical defences, and (iv) antioxidant defences. Enzymatic antioxidant defences include superoxide dismutase (SOD), glutathione peroxidase (GPx) and catalase. Non-enzymatic antioxidants are represented by ascorbic acid (Vitamin C), α- tocopherol (Vitamin E), glutathione (GSH), carotenoids, flavonoids and other antioxidants. Under normal conditions, there is a balance between both the activities and the intracellular levels of these antioxidants. This balance is essential for the survival and health (Lobo *et al* 2010).

1.9. Guar gum

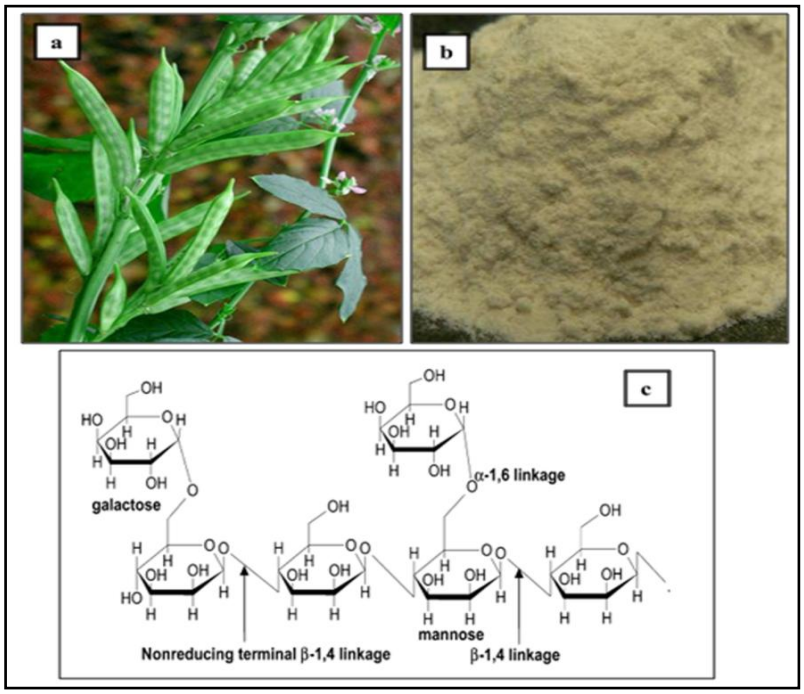

Figure 1. 4. (a) Guar beans (b) Guar gum powder (c) Structure of guar gum.

Guar gum (GG) is a water soluble polysaccharide extracted from the seeds of *Cyamopsis tetragonoloba*, which belongs to Leguminosae family. Also called guaran, it is a non ionic natural polysaccharide derived from the ground endosperm of guar beans (Figure.1.4.a, b). Its backbone consists of linear chains of (1 → 4) - α- D - mannopyranosyl units with β - D-galactopyranosyl units attached by (1 → 6) linkages (Figure.1.4.c.) forming short side-branches (Ma and Pawlik 2005). There are typically 1.5-2.0 mannose residues for every galactose. GG has a chemical composition of 3.5-4% of proteins, 10-13% moisture, 0.06% of phosphorus and 1.07% of ash. The galactomannan units contain 36.6% of D-galactose and 63.1% of D-mannose. The properties of galactomannan mainly depend on the chain length, steric hindrance, abundance of cis-OH group, degree of polymerization and additional substitution. GG hydrates in cold water to form a highly viscous solution in which the single polysaccharide chains interact with each other in a complex way (Tripathy and Das 2013). Its nine hydroxyl groups are available for the formation of hydrogen bonds with other

molecules, but it remains neutrally charged due to the absence of dissociable functional groups. High temperature conditions (50 °C) and extreme pH (pH 3) degrade its structure (Tiraferri *et al* 2008). In solution it remains stable over pH range 5-7. It is insoluble in most hydrocarbon solvents. As the GG polymer is a low-cost, easily available, biodegradable, non-toxic and is obtained from renewable natural resources, it is widely applied in many industrial as well as pharmaceutical fields. It is commonly used as a thickening agent in cosmetics and in sauces, salad dressings and ice creams in the food industry (Barbucci *et al* 2008). There are many reports about GG against a variety of diseases like colon cancer, heart disease and gall stones (Roberfroid 1993). In pharmaceuticals, GG is used as a binder and disintegrant and it has also been used as hydrophilic matrix, for designing oral controlled release dosage forms (Sarmah *et al* 2011). Due to its drug release retarding property and susceptibility to microbial degradation in the large intestine it is widely used for colon delivery. The use of GG in drug delivery is due to its structural characteristic, where its functional groups are used for conjugating it with different molecular weight polymers to create novel derivative molecule with required chemico-physical properties. The existence of reactive -OH groups of GG makes it easily modified to introduce functional groups and thus the capabilities for controlling the release of drugs can be improved. Fahrenbach *et al* (1965) found that guar administration effectively lowered serum total cholesterol levels in normocholesterolemic subjects. GG is rich in dietary fiber, contains 80-85% total dietary fiber, almost in the soluble form it may help to lower cholesterol and glucose levels (Pszczola 2003). One gram of soluble fiber can lower total cholesterol by about 0.045 mmol/l. The serum lipid-lowering effect of GG has been investigated in a large number of human trials. From their meta-analysis, Brown *et al* (1999) estimated that one gram of water-soluble fiber from GG lowered serum total and low density lipoprotein (LDL) cholesterol by 0.026 mmol/l and 0.033 mmol/l respectively. Little information is available in the literature for the possibility of using GG based nanosized materials as drug carriers due to its solubility in water.

1.10. Selenium

Selenium (Se) is an essential trace nutrient required in microgram amounts

(recommended dietary allowance = 55 µg/day; NRC 1989). It is an essential component of GPx, which plays a critical role in protecting aerobic organisms from oxygen radical initiated injury. It is an essential trace element in all mammalian species and it functions mainly through selenoproteins, which contain Se as selenocysteine. GPx and TrxR are the most well characterized selenoenzymes. These selenoproteins as enzymes are involved in various physiological processes such as protection against oxidative stress and redox-based regulation of gene expression (Venardos *et al* 2004). The vital functions of Se in humans are mediated by a group of 25 selenoproteins that contain Se in the form of selenocysteine (Sec), the Se-containing homolog of cysteine. The known human selenoenzymes include GPx, iodothyronine deiodinase, TrxR and methionine sulfoxide reductase B. Se is the only element specified in the genetic code (TGA) and selenocysteine has become recognized as the 21st protein amino acid (Hatfield and Gladyshev 2002). Inadequate Se nutrition is associated with direct impact on health leading to the development of diseases like cardiomyopathy, rheumatoid arthritis, cancer etc. Thus cellular Se status plays an important role in the reduction of oxidative stress in the body. Recently Se nanoparticles are attracting more and more interest due to their biological activity (Riaz and Mehmood 2012). Foods (cereals, grains, vegetables) contain diverse amounts and chemical forms of Se. Whilst all forms of Se are absorbed through intestine. Inorganic forms of Se are incorporated to selenoproteins whereas organic forms of Se are more absorbed by the cells due to its nonspecific incorporation into proteins in place of methionine and have no real biological benefit. High levels of Se lead to the incorporation of Se in place of sulphur leading to increase in selenocysteine available for use in enzymes like GPx and TrxR. Consequently, levels of GPx and TrxR are mainly regulated by inorganic forms of Se rather than organic forms (Roy *et al* 2005). Several literatures are available regarding the supplementation of Se in CVDs. It is able to upregulate the activity of selenocysteine containing enzymes in both animals and cells. Supplementation of rats with 1.5 mg Se/Kg diet, in the form of sodium selenite has been found to significantly reduce the occurrence of reperfusion induced arrhythmias and increase GPx activity in hearts (Tanguy *et al* 2004). Se exerts its biological activity mostly due to its antioxidant mechanisms. The antioxidant mechanisms include increased expression

of antioxidant selenoproteins and the GPx-like, radical scavenging and metal-binding activities of low molecular weight Se metabolites. These mechanisms are generally associated with prevention of disease by Se supplementation due to the relationship between oxidative stress and disease (Weekley and Harris 2013). TrxR which is also an important Se containing enzyme which is present in thioredoxin (Trx) system. The Trx system includes TrxR with Trx and NADPH, constitutes the major intracellular redox system. TrxR has control over the redox environment of the cell and cell growth *via* the regulation of Trx. In addition, the TrxR system is capable of reducing H_2O_2, organic hydroperoxides and lipid hydroperoxides. TrxR may be particularly important in preventing CVD. In addition, Se supplementation prevents the hypoxia/ reoxygenation injury of the isolated neonatal cardiomyocytes (Ostadalova *et al* 2007).

However, Se can also be toxic to organisms, depending on its chemical species and concentration. Se toxicity develops in mammals with a daily intake of one milligram of Se per kilogram of body weight and in cultured cells exposed to micromolar concentrations of Se (Goehring *et al* 1984; Lopez *et al* 1990; Frenkel *et al* 1987). High concentration of Se induce cataract of eye lens. Se toxicity is due to low cellular redox status due to the oxidization of protein thiol groups and glutathione (GSH), and the generation of oxygen radicals. Acute Se toxicity is often related to industrial pollution and could cause respiratory, gastrointestinal health problems (Pedrero and Madrid 2009). Chronic exposure to high levels of Se in food and water could result in hair loss, weak nails, lack of mental alertness, garlic breath odour, excessive tooth decay and discoloration. Due to the health benefits of Se and its protective role in CVD, development of Se nanoparticles have gained much interest. Studies have reported that selenite can be successfully encapsulated into chitosan/TPP nanoparticles, which exhibited enhanced antioxidant activities and controlled release *in vitro* (Luo *et al* 2010).

1.11. Current treatment options in coronary heart disease

Treatment for CHD usually is the same for both women and men. Treatment may include lifestyle changes, medicines, surgical procedures and cardiac rehabilitation.

The goals of treatment are to:

- Relieve symptoms
- Reduce risk factors in an effort to slow, stop or reverse the build-up of plaque
- Lower the risk of blood clots forming
- Widen or bypass plaque-clogged coronary arteries
- Prevent CHD complications
- Decrease cholesterol and blood pressure
- Physically restore blood flow to the heart *via* bypass surgery
- Make lifestyle changes by eating healthy foods, exercising regularly and losing weight

Anti-anginal medications are the mainstay of anti-ischemic management and act to correct the balance between myocardial supply and demand by increasing coronary blood flow, reducing myocardial oxygen requirements or both. These medications include nitrates (which act principally by venous vasodilation, but also probably by coronary dilation), beta-blockers (which act mainly by reducing heart rate and cardiac contractility) and Ca^{2+} channel blockers (which act principally by arterial and coronary vasodilation). The choice of therapy and its effectiveness depend on the underlying cause of ischemia (Cohn 1998). The use of the drugs in combination may result in reduction in myocardial oxygen demand than that achieved with monotherapy also it reduces the undesirable side effects. For example, the reflex tachycardia produced by some calcium channel blockers may be offset by beta-blocker therapy. Ultimately, aspirin and lipid-lowering drugs are also considered in combination therapy. Coronary artery bypass and coronary angioplasty improve myocardial oxygen supply by relieving or circumventing the atherosclerotic obstruction responsible for ischemia.

1.12. Relevance of cell culture in pharmacological studies

Introduction of animal cell culture for drug testing is of great relevance in biotechnological and pharmacological studies. It offers the possibility of observing the effect of drugs on cells without the interference of nervous, humoral and hormonal factors as in intact organism. Viability assessments in a cell culture system have been widely accepted even though differences exist between *in vitro* and *in vivo* systems. Some of the applications for animal cell culture study in biomedical science are to investigate the normal physiology or biochemistry of cells. For example, studies of cell metabolism.

● To test the effect of various chemical compounds or drugs on specific cell types (normal or cancerous cells).

● To study the sequential or parallel combination of various cell types to generate artificial tissues (artificial skin). Possibility of generating artificial tissues is an emerging and intensively studied area of biotechnology known as "tissue engineering".

● To synthesize valuable biologicals from large scale cell cultures. The biologicals include a broad range of cell products and consist of specific proteins or viruses that require animal cells for propagation. For example, therapeutic proteins can be synthesized in large quantities by growing genetically engineered cells in large-scale cultures. The number of such commercially valuable biologicals has increased rapidly over the last decade and has led to the present widespread interest in animal cell culture technology.

Even though animal studies are inevitable in pharmacological study, a preliminary investigation using cell culture and associated assay methods can provide more valuable reports. This can also give an initial idea about the dose and response of chemical on organ system (Schindler 1969; Rowan and Goldberg 1985; Rick 2009). In this study the myoblast cell line H9c2, derived from embryonic rat heart (Kimes and Brandt 1976) has been used as an *in vitro* model. H9c2 cells were found to be closer to normal primary cardiomyocytes with regard to their energy metabolism features. H9c2 cells show electrophysiological and biochemical properties of both skeletal and cardiac tissues, including depolarization in response to acetylcholine and rapid activation of Ca^{2+} currents through L-Type channels (Hescheler *et al* 1991; Mejia-Alvarez *et al* 1994; Wang *et al* 1999). Upon reduction of serum concentration this cell line differentiates from mononucleated myoblasts to myotubes. During the differentiation process, cells retain several elements of the electrical and hormonal signaling pathway of cardiac cells and have therefore become an accepted *in vitro* model pertaining to studies on heart (Eckel 1996; Brostrom *et al* 2000; Wayman *et al* 2001). L'Ecuyer *et al* (2001) demonstrated that H9c2 cells can be used to study free radical production and can be engineered to express foreign genes at controllable levels, making them a suitable system to study molecular responses to oxidative damage. They also demonstrated that H9c2 cells are significantly more sensitive to hypoxia-reoxygenation

injury in terms of loss of cell viability and mitochondrial respiration. Studies of Kuznetsov *et al* (2014) demonstrated that H9c2 cell shows high ATP levels, mitochondrial mass and respiratory activity, as well as higher vulnerability to hypoxia and oxidative stress. In addition, they also reported that H9c2 cells are appropriate models to study the mechanisms of cardiac ischemia-reperfusion injury, to evaluate the efficiency of various therapeutic interventions and in cardioplegic and organ preservation applications (Kuznetsov *et al* 2014).

1.13. Scope and objective of the present work

Polysaccharide nanoparticles remain a hot topic in major medical, pharmaceutical and food industries because of its biodegradability, non-toxicity, water solubility etc. In this view we selected GG which is an abundantly available natural polysaccharide as preferred material for synthesizing nanoparticles for our study. GG which is a galactomannan and has many properties which can be utilized in nutraceutical and pharmaceutical field. Se, a micronutrient that has potential use in the prevention and treatment of disease especially CVD and is used as a therapeutic agent in this study. Diseases in which oxidative stress is implicated, including cancer, cardiovascular and neurodegenerative diseases are particularly attractive targets of Se supplementation. The main significance of the work is the preparation and characterization of guar gum nanoparticle (GGN) and selenium incorporated guar gum nanoparticles (SGG) by nanoprecipitation method and its therapeutic effect was checked against cardiac ischemia and I/R. This is the first attempt on the preparation of GG based nanoparticle by nanoprecipitation method and incorporation of Se to GGN as therapeutic for cardiac disorders.

The objectives of the present work are

1. Preparation and characterization of SGG and its biological evaluation in H9c2 cardiomyoblast.
2. Beneficial properties of SGG against I/R induced alteration in innate antioxidant status and calcium homeostasis in H9c2 cardiomyoblast.
3. Effect of SGG against alteration in mitochondrial functions in I/R.
4. Anti-inflammatory and anti-apoptotic potential of SGG against I/R.

1.14. Societal importance of the present work

Ischemic heart disease and stroke are among the most common causes of death and disability in the world. Globally, India have the highest rate coronary heart diseases. Among different states, Kerala shares more incidence of CHD equally or at a higher level. The result of the present study is expected to generate more knowledge in the physiological and biochemical changes in cardiac myocytes during ischemia. This knowledge could be utilized for selection of new biochemical targets which can be used for better diagnosis and prognosis of cardiac patients. Moreover we are optimistic about the positive outcome of the study in the form selenium based therapeutics (SGG) for human use after detailed investigations on animal and other studies related to drug developments. This study focuses on the possible development of low cost nutraceuticals for prophylactic use in human beings which will be affordable to everybody.

References

1. Abhilash M (2010) Potential applications of nanoparticles. *International Journal of Pharma and Bio Sciences* 1: 1-12.
2. Allemann E, Leroux JC, Gurny R, Doelker E (1993) In vitro extended release properties of drug-loaded poly (DL-lactic acid) nanoparticles produced by a salting out procedure. *Pharm Res* 10: 1732-1737.
3. Anselmi A, Abbate A, Girola F, Nasso G , Biondi-Zoccai GG, Possati G, Gaudino M (2004) Myocardial ischemia, stunning, inflammation, and apoptosis during cardiac surgery: a review of evidence. *Eur J Cardiothorac Surg* 25: 304-311.
4. Arayne MS, Sultana N, Qureshi F (2007) Nanoparticles in delivery of cardiovascular drugs. *Pak J Pharm Sci* 20: 340-348.
5. Athar M, Das AJ (2013) Therapeutic nanoparticles: state-of-the-art of nanomedicine. *Adv Mat Lett* 10.5185/amlett.2013.5475.
6. Baldwin AD, Kiick KL (2010) Polysaccharide-modified synthetic polymeric biomaterials. *Biopolymers* 94: 128-140.
7. Baran ET, Özer N, Hasirci V (2002) In vivo half life of nanoencapsulated L-asparaginase. *J Mater Sci Mater Med* 13: 1113-1121.
8. Barbucci R, Pasqui D, Favaloro R, Panariello G (2008) A thixotropic hydrogel from chemically cross-linked guar gum: synthesis, characterization and rheological behaviour. *Carbohyd Res* 343: 3058-3065.
9. Behera AK, Barik BB, Pandya S, Joshi S (2012) Formulation and evaluation of isoniazid loaded -Σ-polycaprolactone nanoparticles. *J Pharm Res* 5: 798-802.
10. Bernardi P, Krauskopf A, Basso E, Petronilli V, Blachly-Dyson E, Di Lisa F, Forte MA (2006) The mitochondrial permeability transition from in vitro artifact to disease target. *FEBS J* 273: 2077-2099.
11. Boengler K, Heusch G, Schulz R (2011) Mitochondria in postconditioning. *Antioxid Redox Signal* 14: 863-880.
12. Bopassa JC (2012) Protection of the ischemic myocardium during the reperfusion: between hope and reality. *Am J Cardiovasc Dis* 2: 223-236.

13. Brostrom MA, Reilly BA, Wilson FJ, Brostrom CO (2000) Vasopressin-induced hypertrophy in H9c2 heart-derived myocytes. *Int J Biochem Cell Biol* 32: 993-1006.
14. Brown L, Rosner B, Willett WW, Sacks FM (1999) Cholesterol-lowering effects of dietary fiber: a meta-analysis. *Am J Clin Nutr* 69: 30-42.
15. Buzea C, Pacheco I, Robbie K (2007) Nanomaterials and nanoparticles: sources and toxicity. *Biointerphases* 2: MR17-MR71.
16. Carballoa SM, Limb S, Rodrigueza G, Vilac AO, Kruegerb CG, Gunasekaran S, Reed JD (2010) Biopolymer coating of soybean lecithin liposomes via layer-by-layer self-assembly as novel delivery system for ellagic acid. *J Funct Foods* 2: 99-106.
17. Cascone MG, Lazzeri L, Carmignani C, Zhu Z (2002) Gelatin nanoparticles produced by a simple W/O emulsion as delivery system for methotrexate. *J Mater Sci Mater Med* 13: 523-526.
18. Clapham DE (1995) Calcium signaling. *Cell* 80: 259-268.
19. Cohn PF (1998) Treatment of chronic myocardial ischemia: rationale and treatment options. *Cardiovasc Drugs Ther* 12: 217-223.
20. Crompton M (1999) The mitochondrial permeability transition pore and its role in cell death. *Biochem J* 341: 233-249.
21. Di Lisa F, Bernardi P (2009) A CaPful of mechanisms regulating the mitochondrial permeability transition. *J Mol Cell Cardiol* 46: 775-780.
22. Di Lisa F, Canton M, Carpi A, Kaludercic N, Menabò R, Menazza S, Semenzato M (2011) Mitochondrial injury and protection in ischemic pre-and postconditioning. *Antioxid Redox Signal* 14: 881-891.
23. Duncan R (2003) The dawning era of polymer therapeutics. *Nat Rev Drug Discov* 2: 347-60.
24. Eckel J (1996) Direct effects of glimepiride on protein expression of cardiac glucose transporters. *Horm Metab Res* 28: 508-511.
25. Edelmana ER, Nathan A, Katada M, Gates J, Karnovsky MJ (2000) Perivascular graft heparin delivery using biodegradable polymer wraps. *Biomaterials* 21: 2279-2286.
26. Fahrenbach MJ, Riccardi BA, Saunders JC, Lourie IN, Heider JG (1965)

Comparative effects of guar gum and pectin on human serum cholesterol levels. *Circulation* 31: 11-14.

27. Fessi H, Puisieux F, Devissaguet JP, Ammoury N, Benita S (1989) Nanocapsule formation by interfacial polymer deposition following solvent displacement. *Int J Pharm* 55: R1-R4.
28. Frenkel GD, Walcott A, Middleton C (1987) Inhibition of RNA and DNA polymerases by the product of the reaction of selenite with sulfhydryl compounds. *Mol Pharmacol* 31: 112-116.
29. Goehring TB, Palmer IS, Olson OE, Libal GW, Wahlstrom RC (1984) Toxic effects of selenium on growing swine fed corn-soybean meal diets. *J Anim Sci* 59: 733-737.
30. Griffith EJ, Halestrap AP (1993) Protection by Cyclosporin A of ischemia/reperfusion-induced damage in isolated rat hearts. *J Mol Cell Cardiol* 25: 1461-1469.
31. Hans ML, Lowman AM (2002) Biodegradable nanoparticles for drug delivery and targeting. *Curr Opin Solid St M* 6: 319-327.
32. Harmia T, Speiser P, Kreuter J (1986) A solid colloidal drug delivery system for the eye: encapsulation of pilocarpine in nanoparticles. *J Microencapsul* 3: 3-12.
33. Hatfield DL, Gladyshev VN (2002) How selenium has altered our understanding of the genetic code. *Mol Cell Biol* 22: 3565-3576.
34. Hausenloy DJ, Duchen MR, Yellon DM (2003) Inhibiting mitochondrial permeability transition pore opening at reperfusion protects against ischaemia-reperfusion injury. *Cardiovasc Res* 60: 617-625.
35. Hescheler J, Meyer R, Plant S, Krautwurst D, Rosenthal W, Schultz G (1991) Morphological, biochemical, and electrophysiological characterization of a clonal cell (H9c2) line from rat heart. *Circ Res* 69: 1476-1486.
36. Heusch G, Boengler K, Schulz R (2010) Inhibition of mitochondrial permeability transition pore opening: the Holy Grail of cardioprotection. *Basic Res Cardiol* 105: 151-154.
37. Hornig S, Heinze T (2008) Efficient approach to design stable water-dispersible

nanoparticles of hydrophobic cellulose esters. *Biomacromolecules* 9: 1487-1492.

38. Hoyt KR, Stout AK, Cardman JM, Reynolds IJ (1998) The role of intracellular Na^+ and mitochondria in buffering of kainate-induced intracellular free Ca^{2+} changes in rat forebrain neurones. *J Physiol* 509: 103-116.
39. Hunter DR, Haworth RA, Southard JH (1976) Relationship between configuration, function, and permeability in calcium-treated mitochondria. *J Biol Chem* 251: 5069-5077.
40. Javadov SA, Clarke S, Das M, Griffiths EJ, Lim KH, Halestrap AP (2003) Ischaemic preconditioning inhibits opening of mitochondrial permeability transition pores in the reperfused rat heart. *J Physiol* 549: 513-524.
41. Jong WHD, Borm PJA (2008) Drug delivery and nanoparticles: applications and hazards. *Int J Nanomedicine* 3: 133-149.
42. Kimes BW, Brandt BL (1976) Properties of a clonal muscle cell line from rat heart. *Exp Cell Res* 98: 367-381.
43. Kipp JE (2004) The role of solid nanoparticle technology in the parental delivery of poorly water-soluble drugs. *Int J Pharm* 284: 109-122.
44. Kona S, Dong JF, Liu Y, Tan J, Nguyen KT (2012) Biodegradable nanoparticles mimicking platelet binding as a targeted and controlled drug delivery system. *Int J Pharm* 423: 516- 524.
45. Kumpulainen JT, Salonen JT (1999) Natural antioxidants and anticarcinogens in Nutrition, Health and Disease, The Royal Society of Chemistry, UK, pp178-187.
46. Kutala VK, Khan M, Angelos MG, Kuppusamy P (2007) Role of oxygen in postischemic myocardial injury. *Antioxid Redox Signal* 9: 1193-1206.
47. Kuznetsov AV, Javadov S, Sickinger S, Frotschnig S, Grimma M (2014) H9c2 and HL-1 cells demonstrate distinct features of energy metabolism, mitochondrial function and sensitivity to hypoxia-reoxygenation. *Biochim Biophys Acta* 1853: 276-284.
48. Ladilov Y, Efe O, Schäfer C, Rother B, Kasseckert S, Abdallah Y, Meuter K, Dieter Schlüter K, Piper HM (2003) Reoxygenation-induced rigor-type contracture. *J Mol*

Cell Cardiol 35: 1481-1490.

49. L'Ecuyer T, Horenstein MS, Thomas R, Vander Heide R (2001) Anthracycline-induced cardiac injury using a cardiac cell line: potential for gene therapy studies. *Mol Genet Metab* 74: 370-379.
50. Lee JW, Park JH, Robinson JR (2000) Bioadhesive-based dosage forms: the next generation. *J Pharm Sci* 89: 850-866.
51. Lobo V, Patil A, Phatak A, Chandra N (2010) Free radicals, antioxidants and functional foods: impact on human health. *Pharmacogn Rev* 4: 118-126.
52. Lopez S, Miyashita Y, Simons SS (1990) Structurally based selective interaction of arsenite with steroid receptors. *J Biol Chem* 265: 16039-16042.
53. Luo Y, Zhang B, Cheng WH, Wang Q (2010) Preparation, characterization and evaluation of selenite-loaded chitosan/TPP nanoparticles with or without zein coating. *Carbohydr Polym* 82: 942-951.
54. Ma X, Pawlik M (2005) Effect of alkali metal cations on adsorption of guar gum onto quartz. *J Colloid Interface Sci* 289: 48-55.
55. Mebazaa A, Gheorghiade M, Zannad F, Parrillo JE (2008) Acute Heart Failure, Springer-Verlag London limited, pp 931.
56. Medeiros SDV, Cordeiro SL, Cavalcanti JEC, Melchuna KM, Lima AMS, Filho IA, Medeiros AC, Rocha KBF, Oliveira EM, Faria EDB, Sassaki GL, Rocha HAO, Sales VSF (2012) Effects of purified *saccharomyces cerevisiae* (1→ 3) β glucan on venous ulcer healing. *Int J Mol Sci* 13: 8142-8158.
57. Mejia-Alvarez R, Tomaselli GF, Marban E (1994) Simultaneous expression of cardiac and skeletal muscle isoforms of the L-type Ca^{2+} channel in a rat heart muscle cell line. *J Physiol* 478: 315-329.
58. Mohanraj VJ, Chen Y (2006) Nanoparticles – a review. *Trop J Pharm Res* 5: 561-573.
59. Molpeceres J, Guzman M, Aberturas MR, Chacon M, Berges L (1996) Application of central composite designs to the preparation of polycaprolactone nanoparticles by solvent displacement. *J Pharm Sci* 85: 206-213.

60. Mozaffari MS, Liu JY, Abebe W, Baban B (2013) Mechanisms of load dependency of myocardial ischemia reperfusion injury. *Am J Cardiovasc Dis* 3: 180-196.
61. National Research Council (NRC) Committee on Dietary Allowances (1989) Recommended Dietary Allowances, 10th edn. Washington, DC: National Academy Press.
62. Ostadalova I, Vobecky M, Chvojkova Z, Mikova D, Hampl V, Wilhelm J, Ostadal B (2007) Selenium protects the immature rat heart against ischemia/reperfusion injury. *Mol Cell Biochem* 300: 259-267.
63. Pedrero Z, Madrid Y (2009) Novel approaches for selenium speciation in foodstuffs and biological specimens: A review. *Anal Chim Acta* 634: 135-152.
64. Piper HM, Abdallah Y, Schäfer C (2004) The first minutes of reperfusion: a window of opportunity for cardioprotection. *Cardiovasc Res* 61: 365-371.
65. Piper HM, Kasseckert S, Abdallah Y (2006) The sarcoplasmic reticulum as the primary target of reperfusion protection. *Cardiovasc Res* 70: 170-173.
66. Pszczola DE (2003) Plot thickens, as gums: add special effects. *Food Technol Chicago* 57: 34-47.
67. Riaz M, Mehmood KT (2012) Selenium in human health and diseases: A review. *J Postgrad Med Inst* 26: 120-133.
68. Rick NG (2009) Drugs: From discovery to approval. Chapter 1: Trends in drug discovery and development, Wiley-Blackwell, NJ, USA, p 13.
69. Roberfroid M (1993) Dietary fiber, insulin and oligofructose: a review comparing their physiological effects. *Crit Rev Food Sci Nutr* 33: 103-48.
70. Rouzet F, Bachelet-Violette L, Alsac JM, Suzuki M, Meulemans A, Louedec L, Petiet A, Jandrot-Perrus M, Chaubet F, Michel JB, Le Guludec D, Letourneur D (2011) Radio labeled fucoidan as a Pselectin targeting agent for *in vivo* imaging of platelet rich thrombus and endothelial activation. *J Nucl Med* 52: 1433-1440.
71. Rowan AN, Goldberg AM (1985) Perspectives on alternatives to current animal testing techniques in preclinical toxicology. *Ann Rev Pharmacol Toxicol* 25: 225-247.
72. Roy G, Sarma BK, Phadnis PP, Mugesh G (2005) Selenium-containing enzymes in

mammals: chemical perspectives. *J Chem Sci* 117: 287-303.

73. Ruiz-Meana M, Abellán A, Miró-Casas E, Garcia-Dorado D (2007) Opening of mitochondrial permeability transition pore induces hypercontracture in Ca^{2+} overloaded cardiac myocytes. *Basic Res Cardiol* 102: 542-552.
74. Sarmah JK, Mahanta R, Bhattacharjee SK, Mahanta R, Biswas A (2011) Controlled release of tamoxifen citrate encapsulated in cross-linked guar gum nanoparticles. *Int J Biol Macromol* 49: 390-396.
75. Schindler R (1969) Use of cell culture in pharmacology. *Ann Rev Pharmacol* 9: 393-406.
76. Shanmuganathan S, Hausenloy DJ, Duchen MR, Yellon DM (2005) Mitochondrial permeability transition pore as a target for cardioprotection in the human heart. *Am J Physiol Heart Circ Physiol* 289: H237-H242.
77. Sinha VR, Kumria R (2001) Polysaccharides in colon-specific drug delivery. *Int J Pharm* 224: 19-38.
78. Song C, Labhasetwar V, Guzman L, Topol E, Levy RJ (1995) Dexamethasone-nanoparticles for intra-arterial localisation in restonosis in rats. *Proc Intern Symp Control Rel Bioact Mater* 22: 444-445.
79. Spragg DD, Alford DR, Greferath R, Larsen CE, Lee K, Gurtner GC, Cybulsky MI, Tosi PF, Nicolau C, Gimbrone MA Jr (1997) Immuno targeting of liposomes to activated vascular endothelial cells: A strategy for site-selective delivery in the cardiovascular system. *Proc Natl Acad Sci USA* 94: 8795-8800.
80. Suzuki M, Serfaty JM, Bachelet L, Beilvert A, Louedec L, Chaubet F, Michel JB, Letourneur D (2011) In vivo targeted molecular imaging for activated platelets by MRI using USPIO fucoidan in rat abdominal aortic aneuryms model. *J Cardiovasc Mag Reso*13: 372.
81. Tanguy S, Morel S, Berthonneche C, Toufektsian MC, Lorgeril MD, Ducros V, Tosaki A, de Leiris J, Boucher F (2004) Preischemic selenium status as a major determinant of myocardial infarct size in vivo in rats. *Antioxid Redox Signal* 6: 792-796.

82. Tiraferri A, Chen KL, Sethi R, Elimelech M (2008) Reduced aggregation and sedimentation of zero-valent iron nanoparticles in the presence of guar gum. *J Colloid Interface Sci* 324: 71-79.
83. Tripathy S, Das MK (2013) Guar gum: present status and application. *J Pharm Sci Innov* 2: 24-28.
84. Venardos K, Harrison G, Headrick J, Perkins A (2004) Effects of dietary selenium on glutathione peroxidase and thioredoxin reductase activity and recovery from cardiac ischemia–reperfusion. *J Trace Elem Med and Biol* 18: 81-88.
85. Wang W, Watanabe M, Nakamura T, Kudo Y, Ochi R (1999) Properties and expression of Ca^{2+}-activated K^+ channels in H9c2 cells derived from rat ventricle. *Am J Physiol* 276: H1559-1566.
86. Wayman N, McDonald MC, Thompson AS, Threadgill MD, Thiemermann C (2001) 5-aminoisoquinolinone, a potent inhibitor of poly (adenosine 5'-diphosphate ribose) polymerase, reduces myocardial infarct size. *Eur J Pharmacol* 430: 93-100.
87. Weekley CM, Harris HH (2013) Which form is that? The importance of selenium speciation and metabolism in the prevention and treatment of disease. *Chem Soc Rev* 42: 8870-8894.
88. Will O, Purkayastha S, Chan C, Athanasiou T, Darzi AW, Gedroyc W, Tekkis PP (2006) Diagnostic precision of nanoparticle enhanced MRI for lymph-node metastases: a meta-analysis. *Lancet Oncol* 7: 52-60.
89. World Health Organization, World Health Statistics (2008) Department of Measurement & Health Information Systems of the Information, Evidence and Research Cluster. Geneva: WHO Press, pp 29-31.

Chapter 2

Preparation and characterization of selenium incorporated guar gum nanoparticles and its biological evaluation in H9c2 cardiomyoblast

2.1. Introduction

Recently the concept of nanoscience has been incorporated to the medical science for the amplification of the therapeutic potential of the material. A wide range of nanomaterials have been developed for biomedical applications due to their unique properties. The special physicochemical properties of nanomaterial make them entirely different effect on biological system compared to their macro and micro counterparts. There is high demand of antioxidants for control and management of heart diseases due to the importance of oxidative stress in the etiology of the same. Kim *et al* (2011) reported about the use of antioxidants nanoformulations against cardiac diseases like I/R injury, hypertrophy and myocardial infarction associated problems. For example, CuZnSOD protein encapsulated in biodegradable poly (D, L-lactide coglycolide) or PLGA nanoparticles (PLGA-SOD) has shown potential as a therapeutic agent for I/R injury. Other nanoformulated antioxidants studied in models of I/R injury are peroxalate nanoparticles, which instantaneously and specifically decompose H_2O_2, the most abundant ROS generated during I/R injury (Lee *et al* 2008; Lee *et al* 2007). The antioxidant micronutrient like cerium, Se, vanadium etc. have been reported to have therapeutic importance against heart diseases. Among this Se is having special position in biomedical sciences due to its role as an innate antioxidant system of body (discussed in chapter 1). Nanoparticles containing metals of biological importance are attracting much attention of present scenario because of their physical and chemical properties. Taking this into account, the present study was aimed to prepare and characterize SGG and study its interaction with H9c2 by assessing its effect on various vital parameters. For this we conducted batteries of *in vitro* experiments to evaluate its interaction with H9c2 cell lines. In this study GG was used to prepare nanoparticles through nanoprecipitation method with sodium selenite to decrease the toxicity and enhance the antioxidant property of selenite dietary supplement. The physicochemical properties of the nanoparticles were characterized by particle size analysis, transmission electron microscopy (TEM) analysis and X-ray diffraction (XRD) analysis. In order to see the interaction of SGG with cells we systematically investigated

the effect of nanoparticle on H9c2 cells by analyzing various parameters like cell viability, apoptosis, DNA protection, ROS generation, mitochondrial transmembrane potential ($\Delta\Psi m$) and alteration in cytoskeleton properties. This chapter also deals with comparative evaluation of the antioxidant potential of SGG, GGN and Se using *in vitro* cell free systems.

2.2. Experimental methods

2.2.1. Materials

Guar gum powder, mannanase enzyme from *Helix pomatia*, sodium selenite, Triton X-100, isopropanol, phenazine methosulfate (PMS), nicotinamide adenine dinucleotide (NADH), nitrobluetetrazolium (NBT), 2-deoxy D-ribose, thiobarbituric acid (TBA), trichloroacetic acid (TCA), trolox, dimethyl sulfoxide (DMSO), 3-(4,5-dimethylthiazol- 2-yl)-2,5-diphenyl tetrazolium bromide (MTT), sodium tripolyphosphate (TPP), dimethyl sulfoxide (DMSO), 2',7' dichlorodihydrofluorescein diacetate (DCFH-DA), acridine orange (AO), ethidium bromide (EtBr), 2, 3-diaminonaphthalene, 5,5',6,6'-tetrachloro-1,1',3,3' tetraethylbenzimidazolyl carbocyanine iodide (JC-1), 4',6-diamidino-2-phenylindole (DAPI), phallodin and pUC-18 plasmid DNA were purchased from Sigma Chemicals, USA. Ammonium molybdate, ascorbic acid (AA), ferrous sulphate, methanol, hydrogen peroxide (H_2O_2) and potassium ferricyanide were purchased from Merck Specialities Pvt Ltd (India). Tris hydroxymethyl aminomethane hydrochloride (Tris-HCl), potassium hydroxide, and potassium persulphate were purchased from Sisco Research Laboratories, Mumbai (India). Ethylene diamine tetraacetic acid (EDTA), sodium phosphate and sodium hydroxide were purchased from SD Fine Chemicals Ltd (India). Dulbecco's modified Eagle's medium (DMEM) and foetal bovine serum (FBS) were from HiMedia Pvt Ltd India. All other chemicals and solvents used were of analytical grade.

2.2.2. Preparation and characterization of GGN and SGG

The GGN was prepared by nanoprecipitation method (Soumya *et al* 2010). Nanoprecipitation was carried out using the addition of a non-solvent (isopropyl alcohol) to the aqueous solutions of depolymerized sample previously mixed with surfactants (Triton X-100) and cross linker (TPP). Ionic crosslinking using polyanionic cross linker TPP was employed in this method. Vigorous vortexing and sonication were employed in

the procedure to prevent agglomeration of molecules. Triton X-100 was used to modify the surface properties of GG and to ensure the stability of nanoparticles. Besides GGN, SGG nanoparticles were also prepared by the same procedure. Briefly, 1% GG was depolymerised with mannanase enzyme with a pH of 5.2 in citrate phosphate buffer and incubated at 30 °C for 24 h. The hydrolysed suspension of GG was filtered through 0.2 µm syringe filters. The filtered suspension was stored in 4 °C for further characterization. Then through nanoprecipitation method GGN and SGG were prepared with depolymerised GG, 10% Triton X-100, isopropanol and 0.1% TPP. For preparing SGG sodium selenite, was added to the solution containing 1% GG, 10% Triton X-100, isopropanol and 0.1% TPP. The solution was vortexed and sonicated for 10 min at room temperature, filtered with 0.2 µm syringe filters to get uniform nanoparticles. The average particle size (hydrodynamic diameter, Zaverage) of the prepared particles (GGN, SGG) were determined by photon correlation spectroscopy (PCS) using 3000 HSA Zetasizer (UK) equipped with He–Ne laser (633 nm). Photon-correlation spectroscopy requires the viscosity of the medium to be known and determines the diameter of the particle by Brownian motion and light scattering properties (Kreuter 1994). The results obtained by photon-correlation spectroscopy are usually verified by TEM. High-resolution transmission electron microscopy (HRTEM) is an imaging mode of the TEM that allows the imaging of the structure of a sample at an atomic scale (Williams *et al* 2009). Because of its high resolution, it is an invaluable tool to study nanoscale properties of the materials. For this study the morphology and particle size of the samples were analyzed using a high resolution transmission electron microscope, FEI, TECNAI, 30G2s-TWIN microscope. A thin layer of sample was coated on a carbon coated copper grid and dried under vaccum. This sample coated grid was used for the TEM analysis.

XRD of GG, pure sodium selenite and SGG were measured using X-ray diffractometer (XPERT Pro, Philips, Eindhoven, Netherlands) with nickel-filtered Cu-Kα radiation (0.154 nm). Qualitative analysis is possible by comparing the XRD pattern of an unknown material to a library of known patterns. The degree of crystallinity of samples was quantitatively estimated. A smooth curve which connected peak baselines was plotted on the diffractograms. The area above the smooth curve was taken as the crystalline portion and the lower area between smooth curve and the linear baseline in the

samples was taken as the amorphous portion.

2.2.3. Colloidal stability

The colloidal stability of the prepared nanoparticle was investigated by turbidity measurement. Therefore, the nanoparticles were mixed with DMEM medium both in the presence and absence of 10% FBS. The average particle sizes (hydrodynamic diameter, Zaverage) of the prepared particles (GGN, SGG) were determined by using a Zetasizer NanoZS (Malvern, UK).

2.2.4. Cell culture

Rat embryonic cardiomyoblast derived H9c2 cells were obtained from American Type Culture Collection (ATCC) Rockville, MD. Cultures of cardiomyocytes, usually from rat neonatal hearts are widely used to investigate the cellular and molecular changes. H9c2 cells mimic most of the characteristic features of adult cardiac myocytes and this is an ideal cell line to check the effect of drug on myocardium in *in vitro* system. Cells were cultured in DMEM supplemented with 10% FBS, 100 U penicillin/ml and 100 µg streptomycin/ml in 5% CO_2 at 37 ^oC. Cells were passaged regularly and subcultured to 80% confluence before the experiments. Fresh nanoparticle solutions were prepared and checked to ensure consistency of physical chemical and biological properties of nanoparticles. Nanoparticles were freshly prepared before use and vortexed thoroughly before being added to the cells. Experimental design consist of following groups unless otherwise specified (1) control cells (2) cells treated with sodium selenite alone (5, 25 and 50 nM) and (3) cells treated with SGG (5, 25 and 50 nM). Observations were made after 1, 6 and 24 h of incubation.

2.2.5. Evaluation of cell viability

Cell viability was determined by MTT assay. Cells in exponential growth phase were plated at 5×10^4 cells per well in 24-well plate. Then, cells were exposed to various concentrations (5, 25 and 50 nM) of sodium selenite, and SGG for 1, 6 and 24 h and they were subjected to MTT analysis. For this 350 µl of MTT solution (5 mg/ml) was added to each well and incubated for 4 h at 37 ^oC. The formazan crystals thus formed were dissolved in DMSO and the absorbance was read after 45 min in a microplate reader (Biotek Synergy 4, US) at 570 nm and percentage of viable cells were calculated.

2.2.6. Intracellular localization of SGG nanoparticles

Initial experiments were conducted to see whether H9c2 cells uptake nanoparticles. We found that both GGN and SGG emit autofluorescence at blue region (excitation: 360 nm; emission: 435 nm). For cellular uptake studies, cells were seeded in 96-well plate at a density of 5×10^3 per well and treated with various concentrations of SGG (5, 25 and 50 nM) for 1, 6 and 24 h and single concentration (600 µg) of macro guar gum (MGG) as reference. The cells of all experimental groups were subjected to DNA staining with AO (exicitation: 502 nm; emission: 525 nm). Then the cells were subjected to fluorescent imaging by spinning disk microscope (BD PathwayTM Bioimager system, USA).

2.2.7. Estimation of intracellular Se concentration

Cells were treated with various concentrations of Se and SGG (5, 25 and 50 nM) for 24 h to check the influx of Se. For this 100 µl of cell homogenate were digested with 500 µl of HNO_3/ $HClO_4$ (4:1; v/v) at 190 ^oC for 90 min. After cooling to room temperature, 500 µl of 5 M HCl was added and the open glass tubes were heated to 150 ^oC for 30 min. Then 2 ml of 2.5 mM EDTA and 500 µl of diaminonaphthalene reagent was added at room temperature and the mixture were left at 55 ^oC for 30 min. 1 ml portion of cyclohexane was used to extract the piazselenol and fluorescence was measured using a fluorimeter at excitation of 364 nm and emission of 520 nm (Wilkie 1970).

2.2.8. Nanoparticle interaction on plasmid DNA

To check whether nanoparticle prepared has any effect on DNA we conducted experiment on plasmid pUC 18. The reaction mixture consisting of plasmid DNA and various concentrations of SGG was subjected to agarose gel electrophoresis and visualized by EtBr staining. In addition, we also conducted study to see whether SGG protect DNA from hydroxyl radical induced damage. For this, the reaction was conducted at a total volume of 14 µl containing 2 µl of plasmid pUC 18 DNA (50 ng DNA/µl) in 5 µl of 5, 25 and 50 nM concentration of Se and SGG, 7 µl of Fenton's reagent. The DNA (supercoiled, linear and open circular) was analyzed on 1% agarose gels and visualized. Ellagic acid was used as positive control.

2.2.9. DNA integrity

Briefly the cells in all experimental groups were stained with AO (excitation: 502 nm; emission: 525 nm) and EtBr (excitation: 510 nm; emission: 595 nm) to detect apoptosis and processed for fluorescent imaging to see alteration with various treatments. The working stain (100 µg/ml of AO and 100 µg/ml EtBr in phosphate buffered saline) was added to cells and was examined under spinning disc fluorescent microscope.

2.2.10. ROS generation with nanoparticles

Oxidative stress in response to nanoparticle incubation was measured by determining intracellular ROS generation. Intracellular ROS was determined by oxidative conversion of cell-permeable DCFH-DA to fluorescent 2', 7' dichlorofluorescein (DCF). For this H9c2 cells were seeded in 96-well plate and treated with different concentrations of Se and SGG (5, 25 and 50 nM) with different time duration. DCFH-DA stain in serum free medium was co-incubated with H9c2 cells at 37 °C for 20 min. After three washes, DCF fluorescence was measured by fluorimetry (excitation: 488 nm; emission: 525 nm) in multiwell plate reader and fluorescent imaging was done to detect the differences in the intensity of fluorescence emitted.

2.2.11. Alteration in $\Delta\Psi m$

The cells were seeded in 96-well plate in 200 µl of culture medium and treated with different concentration of Se and SGG (5, 25 and 50 nM) for 24 h. The experiment was done as per the protocol provided with the kit (JC-1 kit, Sigma). After respective treatments the cells were stained with JC-1 stain for 20 min at 37 °C and wash with growth medium. The shift of fluorescence was visualized under spinning disk microscope and fluorescence intensity was measured in multiwell plate reader. In normal cells, the JC-1 dye concentrates in the mitochondrial matrix where it forms red fluorescent aggregates because of the electrochemical potential gradient. Dissipation of $\Delta\Psi m$ prevents the accumulation of JC-1 in the mitochondria and thus it is dispersed throughout the cell, leading to a shift from red (J-aggregates) to green fluorescence (JC-1 monomers) and visualized under spinning disk microscope. For JC-1 monomers, the fluorimeter was set at 490 nm excitation and 530 nm emission wavelengths and for J-aggregates, the fluorimeter was set at 525 nm excitation and 590 nm emission wavelengths. Valinomycin (1 mg/ml) was used as positive control.

2.2.12. Cytoskeleton integrity

Phalloidin staining was used to determine cytoskeletal integrity of the cells upon nanoparticle treatment. The cells from experimental groups were washed with PBS and fixed with 4% paraformaldehyde in PBS for 10 min, permeabilized and dehydrated with cold 100% acetone for 3-5 min. Phalloidin stain (excitation: 488 nm; emission: 525 nm) was added and kept at room temperature for 30 min. Nucleus was counterstained with DAPI (excitation: 360 nm; emission: 450 nm) and visualized.

2.2.13. Antioxidant potential

2.2.13.1. Hydroxyl radical scavenging activity

The hydroxyl radical scavenging activity was measured by the deoxyribose method (Halliwell *et al* 1987) with slight modifications. Different concentrations of samples were mixed with an adequate amount of potassium buffer (pH 7.4). To this freshly prepared 0.1 ml of $FeCl_3$ (200 µM), 0.05 ml of H_2O_2 (1 mM), 0.1 ml of EDTA (1.04 mM), 0.05 ml of deoxyribose (28 mM) and freshly prepared 0.05 ml of ascorbic acid (1 mM) were added and then the mixture was incubated at 37 ^oC for 1 h. To that 2% TCA (0.5 ml) and 1% TBA (0.5 ml) were added and the mixture was heated in a water bath at 100 ^oC for 20 min. Absorbance of the resulting solution was measured at 532 nm. The absorbance of blank was also measured under similar conditions using catechin as the standard. The IC_{50} value was obtained from a dose response curve plotted between the percentage of inhibition and concentrations.

2.2.13.2. Total reducing power

Total reducing power (TRP) of the samples (Se, GGN and SGG) was determined colorimetrically using gallic acid as standard at the wavelength of 700 nm (Oyaizu 1986). Samples of different concentrations were mixed with distilled water, 200 mM phosphate buffer (pH 6.6) and 1% potassium ferricyanide. The mixture was incubated for 20 min at 50 °C. 10% TCA was added to the mixture, followed by vigorous vortexing for 10 min and the upper layer was mixed with distilled water and 0.1% of $FeCl_3$. The absorbance of the resultant solutions was read at 700 nm against blank. Increased absorbance indicates increased reducing power.

2.2.13.3. Metal chelating activity

The chelation of ferrous ions by the Se, GGN and SGG was estimated using

ferrozine (Rani *et al* 2010). Ferrozine can quantitatively form complexes with Fe^{2+}. In the presence of chelating agent the complex formation is disrupted resulting in the reduction of red colour of the complex. Measurement of colour reduction leads to the estimation of metal chelating activity. EDTA was used as the standard. The absorbance of red colour was read at 562 nm.

2.2.14. Statistical analysis

Results were expressed in mean and standard deviation (SD) of the control and treated cells from three independent experiments with duplicates (n=6). Data were subjected to one-way ANOVA followed by the Bonferroni test (Sokal and Rohlf 2009) to calculate the statistical difference among the groups using SPSS for Windows, standard version 11.5.1 (SPSS, Inc.) and significance was accepted at $P \leq 0.05$.

2.3. Results

2.3.1. Particle size measurements

In the present study GGN and SGG were prepared by nanoprecipitation method. Particle size analysed by PCS indicated the presence of fine spherical nanoparticles of size of ~41–132 nm with a polydispersity index (PDI) of 0.4 (Figure.2.1.a). In SGG the size of the nanoparticle had increased to ~69–173 nm range upon Se incorporation (Figure.2.1.b). This result is expected since selenite carried negative charges and electrostatically interacted with GG which would promote formation of nanoparticles through ionic cross-linking. Particle size is one of the most important parameters determining biocompatibilities and bioactivities of materials of therapeutic importance.

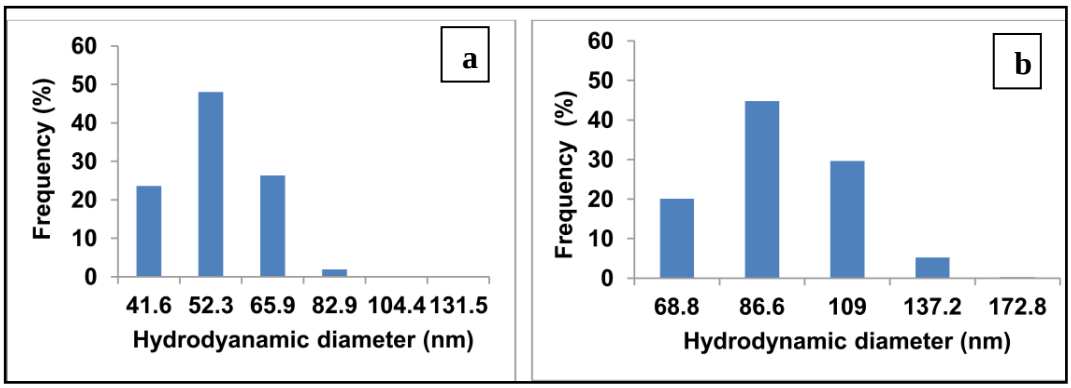

Figure 2. 1. Particle size distribution of (a) GGN and (b) SGG. The prepared nanoparticles were subjected to particle size analysis. (a) GGN had an average particle size varies from 41 to 132 nm range and (b) SGG nanoparticle prepared by nanoprecipitation method shows an increase in particle size from 69 to 173 nm.

2.3.2. Transmission electron microscopic images of GGN and SGG

The TEM analysis of GGN revealed the presence of fine spherical nanoparticle of size 40 nm range with few larger particles. It was found that the sizes observed by DLS were larger than those determined by TEM images. This might be due to the fact that GG binds to the surface of the Se which in turn creates a layer and this has made the particles appear larger. TEM images also confirmed that upon Se incorporation the size of GGN had increased to 50–100 nm (Figure.2.2.a, b). An elemental composition analysis by TEM-EDX showed the presence of strong signals from the Se atoms together with signal of C, Na and O atom from SGG (Figure.2.2.c) confirming the presence of Se in SGG.

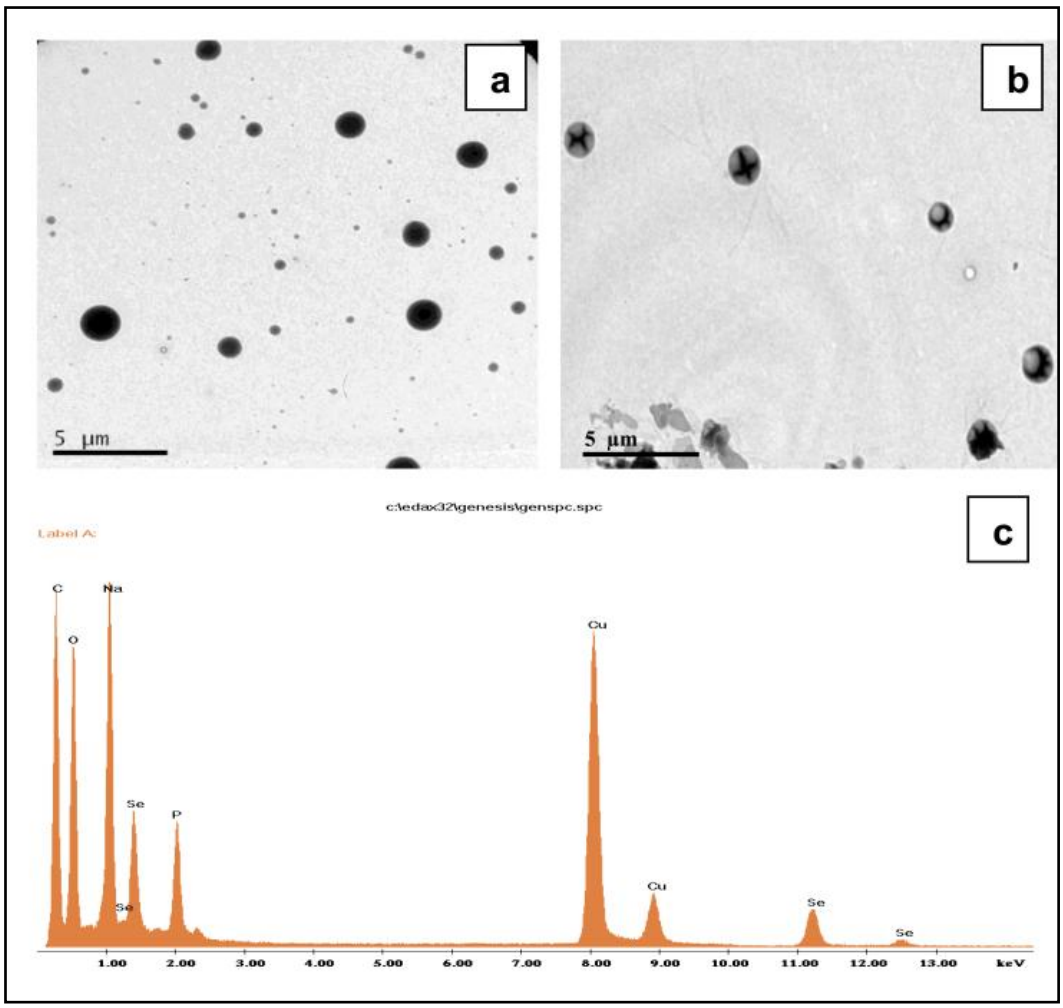

Figure 2. 2. TEM images of (a) GG showing spherical morphology with a size of 40 nm with few larger particles (b) SGG were also spherical in shape, upon incorporation of Se the particle size has been increased to the range of 50–100 nm (c) EDX spectrum of SGG show the presence of Se peaks, thereby confirming the presence of Se in SGG.

2.3.3. XRD characterization of nanoparticles

In nanoparticle preparation it is very important to control the particle size, shape and morphology. To determine the crystalline property of nanoparticles, SGG was characterized by XRD as it is an important analysis tool in nanomaterial science. Figure 2.3.a, b and c show the powder X-ray diffraction patterns of GG, sodium selenite and SGG respectively. XRD of GG (Figure.2.3.a) was amorphous because of its polymeric nature. XRD pattern of pure sodium selenite was compared with the standard JCPDS file data 32-1153. Peaks corresponding to sodium selenite had been observed in figure 3.c, confirming the incorporation of Se in SGG.

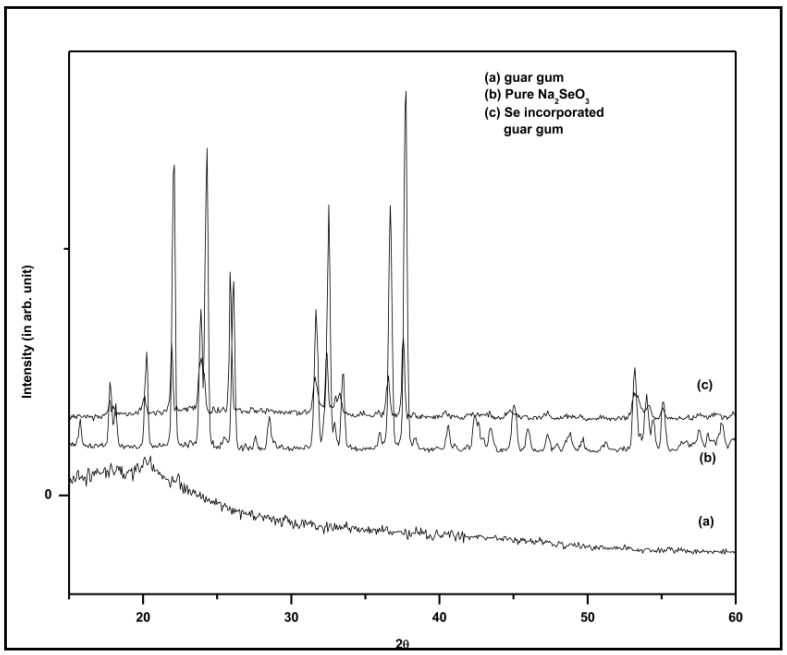

Figure 2. 3. XRD images of (a) GG (b) Sodium selenite and (c) SGG. GGN appears amorphous in nature in their morphology as per XRD data (Figure.3.a). While sodium selenite appears crystalline nature in the XRD pattern (Figure 3.b). The presence of major peaks of Se in SGG confirms the incorporation of Se in GGN (Figure.3.c).

2.3.4. Behaviour of nanoparticles in cell culture medium

The agglomeration of nanoparticles in liquid medium is of great importance in nanomedicine. The size of the SGG in cell culture medium without serum was found to be 286.3 nm with a PDI value of 0.5 (Figure.2.4a.b) while that in serum containing medium was 22.83 nm with a PDI value of 0.5 (Figure.2.4a.a). The particle size observed in DLS was considerably decreased from the previous results due to the enhanced repulsive interparticle interactions, especially with proteins in serum containing medium

(Gil *et al* 2009). The multimodal peak obtained for GGN in solution for both serum containing and serum free medium indicates a broad distribution of particles in agreement with the primary DLS results (Figure.2.4b.a, b). The observed PDI value ranging from 0.1-0.5 indicates that SGG possess the ability to remain as primary particles in cell culture medium with and without 10% FBS, suggesting that the SGG is relatively non-toxic in solution and the particles are remaining as homogeneous in nature.

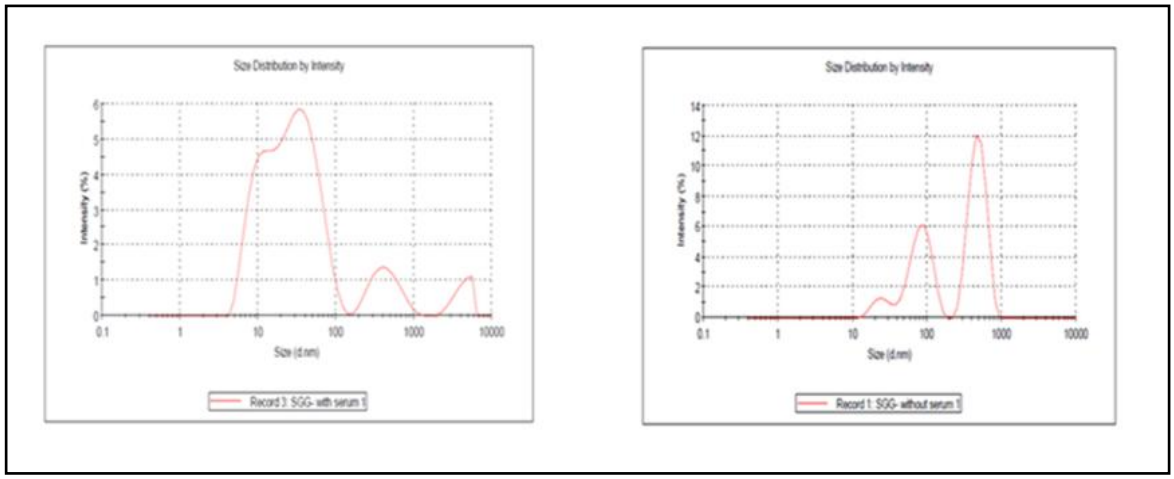

Figure 2. 4a. Particle size distribution for (a) SGG in serum containing DMEM (b) SGG in serum free DMEM

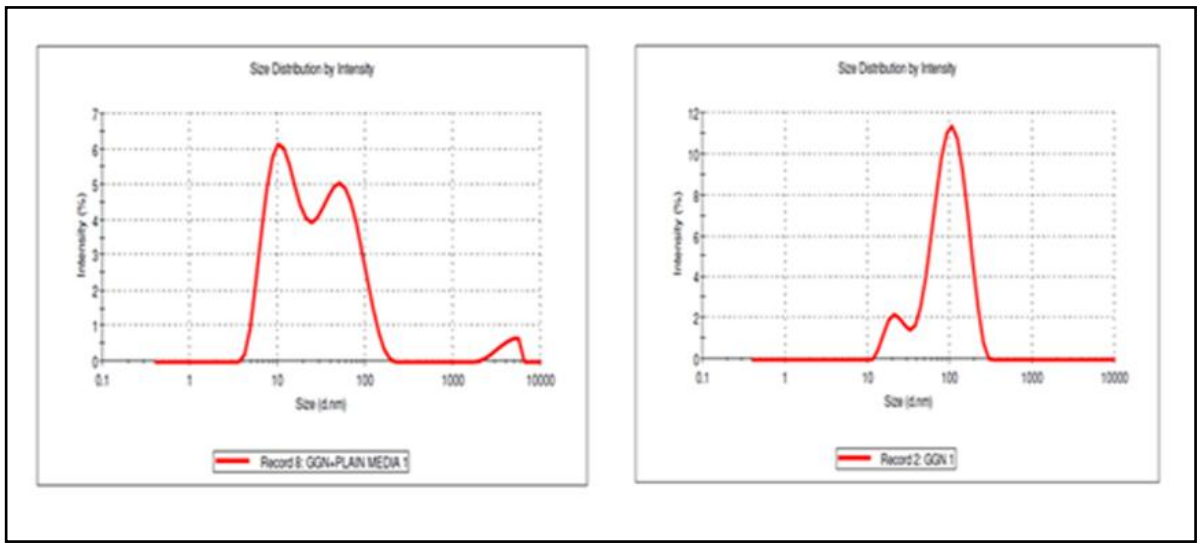

Figure 2. 4b. Particle size distribution for (a) GGN in serum free DMEM (b) GGN in serum containing DMEM

2.3.5. Morphological analysis of cells upon treatment with nanoparticles

The cytotoxicity of the SGG was verified for its biomedical application. H9c2

myoblast are spindle to stellate shaped that can be mono or multinucleated. The morphological examination of the cells treated with different doses of both SGG and Se showed normal cell morphology up to 50 nM for 24 h exposure (Figure.2.5).

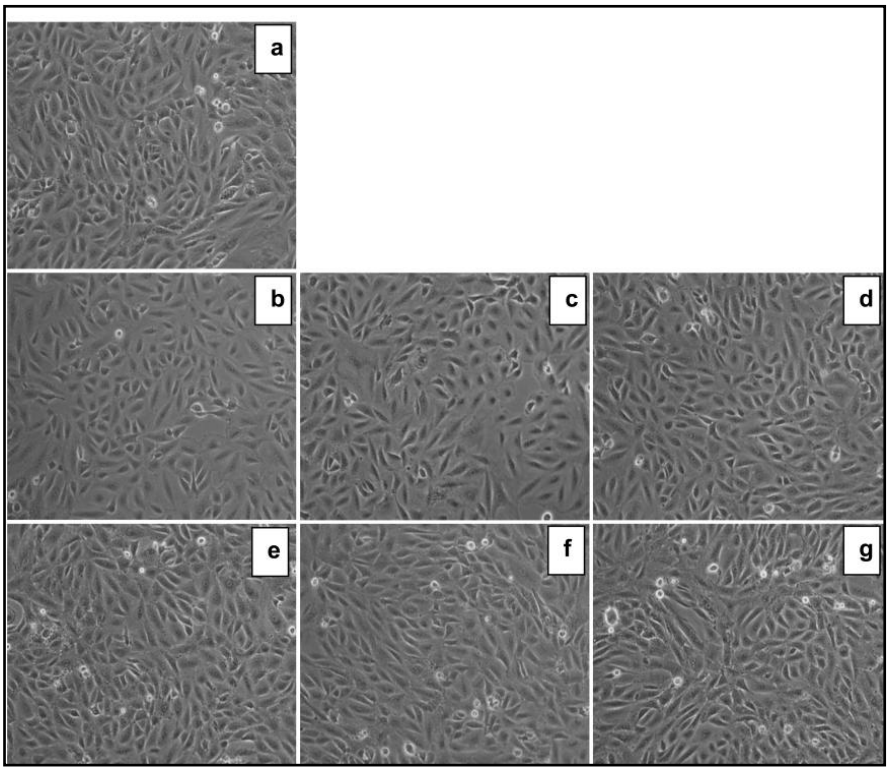

Figure 2. 5. Morphological examination of cells with nanoparticles. Images of H9c2 cells from different experimental groups under phase-contrast microscope (10x). (a) control cells; (b, c, d) cells treated with 5, 25 and 50 nM Se; (e, f, g) cells treated with 5, 25 and 50 nM SGG, respectively.

2.3.6. MTT assay

Nanomaterials are used increasingly in cosmetics, medical imaging, disease diagnosis and drug delivery. However more and more evidence indicates that reduction to nanoscale causes marked differences in properties compared with macroscale. In order to evaluate the cytotoxicity of the newly synthesized SGG and the bulk Se, H9c2 cells were treated with various concentrations (5, 25 and 50 nM) for various duration (1, 6 and 24 h). The results showed that 5 and 25 nM of Se and SGG nanoparticle for 1, 6 and 24 h of incubation were non-toxic. But higher dose (50 nM) of Se and SGG showed significant toxicity of 17.4% and 14.59% after 24 h incubation respectively (Table 2.1).

Table 2. 1. Viability of H9c2 cardiac myoblast cells treated with sodium selenite, GGN and SGG

	Concentration	% toxicity		
		1 h	6 h	24 h
Sodium selenite (nM)	5	1.73 ± 0.39	5.41 ± 0.87	11.39 ± 1.84
	25	2.38 ± 0.43	6.18 ± 0.63	13.66 ± 1.07
	50	9.05 ± 0.48	11.36 ± 0.87	14.59 ± 1.12
GGN (µg)	5	2.63 ± 0.37	6.50 ± 0.87	10.33 ± 1.72
	25	4.44 ± 0.89	7.43 ± 1.00	13.59 ± 0.99
	50	5.14 ± 0.30	9.34 ± 0.89	14.60 ± 1.47
SGG (nM)	5	1.79 ± 0.64	3.38 ± 1.03	7.21 ± 1.23
	25	2.61 ± 0.93	6.30 ± 0.80	10.31 ± 2.32
	50	10.87 ± 1.12	12.54 ± 0.67	17.40 ± 1.51

2.3.7. Uptake of SGG by H9c2 cell

To evaluate the cellular uptake of SGG and MGG we utilized autofluorescence property of GG. For this, cells were incubated with various concentrations (5, 25 and 50 nM) of SGG and MGG for 1, 6 and 24 h and counter stained with AO that stains the double and single stranded DNA of live cells which appears green in color and were subjected to fluorescence imaging by spinning disk microscope. We observed presence of fluorescence in the SGG treated cells (Figure.2.6A, 6B, 6C) whereas no fluorescent emission was observed in MGG treated cells (Figure.2.6A.b, 6B.b, 6C.c). This observation reveals the presence of SGG in cells not MGG. In addition, fluorescent data showed uptake of nanoparticle was dose and duration dependent. The maximal cellular uptake was found in 24 h exposure with high dose (Figure.2.6C).

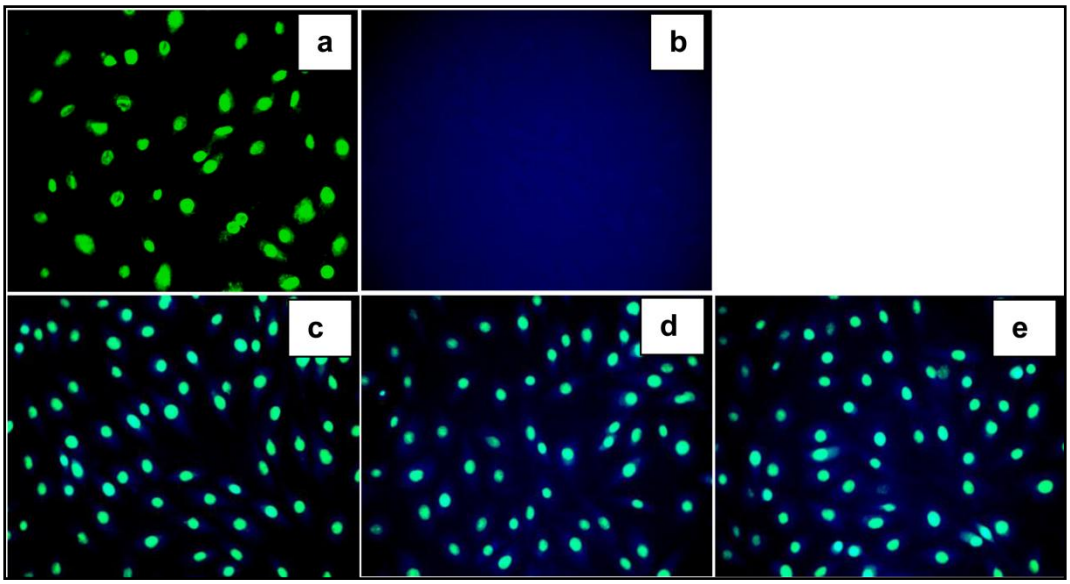

Figure 2. 6A. Uptake of nanoparticle by H9c2 cardiac myoblasts for 1h incubation with various concentrations of SGG.(a) control; (b) MGG; (c, d, e) cells treated with 5, 25 and 50 nM SGG.

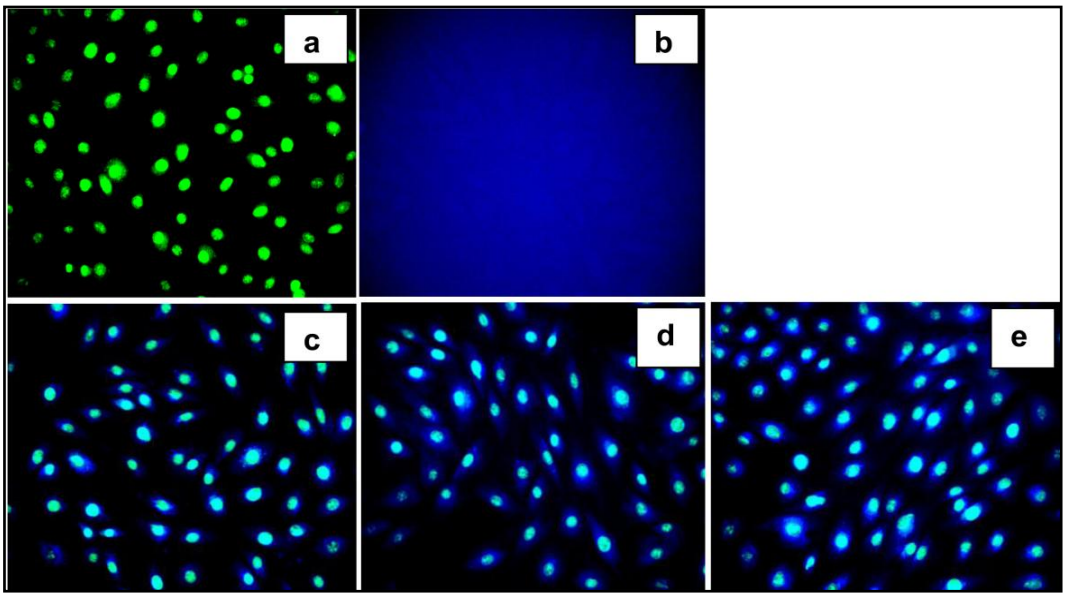

Figure 2. 6B. Uptake of nanoparticle by H9c2 cardiac myoblasts for 6 h incubation with various concentrations of SGG.(a) control; (b) MGG; (c, d, e) cells treated with 5, 25 and 50 nM SGG.

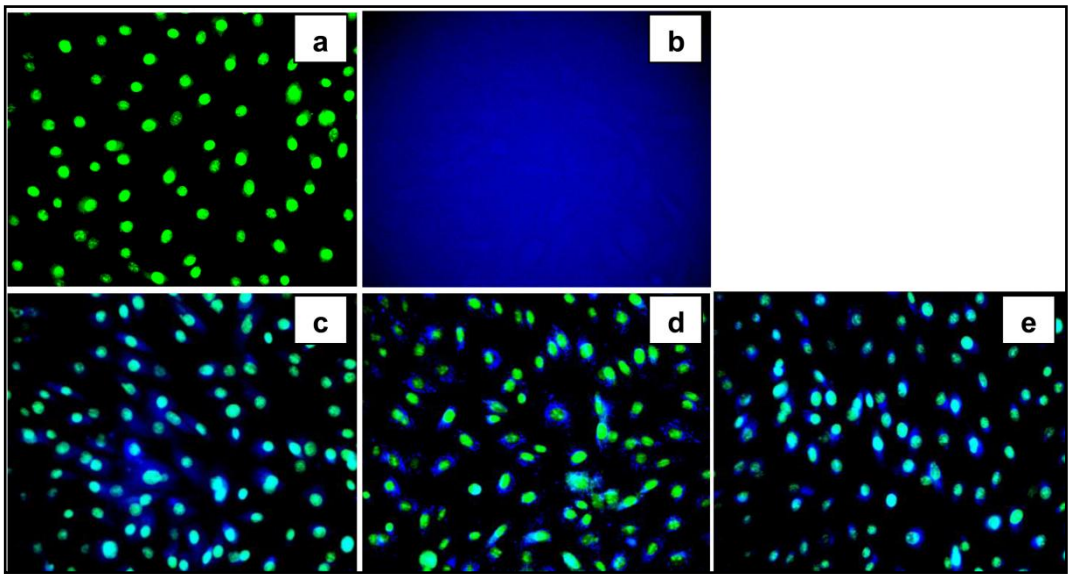

Figure 2. 6C. Uptake of nanoparticle by H9c2 cardiac myoblasts for 24 h incubation with various concentrations of SGG.(a) control; (b) MGG; (c, d, e) cells treated with 5, 25 and 50 nM SGG.

2.3.8. Differential Se uptake by H9c2 cells

We examined the cellular uptake of Se from sodium selenite and SGG in H9c2 cell lines with diaminonaphthalene reagent. For this, cells were treated with different concentrations of sodium selenite (5, 25 and 50 nM) and SGG (5, 25 and 50 nM) for 24 h. Analysis showed that 25 nM of SGG was found to have more effective uptake of Se (7.2 nM) which was found to be significantly greater than Se uptake from sodium selenite (5.2 nM). Beyond 25 nM, concentration did not show any influence on Se uptake whether in SGG or sodium selenite (Figure.2.7). The more cell permeability of nanoparticle will enable to have more drug bioavailability at target site for better therapeutic property. This also reduces the dose of drug required for recovery and reduces the adverse effect of drug.

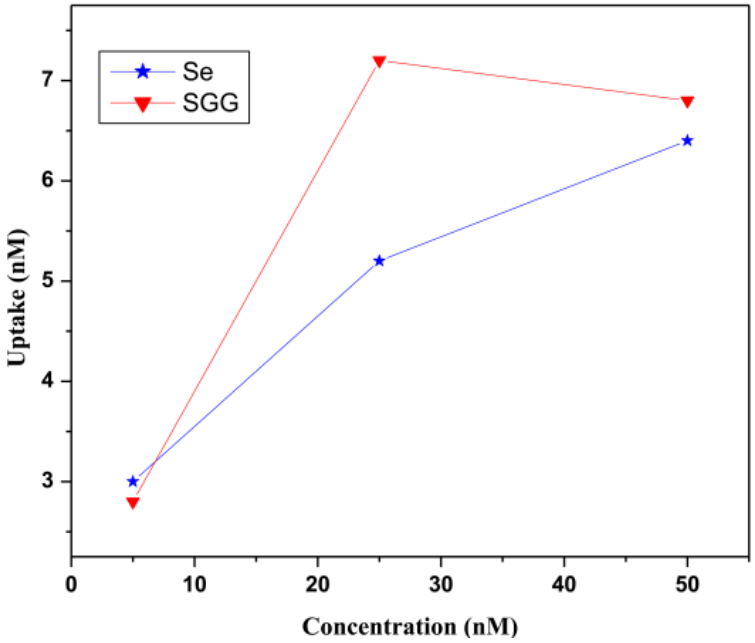

Figure 2. 7. *In vitro* cellular uptake of Se from sodium selenite and SGG. Se uptake study using diaminonaphthalene method shows that uptake of Se by cell is higher for SGG (red) than sodium selenite (blue). 25 nM of both Se and SGG showed maximum uptake of Se by cells.

2.3.9. Effects of SGG on apoptosis

In order to characterize the safety profile of the SGG we investigated whether SGG induce apoptosis in H9c2. To evaluate apoptosis inducing property of SGG, cells were stained with AO/EtBr and it was found that the exposure of H9c2 cells with different concentrations of 5, 25 and 50 nM of Se and SGG nanoparticle for 24 h did not cause apoptosis (Figure.2.8). SGG was effective to protect the cells from apoptosis at 50 nM for 24 h and this property of SGG will definitely help us to use this nanoparticle for therapeutic purpose against various disorders.

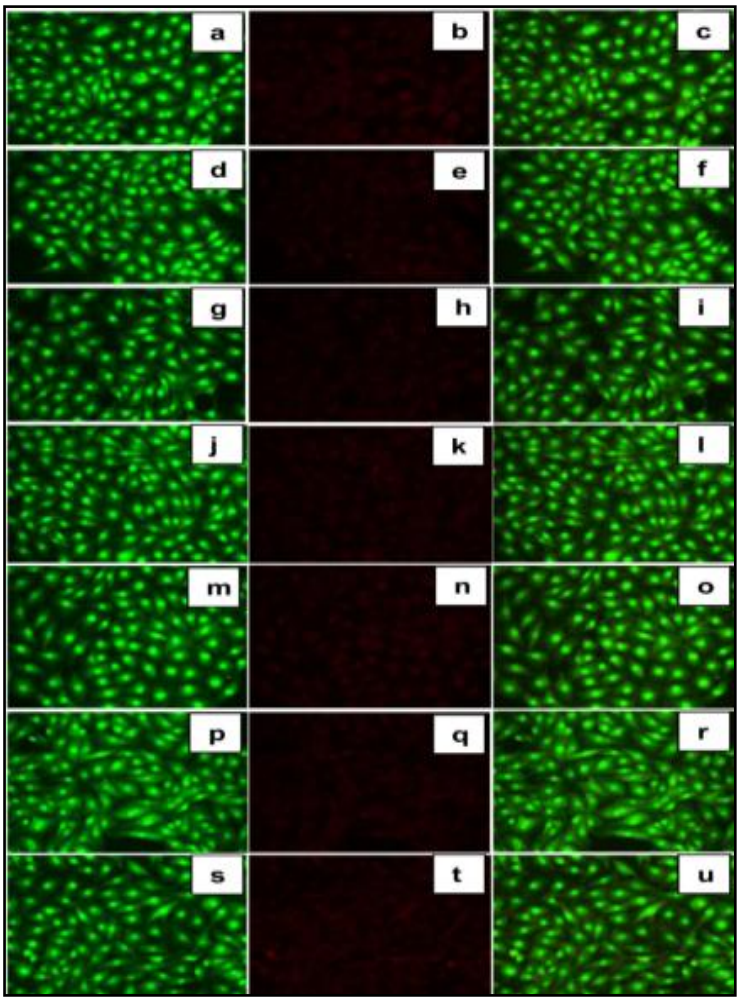

Figure 2. 8. Alteration in DNA integrity with Se and SGG. Photomicrographs of H9c2 cells under AO/EB staining to check induction of apoptosis with Se and SGG (20x); (c) merged images of control cells; (f, i ,l) merged images of cells treated with 5, 25 and 50 nM Se; (o, r, u) merged images of cells treated with 5, 25 and 50 nM SGG.

2.3.10. DNA protection assay

Oxidative DNA damage has been implicated in various degenerative diseases. Sodium selenite is reported to inhibit oxidative DNA damage caused by iron (Fe^{2+}) in the presence of H_2O_2, in a cell free system, which contained plasmid DNA, Fe^{2+} and H_2O_2 (Ramoutar and Brumaghim 2007). The effect of GGN and SGG on Fe^{2+} dependent hydroxyl radical induced DNA damage of pUC18 plasmid was studied. The treatment of supercoiled (SC) DNA with Fenton's reagent directed to the alteration of DNA to open circular form (OC). The addition of SGG nanoparticles to the reaction mixture substantially decreased the DNA strand scission and retained the SC form, thus

effectively protect DNA, in a dose dependent manner (Figure.9A). In addition we also checked whether it induce breakage or nick or ladder formation on plasmid DNA (pUC18) by agarose gel electrophoresis (Figure.9B). It did not affect plasmid DNA.

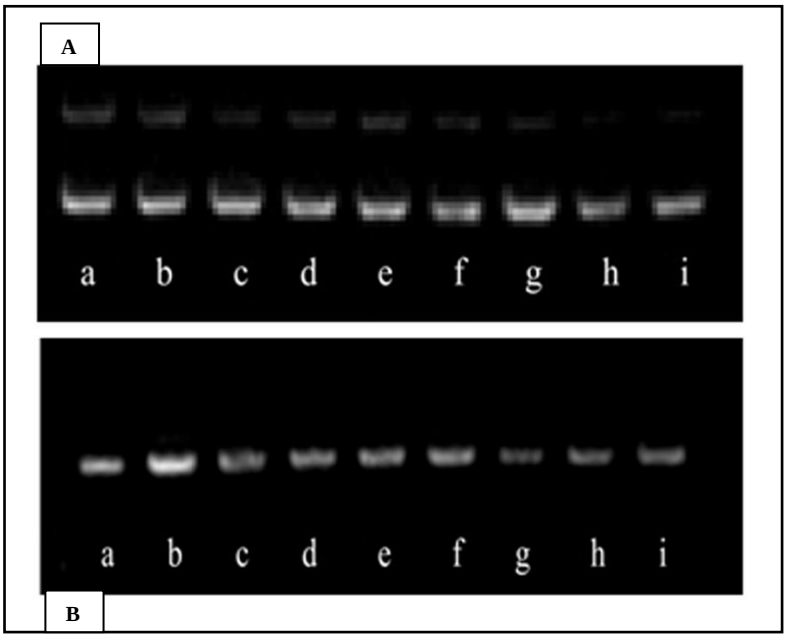

Figure 2. 9A. DNA damage protection assay with Fenton's reagent. (a) control (pUC 18 plasmid); (b) plasmid+Fenton's reagent (c) positive control (ellagic acid 50 nM) (d, e and f) 5, 25 and 50 nM Se; (g, h, i) 5, 25 and 50 nM SGG. **B.** The effect of nanoparticle on plasmid DNA (a) control (pUC 18 plasmid); (b, c) positive control (ellagic acid 5, 50 nM); (d, e, f) 5, 25 and 50 nM Se; (g, h, i) 5, 25 and 50 nM SGG.

2.3.11. Effect of SGG on ROS

Induction of oxidative stress is one of the common mechanisms of toxicity of nanoparticles (Soenen *et al* 2011). Oxidative stress occurs when generation of ROS exceed the capacity of antioxidant defense mechanism. It elicits a wide variety of physiological and cellular events including stress, inflammation, DNA damage and apoptosis. In the present study, attempts were made to evaluate ROS generation with various doses of nanoparticle to see whether they induce oxidative stress in H9c2 cells and it was found that treatment with various doses (5, 25 and 50 nM) of Se and SGG caused mild ROS generation (41%) after one hour and gradually reduced to (8%) in a span of 24 h (Figure.2.10C). It is interesting to note that the initial outburst of ROS did not cause any morphological alteration or toxicity on cells (Figure.2.10A). This temporary elevation of ROS (Figure.2.10A) may be due to over reaction of cells for self adaptation to the presence of the foreign material.

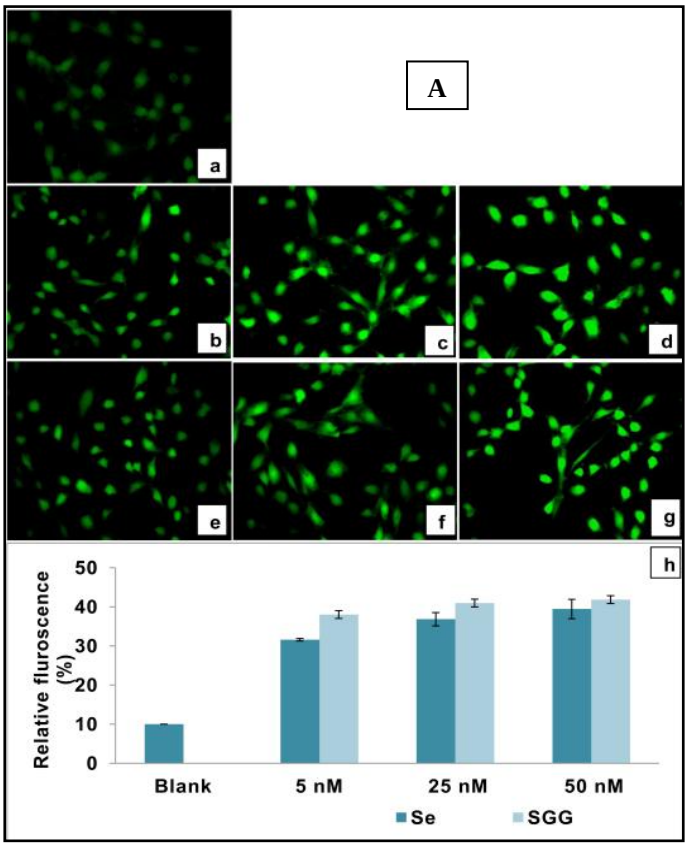
A
a
b
c
d
e
f
g
h
Relative fluroscence (%)
50
40
30
20
10
0
Blank
5 nM
25 nM
50 nM
Se
SGG

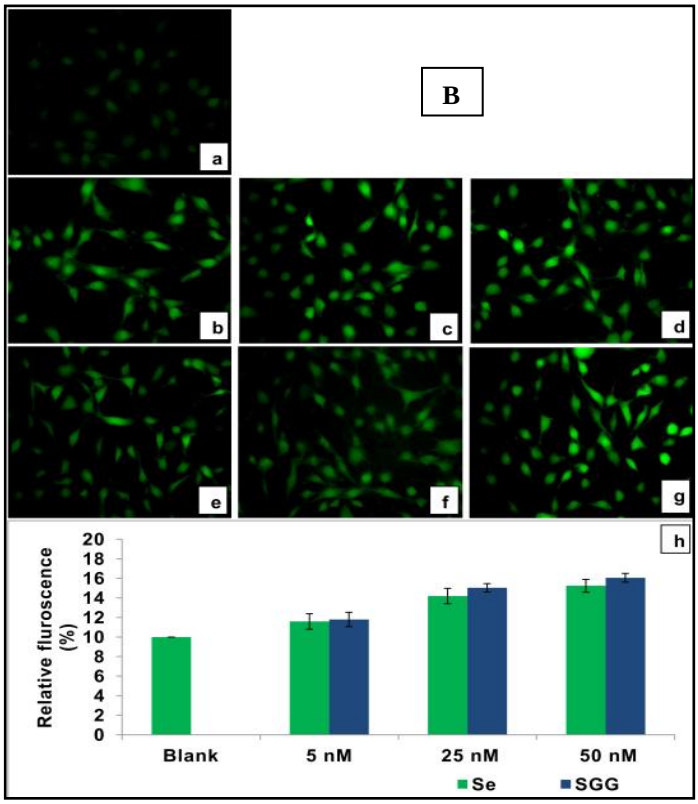
B
a
b
c
d
e
f
g
h
Relative fluroscence (%)
20
18
16
14
12
10
8
6
4
2
0
Blank
5 nM
25 nM
50 nM
Se
SGG

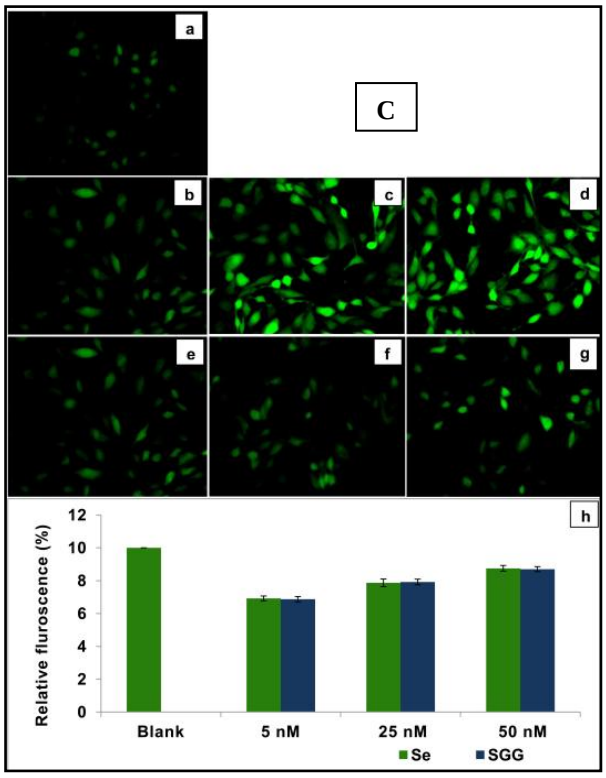

Figure 2. 10A. Evaluation of ROS with various doses of Se and SGG after 1 h. (a) control cells; (b, c, d) cells treated with 5, 25 and 50 nM Se, respectively; (e, f, g) cells treated with 5, 25 and 50 nM of SGG, respectively; (h) The fluorometric analysis supports the microscopic data. **B.** Evaluation of ROS with various doses of Se and SGG after 6 h. (a) control cells; (b, c, d) cells treated with 5, 25 and 50 nM Se, respectively; (e, f, g) cells treated with 5, 25 and 50 nM of SGG, respectively; (h) The fluorometric analysis data. **C.** Evaluation of ROS with various doses of Se and SGG after 24 h. (a) control cells; (b, c, d) cells treated with 5, 25 and 50 nM Se, respectively; (e, f, g) cells treated with 5, 25 and 50 nM of SGG, respectively; (h) The fluorometric analysis data.

2.3.12. Alteration in Δψm of mitochondria

Mitochondria are the vital organelle which play significant role in the physiology of the cells and it is the centre of target for foreign particles interaction (El-Ansary and Al-Daihan 2009). In this study we verified the effect of various concentration of SGG on mitochondria of H9c2 cells. H9c2 cells are known for the high content of mitochondria to meet its metabolic need. Intact mitochondrion is very much essential for the normal well being of cells as it control many sensitive functions related to energy metabolism. Exposure of H9c2 to Se and SGG for different time duration (1, 6 and 24 h) did not cause much alteration in Δψm, as measured with JC-1 probe with an average ratio of red:green fluorescence (Figure.2.11A, 11B). But high dose (50 nM) caused some alterations in Δψm in the case of 24 h of incubation (Figure.2.11C).

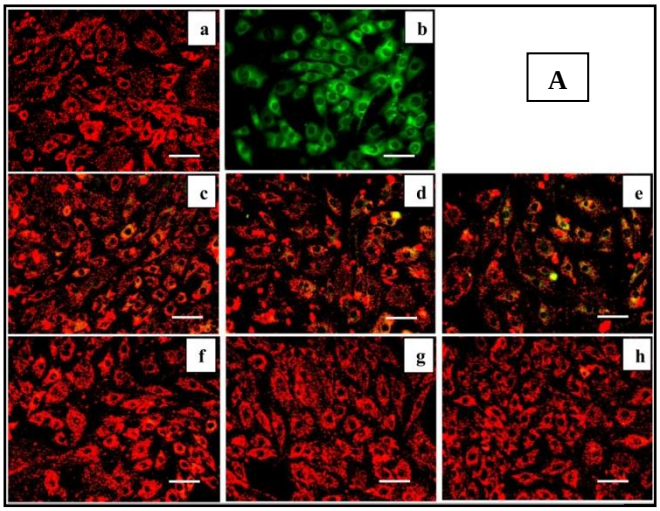
a
b
A
c
d
e
f
g
h

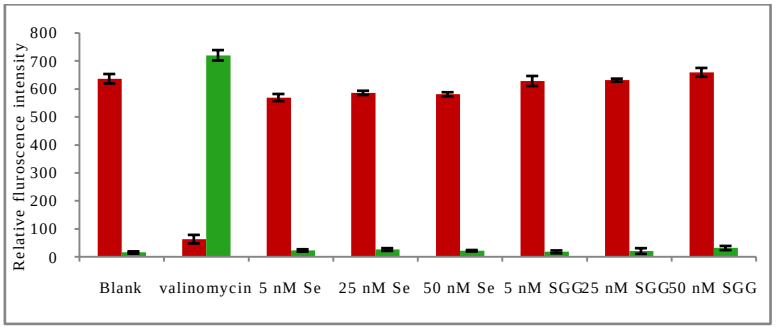
Relative fluroscence intensity
800
700
600
500
400
300
200
100
0
Blank
valinomycin
5 nM Se
25 nM Se
50 nM Se
5 nM SGG
25 nM SGG
50 nM SGG

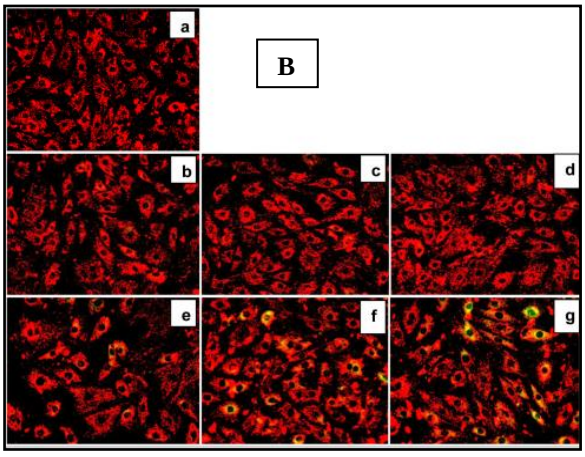
a
B
b
c
d
e
f
g

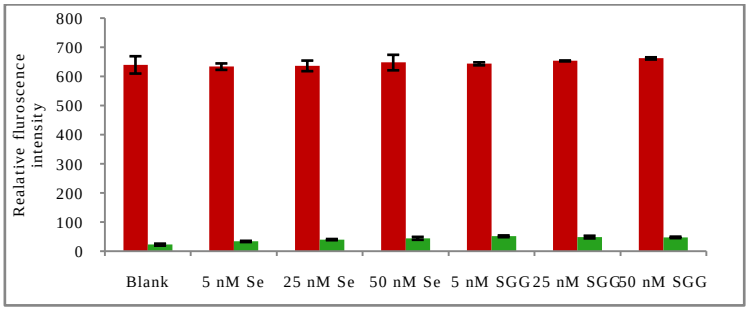
Realative fluroscence intensity
800
700
600
500
400
300
200
100
0
Blank
5 nM Se
25 nM Se
50 nM Se
5 nM SGG
25 nM SGG
50 nM SGG

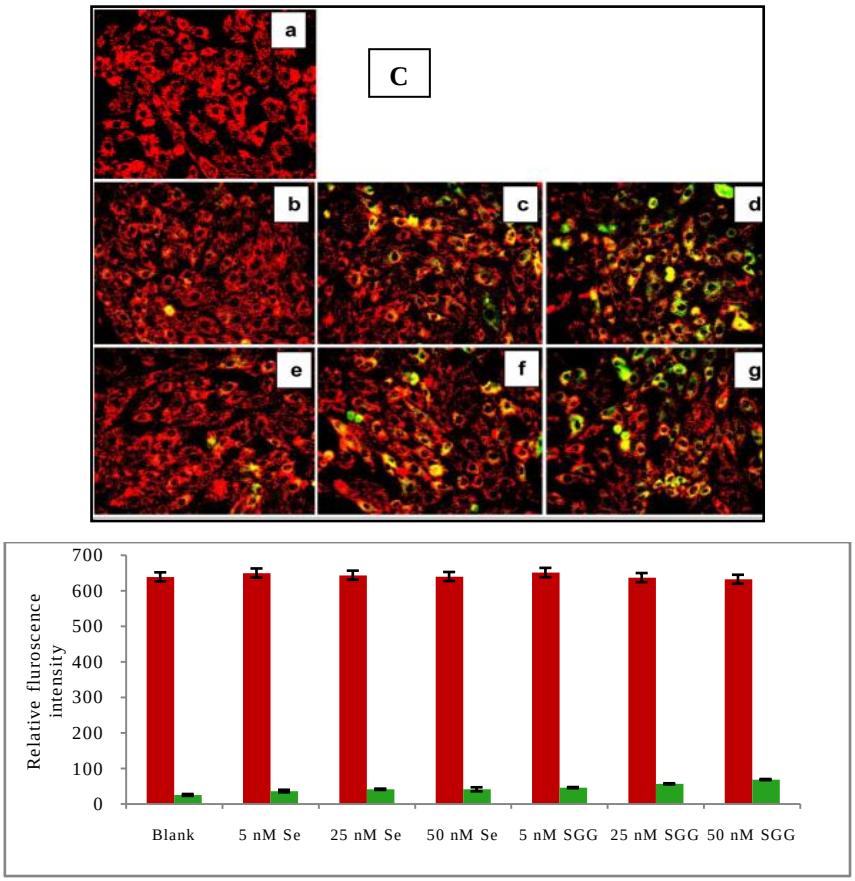

Figure 2. 11A. Mitochondrial transmembrane potential with Se and SGG for 1 h. Images of H9c2 cells stained with JC-1 for mitochondrial study (20x). (a) control cells; (b) positive control valinomycin; (c, d, e) cells treated with 5, 25 and 50 nM Se, respectively; (f, g, h) cells treated with 5, 25 and 50 nM SGG, respectively; (i) relative fluorescence also showed a similar trend. **B.** Mitochondrial transmembrane potential with Se and SGG for 6 h. (a) control cells; (b, c, d) cells treated with 5, 25 and 50 nM Se, respectively; (e, f, g) cells treated with 5, 25 and 50 nM SGG, respectively; (h) relative fluorescence also showed a similar trend.**C.** Mitochondrial transmembrane potential with Se and SGG for 24 h. (a) control cells; (b, c, d) cells treated with 5, 25 and 50 nM Se, respectively; (e, f, g) cells treated with 5, 25 and 50 nM SGG, respectively; (h) relative fluorescence also shows a similar trend.

2.3.13. Effects of SGG on cell cytoskeleton

To check the effect of cellular uptake of nanoparticles on cytoskeleton organization of cardiac myoblast, F-actin component of cytoskeleton was stained using phalloidin. Staining revealed that there was no alteration in structure with Se and SGG treated group (Figure.2.12.b-g). All the groups had an intact filamentous network structure confirming the original structure. Nanoparticles upto 50 nM were safe in holding intact the mesh like architecture of the cells even at 24 h (Figure.2.12.d, g).

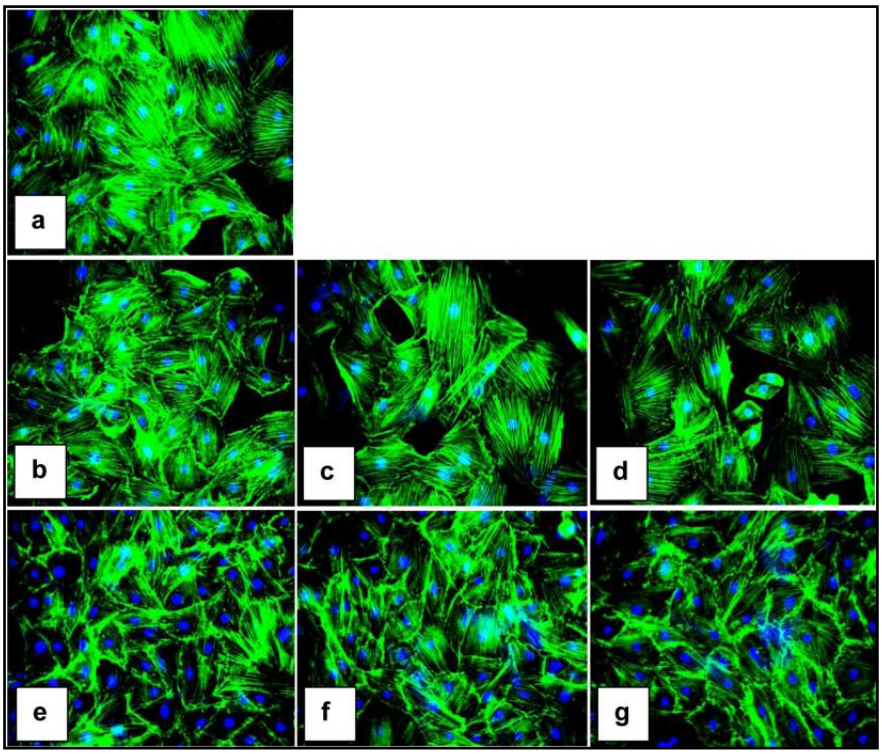

Figure 2. 12. Effect of Se and SGG on cytoskeleton of H9c2 cells. Fluorescent microscopic images of H9c2 cells stained with phalloidin (20x). (a) control cells; (b, c, d) cells treated with 5, 25 and 50 nM Se, respectively; (e, f, g) cells treated with 5, 25 and 50 nM SGG, respectively. The green colour indicates the cytoskeleton F-actin stained with phalloidin. The blue colour indicates the nucleus stained with DAPI. There were no significant alterations in cytoskeleton with any groups.

2.3.14. Total reducing power

To evaluate the antioxidant potential of Se, GGN and SGG various cell free assays like total reducing power, metal chelation and hydroxyl radical scavenging were checked. The high absorbance value of the test materials at 700 nm indicates potential reductive ability. TRP values of Se, GGN and SGG were compared with gallic acid as the standard. Reducing power (absorbance values) of Se, GGN and SGG was 0.028±0.004, 0.098±0.003 and 0.234±0.006, respectively (Table 2.2). From these the reducing power of SGG was found to be significantly higher than those of Se and GGN. In this assay, the yellow colour of the solution changed depending on the reducing power of each material. The data showed that the SGG have the significant ability to interact with free radicals to convert them to nonreactive species, thus terminating the radical chain reaction.

2.3.15. Metal chelation

Chelation of the metal ions is the main strategy to avoid ROS generation. Here,

the IC_{50} of SGG for metal chelating activity was 3.6±0.05 µg/ml which was better than the positive standard EDTA (12.72±0.68 µg/ml) indicating the potential metal chelating capacity of SGG (Table 2.2). The IC_{50} of the chelating effect of Se and GGN was 12.11 ±0.01 µg/ml and 4.1±0.1 µg/ml, respectively.

2.3.16. Hydroxyl scavenging activity

The IC_{50} of Se, GGN and SGG for hydroxyl radical scavenging activity was 63.79±1.82, 11.97±1.13, 5.68±0.285 µg/ml respectively (Table 2.2). Catechin was used as the standard with IC_{50} of 9.22±0.94 µg/ml respectively. Hydroxyl radical is an extremely reactive free radical formed in biological systems and has been implicated as a highly damaging species in free radical pathology (Li *et al* 2008). This radical has a capacity to join nucleotides in DNA and cause strand breakage that contributes to carcinogenesis, mutagenesis and cytotoxicity (Moskovitz *et al* 2002). Here also SGG showed excellent hydroxyl scavenging activity compared to other materials and the positive control. These assays evaluate the scavenging potential of particles with respect to specific reactive radicals. Evaluation of antioxidant potential of the various test material revealed SGG exhibited better antioxidant activities like high reducing power, metal chelation capacity and hydroxyl radical scavenging activity compared to GGN and Se.

Table 2. 2. Antioxidant chemical assays with Se, GGN and SGG.

	TRP	**Metal chelation IC_{50} (µg/ml)**	**Hydroxyl RSA IC_{50} (µg/ml)**
GGN	0.098±0.003	4.1±0.1	11.97±1.13
SGG	0.234±0.006	3.6±0.05	5.68±0.285
Se	0.028±0.004	12.11±0.01	63.79±1.82
GA	1.236±0.13	-	-
EDTA		12.72±0.68	
Catechin			9.22 ± 0.94

Se: Sodium Selenite; GGN: guar gum nanoparticle; SGG: selenium incorporated guar gum nanoparticle; GA: gallic acid; RSA: radical scavenging activity. Each value represents mean ± SD (n=6).

2.4. Discussion

Nanoparticle characterization is indispensable for understanding and controlling of nanoparticle synthesis and applications. In the present study, the techniques used for these were particle size analysis, TEM and XRD. This chapter deals with preparation and characterization of SGG and its interaction with H9c2 by assessing its effect on various vital parameters. For this we conducted *in vitro* experiments to evaluate its interaction with H9c2 cell lines.

Although, biochemicals may often be used for the synthesis of nanomaterials, the biogenic synthetic route is frequently applied due to its ease and simplicity and also because no hazardous and toxic residues are released in the environment (Mukherjee *et al* 2002; Mukherjee *et al* 2001). There are reports that the reduction of sodium selenite ($Na_2SeO_{3)}$ to Se nanoparticles by the biomolecules in the polysaccharide is by functional groups such as alcohol, aldehyde etc. (Husen and Siddiqi 2014). Important and challenging aspect of nanoparticle characterization is measurement under conditions that resemble *in vitro* or *in vivo* environment. It was shown in several studies (Ji *et al* 2010; Maiorano *et al* 2010; Metin *et al* 2011; Fatisson *et al* 2012; Allouni *et al* 2009; Lordan *et al* 2012; Safi *et al* 2011; Zhang *et al* 2009; Santander-Ortega *et al* 2007) that stability of nanoparticles in different culture media can be severely reduced depending on ionic and protein composition consequently affecting nanoparticles characteristic and functionality in *in vitro* and *in vivo* applications. Literature also demonstrated that characterization of nanoparticles in relevant media is necessary for evaluation of toxicity (Fatisson *et al* 2012). The stability of nanoparticles is a complex combination of nanoparticles surface properties, media compositions and nanoparticle concentrations, so it is essential to characterize the nanoparticles in physiologically relevant media which is crucial for understanding of their interaction with biological systems. Pavlin and Bergar (2012) reported about nanoparticles functionalized with polyacrilic acid are relatively very stable in different culture media, where level of aggregation depends on medium composition. Our study also the shows that the SGG particles showed more stability in serum medium than medium without serum. Compared with GGN in serum and serum free medium SGG particles have more stability. On the other hand there are several reports (Ji *et al* 2010; Allouni *et al* 2009; Zhang *et al* 2009) identifying the increased stability of nanoparticles

(TiO2) by the addition of the serum in the medium with the stabilization mechanism being again opsonization of the nanoparticle surface with proteins and peptides, which form stabilizing protein corona. This was similar to our results.

An important factor that usually contributes to nanomaterial based drug cytotoxicity is cellular uptake (Sohaebuddin *et al* 2010). GG is a non-ionic polysaccharide that is abundantly present in nature and has many properties desirable for drug delivery applications. Due to the presence of various functional groups on molecular chains polysaccharides can be easily modified chemically and biochemically, resulting in different kind of derivatives (Liu *et al* 2008). As they are highly stable, safe, non-toxic, hydrophilic, biodegradable and the cost of processing is very low, they are used as ideal material for drug delivery. Among polysaccharides GG is a potential candidate for drug delivery application due to its drug release retarding property and susceptibility to microbial degradation in the large intestine (Bayliss and Houston 1986). It is established fact that nanoparticles can efficiently intrude in cell by exploiting endocytosis machinery. But only specialised cells such as macrophages are capable of phagocytosis. On the other hand almost all cells internalize nanoparticles by pinocytosis. There are many factors like physicochemical properties like size, shape, surface charge and surface chemistry that was essential for modulating cellular uptake efficiency.

Se is a trace element with wide commercial applications, due to its special chemical and physical properties. Se nanoparticles attracted more attention due to their high bioavailability and antioxidant activities, low toxicity and novel therapeutic property (Li *et al* 2011; Yang *et al* 2012; Wu *et al* 2012; Zhang *et al* 2013). There are reports to suggest that nanoencapsulation of Se in polysaccharide like chitosan increase cellular Se level (Zhang *et al* 2011). Se in encapsulated stage desensitizes the cells to Se compounds and decrease damage to cells in contrast to application of native Se to the cells (Zhang *et al* 2011). This explains why more Se in GG encapsulated form is taken up by the cells. Another reason for the minimum toxicity with SGG is due to the fact that SGG are not metabolically available for the induction of any type of cell damage.

Induction of apoptosis is considered an important cellular event that can account for the cancer preventive effects of Se compounds. Apoptosis induced by supranutritional doses of seleno compounds are described in various types of neoplastic cells, including

prostate, colon and liver cancer, leukemia and lymphoma. Se in encapsulated form at nanoparticle size upregulates selenoenzyme (Sanmartı´n *et al* 2012). DNA protection property of SGG will have therapeutic potential as in some metabolic disorders like diabetes, hydroxyl radical induced DNA damages are very common. From these results it is again clear that SGG prepared by nanoprecipitation is safe as well as it has therapeutic potential to use for biomedical research applications. There are reports that Se nanoparticles prevented DNA damage when cells were exposed to UV-light (Prasad *et al* 2013). In this study SGG inhibits oxidative DNA damage caused by iron (Fe^{2+}) which contained plasmid DNA. A mild increase in oxidative stress seen in cells act as a cell signaling mechanism required to trigger several responses to the foreign particle (Ruiz-Meana *et al* 2010). These results again confirm the suitability of SGG for biomedical application without any adverse effect. Normal cytoskeleton is essential to keep the morphology and physical structure of the body intact. One possible sign of cellular stress induced by uptake of nanosized materials is alterations to the cytoskeleton network (Soenen *et al* 2011).

There is not even a single report on SGG nanoparticle and investigation on interaction with cell and this is the first report in this regard. But there are reports of preparation of Se nanoparticles with hyperbranched polysaccharide in water (Zhang *et al* 2010). However, it was not prepared for any biological applications. In addition Se nanoparticles with spirulina polysaccharide had been prepared by some groups (Yang *et al* 2012) for evaluation of its anticancer activities and uptake of Se nanoparticle by cells. They reported enhanced cytotoxicity and uptake by melanocytes. In the case of GG, there are reports on silver nanoparticle preparation using polyacrylamide/guar gum graft copolymers for some chemical purpose (Abdel-Halim *et al* 2011). Green synthesis had also been exploited for preparation of biopolymer (GG) silver nanoparticle composite for application in optical sensor for ammonia detection (Pandey *et al* 2012). Overall results clearly reveal SGG prepared in this study exhibit potent therapeutic potential with respect to oxidative stress, apoptosis, DNA protection, $\Delta\Psi m$ and cytoskeleton. Moreover the cytotoxicity was minimum with SGG which is a great advantage of this particle for biomedical applications.

To prevent the detrimental effects of free radicals in the human body, antioxidants gain increasing interest. In addition, there is a preference for antioxidants from natural sources due to low adverse effects and high tolerance to the human body (Abdalla and Rooze 1999). The methods for evaluation of the antioxidant status and oxidative damage are many and varied. The simplest ones are purely chemical *in vitro* reactions or tests in cell cultures. They can yield useful information about mechanisms of action; currently, there is no single antioxidant assay for quality grading because of the lack of standard quantification methods. Keeping these facts in mind, we checked the antioxidant potentials of Se, GGN and SGG employing various cell free assays like total reducing power, metal chelation and hydroxyl radical scavenging. These assays evaluate the scavenging potential of particles with respect to specific reactive radicals. Evaluation of the antioxidant potential of the various test materials revealed that SGG exhibited better antioxidant activities like high reducing power, metal chelation capacity and hydroxyl radical scavenging activity compared to GGN and Se.

Redox active metals catalyse oxygen radical formation thus causes tissue injury during I/R sequence (Spencer *et al* 1998). This concept is based on the basic chemistry of oxygen radicals in which trace amounts of transition metals are required to catalyst the formation ROS such as the OH^{-}. Transition metals such as Fe^{2+} and Cu^{+} are present in the myocardium and can act as catalyst for the formation of oxygen free radicals during reperfusion after myocardial ischemia. There are reports to suggest that transition metal chelators such as desferrioxamine can reduce the production of such radicals and may thereby attenuate postischemic myocardial dysfunction (Spencer *et al* 1998). Studies investigating the role of transition metals as a catalyst for the formation of oxygen free radicals during I/R primarily focussed on iron; Fe^{2+} chelators results in improvement in myocardial functional and metabolic recovery after I/R, presumably by preventing oxygen free radical generation (Bolli *et al* 1990; Farber *et al* 1988; Maruyama *et al* 1991; Bolli *et al* 1987). Hydroxyl radical is an extremely reactive free radical formed in biological systems and has been implicated as a highly damaging species in free radical pathology (Li *et al* 2008). This radical has a capacity to join nucleotides in DNA and cause strand breakage that contributes to carcinogenesis, mutagenesis and cytotoxicity (Moskovitz *et al* 2002). Gao *et al* (2002) reported the antioxidant properties of hollow

spherical nanoparticles of Se. The size of nanoparticles plays an important role in their biological activity as 5-200 nm nano-Se can directly scavenge free radicals *in vitro* in a size dependent fashion (Peng *et al* 2007). Barnaby *et al* (2011) reported Se nanoparticles which is prepared using gallic acid exhibit good antioxidant activity. There are reports regarding the antioxidant property of GG (Iqbal *et al* 2013). Based on these report we checked the antioxidant properties of Se, GGN and SGG and the results showed that SGG has better activity compared to native Se and GGN to scavenge free radicals.

Conclusion

The present study demonstrated that SGG can be successfully prepared under mild conditions *via*, nanoprecipitation method. Physicochemical properties, such as particle size, TEM, XRD data confirmed the nanoscale structure of the prepared material and proper incorporation of SGG. Elaborate investigations on the interaction of nanoparticle on biological system had been conducted on H9c2 and confirmed the safety of nanoparticle on biological system (H9c2). On the basis of these results SGG was found to be an ideal nanomaterial for further research with promising therapeutic properties especially for cardiac problems.

References

1. Abdalla AE, Rooze JP (1999) Effect of plant extracts on the oxidative stability of sunflower oil and emulsion. *Food Chem* 64: 323-329.
2. Abdel-Halim ES, El-Rafie MH, Al-Deyab SS (2011) Polyacrylamide/guar gum graft copolymer for preparation of silver nanoparticles. *Carbohyd Polym* 85: 692-697.
3. Allouni ZE, Cimpan MR, Hol PJ, Skodvin T, Gjerdet NR (2009) Agglomeration and sedimentation of TiO_2 nanoparticles in cell culture medium. *Colloids Surf B* 68: 83-87.
4. Barnaby S, Sarker N, Dowdell A, Banerjee I (2011) The spontaneous formation of selenium nanoparticles on gallic acid assemblies and their antioxidant properties. *The Fordham Undergraduate Research Journal* 1: 41-46.
5. Bayliss CE, Houston AP (1986) Degradation of guar gum by faecal bacteria. *Appl Environ Microbiol* 48: 626-632.
6. Bolli R, Patel BS, Zhu WX, O'Neill PG, Hartley CJ, Charlat ML, Roberts R (1987) The iron chelator desferrioxamine attenuates postischemic ventricular dysfunction. *Am J Physiol* 253: 1372-1380.
7. Bolli R, Patel BS, Jeroudi MO, Li XY, Triana JF, Lai EK, McCay PB (1990) Iron-mediated radical reactions upon reperfusion contribute to myocardial "stunning". *Am J Physiol* 259: H1901-H1911.
8. El-Ansary A, Al-Daihan S (2009) On the toxicity of therapeutically used nanoparticles: An overview. *J Toxicol* doi: 10.1155/2009/754810.
9. Farber NE, Vercelotti GM, Jacob HS, Pieper GM, Gross GJ (1988) Evidence for a role of iron-catalyzed oxidants in functional and metabolic stunning in the canine heart. *Circ Res* 63: 351-360.
10. Fatisson J, Quevedo IR, Wilkinson KJ, Tufenkji N (2012) Physicochemical characterization of engineered nanoparticles under physiological conditions: Effect of culture media components and particle surface coating. *Colloids Surf B* 91: 198-204.
11. Gao X, Zhang J, L Zhang (2002) Hollow sphere selenium nanoparticles: their in-vitro anti hydroxyl radical effect. *Adv Mater* 14: 290-293.

12. Gil GO, Pr´evost S, Losik M, Hermes F, Schlaad H, Hellweg T (2009) Polypeptide hybrid copolymers as selective micellar nanocarriers in nonaqueous media. *Colloid Polym Sci* 287: 1295-1304.
13. Halliwell B, Gutteridge JM, Aruoma OI (1987) The deoxyribose method: a simple "test-tube" assay for determination of rate constants for reactions of hydroxyl radicals. *Anal Biochem* 165: 215-219.
14. Husen A and Siddiqi KS (2014) Plants and microbes assisted selenium nanoparticles: characterization and application. *J Nanobiotechnology* 12: 28 doi;10 1186/s12951-014-0028-6.
15. Iqbal DN, Hussain EA, Naz N (2013) Synthesis and characterization of guar gum derivatives with antioxidant moieties. *Int J Pharm Bio Sci* 4: 305-316.
16. Ji Z, Jin X, George S, Xia T, Meng H, Wang X, Suarez E, Zhang H, Hoek EMV, Godwin H, Nel AE, Zink JI (2010) Dispersion and stability optimization of TiO_2 nanoparticles in cell culture media. *Environ Sci Technol* 44: 7309-7314.
17. Kim KS, Khang G, Lee D (2011) Application of nanomedicine in cardiovascular diseases and stroke. *Curr Pharm Des* 17: 1825-1833.
18. Kreuter J (1994) Nanoparticles In: colloidal drug delivery systems, Marcel Dekker, New York, vol 66, pp 219-342.
19. Lee D, Erigala VR, Dasari M, Yu J, Dickson RM, Murthy N (2008) Detection of hydrogen peroxide with chemiluminescent micelles. *Int J Nanomedicine* 3: 471-476.
20. Lee D, Khaja S, Velasquez-Castano JC, Dasari M, Sun C, Petros J, Taylor WR, Murthy N (2007) In vivo imaging of hydrogen peroxide with chemiluminescent nanoparticles. *Nat Mater* 6: 765-769.
21. Li B, Lu F, Wei X, Zhao R (2008) Fucoidan: Structure and bioactivity. *Molecules* 13: 1671-1695.
22. Li Y, Li X, Wong YS, Chen T, Zhang H, Liu C, Zheng W (2011) The reversal of cisplatin induced nephrotoxicity by selenium nanoparticles functionalized with 11-mercapto-1-undecanol by inhibition of ROS mediated apoptosis. *Biomaterials* 32: 9068-9076.
23. Liu Z, Jiao Y, Wang Y, Zhou C, Zhang Z (2008) Polysaccharides-based

nanoparticles as drug delivery systems. *Adv Drug Deliver Rev* 60: 1650-1662.

24. Lordan S, Higginbotham CL (2012) Effect of serum concentration on the cytotoxicity of clay particles. *Cell Biol Int* 36: 57-61.
25. Maiorano G, Sabella S, Sorce B, Brunetti V, Malvindi MA, Cingolani R, Pompa PP (2010) Effects of cell culture media on the dynamic formation of protein−nanoparticle complexes and influence on the cellular response. *ACS Nano* 4: 7481-7491.
26. Maruyama M, Pieper GM, Kalyanaraman B, Hallaway PE, Hedlund BE, Gross GJ (1991) Effect of hydroxyethyl starch conjugated deferoxamine on myocardial functional recovery following coronary occlusion and reperfusion in dogs. *J Cardiovasc Pharmacol* 17: 166-175.
27. Metin CO, Lake LW, Miranda CR, Nguyen QP (2011) Stability of aqueous silica nanoparticle dispersions. *J Nanopart Res* 13: 839-850.
28. Moskovitz J, Yim KA, Choke PB (2002) Free radicals and disease. *Arch Biochem Biophys* 397: 354-359.
29. Mukherjee P, Ahmad A, Mandal D, Senapati S, Sainkar SR, Khan MI, Ramani R, Parischa R, Ajayakumar PV, Alam M, Sastry M, Kumar R (2001) Bioreduction of $AuCl_4$−ions by the fungus, Verticillium sp. and surface trapping of the gold nanoparticles formed. *Angew Chem Int Edit* 40: 3585-3588.
30. Mukherjee P, Senapati S, Mandal D, Ahmad A, Khan MI, Kumar R, Sastry M (2002) Extracellular synthesis of gold nanoparticles by the fungus *Fusarium oxysporum*. *Chembiochem* 3: 461-463.
31. Oyaizu M (1986) Studies on products of browning reactions: antioxidative activities of browning products of browning reaction prepared from glucosamine. *Jpn J Nutr* 44: 307-315.
32. Pandey S, Goswami GK, Nanda KK (2012) Green synthesis of biopolymer silver nanoparticle nanocomposite: an optical sensor for ammonia detection. *Int J of Biol Macromol* 51: 583-589.
33. Pavlin M, Bregar VB (2012) Stability of nanoparticle suspensions in different biologically relevant media. *Dig J Nanomater Bios* 7: 1389-1400.
34. Peng D, Zhang J, Liu Q, Taylor EW (2007) Size effect of elemental selenium

nanoparticles (Nano-Se) at supranutritional levels on selenium accumulation and glutathione S-transferase activity. *J Inorg Biochem* 101: 1457-1463.

35. Prasad KS, Patel H, Patel T, Patel K, Selvaraj K (2013) Biosynthesis of Se nanoparticles and its effect on UV-induced DNA damage. *Colloids and Surf B Biointerfaces* 103: 261-266
36. Ramoutar RR, Brumaghim JL (2007) Effects of inorganic selenium compounds on oxidative DNA damage. *J Inorg Biochem* 101: 1028-1035.
37. Rani MP, Venkatesan J, Raj SB, Sasidharan IS, Padma Kumari Amma KP (2010) Antioxidant and cytotoxic potential of acetone and methanolic extracts of fresh and dry barks of *Cinnamomum zeylanicum verum*: in vitro study. *J Cell Tissue Res* 10: 2131-2138.
38. Ruiz-Meana M, Fernandez-Sanz C, Garcia-Dorado D (2010) The SR–mitochondria interaction: a new player in cardiac pathophysiology. *Cardiovasc Res* 88: 30-39.
39. Safi M, Courtois J, Seigneuret M, Conjeaud H, Berret JF (2011) The effects of aggregation and protein corona on the cellular internalization of iron oxide nanoparticles *Biomaterials* 32: 9353-9363.
40. Sanmartı´n C, Plano D, Sharma AK, Palop JA (2012) Selenium compounds, apoptosis and other types of cell death: an overview for cancer therapy. *Int J Mol Sci* 13: 9649-9672.
41. Santander-Ortega MJ, Csaba N, Alonso MJ, Ortega-Vinuesa JL, Bastos-Gonzalez D (2007) Stability and physicochemical characteristics of PLGA, PLGA:poloxamer and PLGA: poloxamine blend nanoparticles: a comparative study. *Colloids Surface A* 296: 132-140.
42. Soenen SJ, Gil PR, Montenegro JM, Parak WGJ, Smedt SCD, Braeckman K (2011) Cellular toxicity of inorganic nanoparticles: common aspects and guidelines for improved nanotoxicity evaluation. *Nano Today* 6: 446-465.
43. Sohaebuddin SK, Thevenot PT, Baker D, Eaton JW, Tang L (2010) Nanomaterial cytotoxicity is composition, size, and cell type dependent. *Part Fibre Toxicol* 7: 1-17.
44. Sokal RR, Rohlf FJ, In the principles and practice of statistics in biological research, Dover Publications, New York, 2nd edn, 2009, ch. 8, pp. 160–184.

45. Soumya RS, Ghosh SK, Abraham ET (2010) Preparation and characterization of guar gum nanoparticles. *Int J of Biol Macromol* 46: 267-269.
46. Spencer KT, Lindower PD, Buettner GR, Kerber RE (1998) Transition metal chelators reduce directly measured myocardial free radical production during reperfusion. *J Cardiovasc Pharmacol* 32: 343-348.
47. Wilkie JB (1970) Improvement in the 2,3-diaminonaphthalene reagent for microfluorescent determination of selenium in biological materials. *J Agric Food Chem* 18: 944-945.
48. Williams DB, Carter CB (2009) Transmission Electron Microscopy: A Textbook for Materials Science, NY: Springer; 2 nd edn, New York, vol 3.
49. Wu H, Li X, Liu W, Chen T, Li Y, Zheng W, Man CWY, Wong MK, Wong KH (2012) Surface decoration of selenium nanoparticles by mushroom polysaccharides–protein complexes to achieve enhanced cellular uptake and antiproliferative activity. *J Mater Chem* 22: 9602-9610.
50. Yang F, Tang Q, Zhong X, Bai Y, Chen T, Zhang Y, Li Y, Zheng W (2012) Surface decoration by Spirulina polysaccharide enhances the cellular uptake and anticancer efficacy of selenium nanoparticles. *Int J Nanomedicine* 7: 835-844.
51. Zhang S, Luo Y, Zeng H, Wang Q, Tian F, Song J, Cheng WH (2011) Encapsulation of selenium in chitosan nanoparticles improves selenium availability and protects cells from selenium-induced DNA damage response. *J Nutr Biochem* 22: 1137-1142.
52. Zhang Y, Chen Y, Westerhoff P, Crittenden J (2009) Impact of natural organic matter and divalent cations on the stability of aqueous nanoparticles. *Water Res* 43: 4249-4257.
53. Zhang Y, Li X, Huang Z, Zheng W, Fan C, Chen T (2013) Enhancement of cell permeabilization apoptosis-inducing activity of selenium nanoparticles by ATP surface decoration. *Nanomedicine* 9: 74-84.
54. Zhang Y, Wang J, Zhang L (2010) Creation of highly stable selenium nanoparticles capped with hyperbranched polysaccharide in water. *Langmuir* 26: 17617-17623.

Chapter 3

Beneficial properties of selenium incorporated guar gum nanoparticles against I/R induced alteration in innate antioxidant status and calcium homeostasis in H9c2 cardiomyoblast

3.1. Introduction

Many research have shown the role of antioxidants for the treatment and prevention of disease because of the ability of same to ameliorate oxidative damage caused by ROS (Valko *et al* 2006; Seifried *et al* 2007). Antioxidants like polyphenols, sulfur and Se containing compounds, enzymatic antioxidants such as SOD and GPx, and micronutrients such as vitamins C and E have been extensively investigated and numerous studies have demonstrated their antioxidant properties (Valko *et al* 2006; Rice-Evans *et al* 1997; Ramoutar and Brumaghim 2007a; Ramoutar and Brumaghim 2007b; Perron *et al* 2008; Battin *et al* 2006; Battin *et al* 2008; Mates *et al* 1999; Burton and Traber 1990; Padayatty *et al* 2003). I/R cycle generates ROS which trigger lipid peroxidation, protein oxidation, enzyme inactivation, as well as impair physiological functions like blocking of ion channels, restricting glycolysis, promoting mitochondrial calcium release etc. (Depre and Taegtmeyer 2000; Szabados *et al* 1999; Halmosi *et al* 2001; Halmosi *et al* 2002). Innate antioxidant enzymes, such as GPx and SOD are the specific oxygen free radical scavengers and can protect the cell against ROS induced damage. The protective effects of Se compounds against disease are mainly due to radical scavenging and enzymatic decomposition of oxygen metabolites (Mugesh and Singh 2000). Se nanoparticles have gained more attention in recent times due to their high antioxidant activities and low toxicity (Wang *et al* 2007; Zhang *et al* 2008). In addition, Se nanoparticles have excellent bioavailability and high biological activity (Tanaka *et al* 2000). It is interesting to know that nano-Se has a 7-fold lower acute toxicity than sodium selenite in mice (Zhang *et al* 2001). Se has an important role in preventing CVD through the ability of GPx to combat the oxidative modification of lipids and to reduce aggregation of platelets (Neve 1996). Depletion of Se causes extensive damage to many tissues including myocardium (Burk 1989). In this regard, there were some studies on Se deficiency (Tonfektsian *et al* 2000) but little is known about the effect of Se, particularly with respect to cardiac cells and heart diseases.

In previous chapter we had seen the safety profile and interaction of Se and SGG

with cardiac myoblast. The present chapter deals with the comparative beneficial effect of Se, GGN and SGG against ischemia induced alteration in innate antioxidant status and Calciumhomeostasis in ischemia and I/R.

3.2. Experimental methods

3.2.1. Materials

Sodium chloride (NaCl), potassium chloride (KCl), magnesium sulphate ($MgSO_4$), calcium chloride ($CaCl_2$), sodium lactate, ferric chloride ($FeCl_3$), hydrogen peroxide (H_2O_2), 4-(2-hydroxyethyl)-1-piperazineethanesulfonic acid (HEPES), MTT, DCFH-DA were purchased from Sigma Aldrich (St. Louis, USA). All cell based assay kits used were from Cayman Chemicals, USA. All other chemicals and solvents used were of analytical grade.

3.2.2. Induction of ischemia in H9c2 cardiomyoblast

For this cells (H9c2) were seeded in 24 well plates supplemented with 10% v/v FBS, DMEM and the medium was changed every 48 h. The *in vitro* model of ischemia/reoxygenation (I/R) employed in the present study was similar to that described by Koyama *et al* (1991). For this, H9c2 cardiac myoblasts were maintained initially with normal DMEM medium equilibrated with a gas mixture of 95% O_2 and 5% CO_2 and the pH was adjusted to 7.4 at 37 °C (control) and then confluent cardiomyoblast in 24-well plates were exposed to hypoxia with simulated ischemia buffer (98.5 mM NaCl,10 mM KCl, 1.2 mM $MgSO_4$, 1.0 mM $CaCl_2$, 20 mM HEPES, 40 mM sodium lactate, pH 6.8, 37 °C) in ischemic chamber (New Brunswick Eppendrof Galaxy 48 R, USA) with 94.9% N_2 and 5% CO_2 for half an hour and then reoxygenated for 1 h with DMEM medium 95% O_2 and 5% CO_2 at 37 °C (DMEM medium) along with test materials (Se, GGN and SGG).

Experimental groups

Group I: H9c2 were incubated in normal medium supplemented with 10% FBS and 5% CO_2 during the entire experimental period.

Group II: Cells were incubated with ischemic buffer for 30 min (ischemia).

Group III: Cells were incubated with ischemic buffer for 30 min (ischemia) followed by reperfusion with normal medium for 1 h.

Group IV: After ischemia, cardiomyoblasts were incubated with nascent sodium selenite (5 nM) for 1 h.

Group V: After ischemia, cardiomyoblasts were incubated with nascent sodium selenite (25 nM) for 1 h.

Group VI: After ischemia, cardiomyoblasts were incubated with GGN (60 µg) for 1 h.

Group VII: After ischemia, cardiomyoblasts were incubated with GGN (300 µg) for 1 h.

Group VIII: After ischemia, cardiomyoblasts were incubated with SGG (5 nM) for 1 h.

Group IX: After ischemia, cardiomyoblasts were incubated with SGG (25 nM) for 1 h.

3.2.3. Cell morphology

The cells subjected to ischemia, I/R and treatment with Se, GGN and SGG were observed under phase contrast microscope (Nikon Eclipse TS100) to study the morphological changes.

3.2.4. Cell viability

Cell viability was determined by MTT assay after ischemia, I/R and treatment with Se, GGN and SGG. MTT solution was added into plates at a final concentration of 0.5 mg/ml and incubated for 3 h at 37 °C. Then the culture medium was discarded and 0.5 ml DMSO was added to each well to dissolve dark blue formazan crystals. The absorbance was measured at 570 nm (Biotek Synergy 4, US) and the percentage toxicity was calculated.

3.2.5. Lactate dehydrogenase level

The lactate dehydrogenase (LDH) release from all experimental groups was determined using the Cayman assay kit, USA. This assay measures cell death in response to chemical compound using a coupled two step reactions. In the first step, LDH catalyzes the reduction of NAD^+ to NADH and H^+ by oxidation of lactate to pyruvate and in the second step diaphorase uses the newly formed NADH and H^+ to catalyze the reduction of a tetrazolium salt to highly colored formazan which absorbs strongly at 490 nm. The amount of formazan formed was proportional to the amount of LDH released into the culture medium as a result of cytotoxicity. After respective treatments with Se, GGN and SGG cells were trypsinized and were centrifuged at 400×g for 5 min. Then 100 µl of supernatant and standard were transferred to a 96 well plate. 100 µl of reaction solution were added to each well and incubated the plate with gentle shaking for 30 min at room

temperature. The absorbance was read at 490 nm with a plate reader.

3.2.6. GSH level

GSH activity was assayed spectrophotometrically according to manufacturer's instruction (Cayman, USA).The principle of this assay is that sulfhydryl group of GSH reacts with DTNB (5,5'dithio-*bis*-2-(nitrobenzoic acid)) and produces a yellow coloured 5-thio-2-nitrobenzoic acid (TNB). The mixed disulfide that is concomitantly produced during this reaction is reduced by glutathione reductase to recycle the GSH and produce more TNB. The rate of TNB production is directly proportional to this recycling reaction which in turn is directly proportional to the concentration of GSH in the sample. The absorbance of TNB was noted at 407 nm. For assay the cells after respective treatments were collected and centrifuged (2,000×g) for 10 min at 4 °C. The cell pellets were homogenised in 2 ml of cold buffer and was centrifuged at 10,000×g for 15 min at 4 °C. After that the supernatant was deproteinized. 50 µl standard and sample were added to the designated wells and covered with the plate cover. The assay cocktail mixture containing MES buffer, reconstituted cofactor mixture, reconstituted enzyme mixture, water and reconstituted DTNB was prepared and 150 µl of assay cocktail mixture was added to each well containing sample and standard and incubated in dark on a shaker. The absorbance was measured at 407 nm at five min intervals for 30 min.

Alteration in GSH was also detected by fluorescent imaging (BD Pathway ™ Bioimager system, USA) using Cayman kit. This assay kit employs a cell permeable dye monochlorobimane which reacts with GSH to generate a highly fluorescent product with excitation emission wavelengths of 380 nm and 460 nm. After respective treatments, 100 µl of the substrate solution was added to each well and incubated for 30 min at 37 °C. The supernatant was discarded and 200 µl assay buffer was added to each well. The fluorescence was analysed in spinning disc fluorescent microscope at excitation and emission wavelengths of 380 nm and 460 nm.

3.2.7. GPx activity

GPx activity was assayed spectrophotometrically using Cayman assay kit, which is based on the reduction of oxidized glutathione coupled to the oxidation of NADPH. The disappearance of NADPH was monitored at 340 nm. One unit of GPx activity was defined as the amount of enzyme that will cause the oxidation of NADPH to $NADP^+$ per

min at 25 °C. For assay the cells after respective treatments were collected by centrifugation (2000×g) for 10 min at 4 °C. The cell pellets were homogenized in cold buffer (50 mM tris-HCl, pH 7.5, 5 mM EDTA and 1 mM DTT) and centrifuged (10,000× g) for 15 min at 4 °C. The supernatant was used for the assay. 100 µl of assay buffer, 50 µl of co-substrate mixture and 20 µl supernatant (samples) were added to the subsequent wells. Then 20 µl of cumene hydroperoxide were added to all wells for initiating the reaction. The absorbance was read once in every min at 340 nm to get 5 time points using a plate reader.

3.2.8. Total antioxidant level

Total antioxidant activity of the samples was assayed as per Cayman protocol. This assay was based on the ability of antioxidants in the sample to inhibit the oxidation of ABTS* (2, 2'- Azino-di-[3-ethylbenzthiazoline sulphonate]) to reduced ABTS**$^{+}$ by metmyoglobin. The amount of ABTS**$^{+}$ produced was monitored by measuring the absorbance at 405 nm. For performing the assay after respective treatment the cells were collected by centrifugation (2000×g) for 10 min at 4 °C. The pellets were sonicated and centrifuged at 10,000×g for 15 min at 4 °C. For assay, 10 µl of the sample (supernatant) and 10 µl standard was added in two different wells. 10 µl metmyoglobin and 150 µl of chromogen was added to both wells. The reaction was initiated by adding H_2O_2. The wells were incubated for 5 min at room temperature and then absorbance was read at 405 nm.

3.2.9. Catalase and SOD activity

Catalase activity was assayed according to the method of Cohen *et al* (1970) and expressed as 1 µM of H_2O_2 decomposed per minute at 25 °C. The protein concentration was measured by the method of Bradford (1976). The disappearance of H_2O_2 activity was spectrophotometrically assayed at 240 nm. SOD was assayed by the method of Kakkar *et al* (1984). The assay mixture contained 1.2 ml of sodium pyrophosphate buffer (pH 8.3, 0.52 M), 0.1 ml (186 µM) phenazine methosulfate, 0.3 ml (300 µM) nitroblue tetrazolium, and 0.2 ml NADH (780 µM) and finally made up in to a volume of 3 ml with addition of distilled water. The reaction was started by the addition of NADH. After incubation at 30 °C for 90 seconds the reaction was stopped by the addition of glacial acetic acid. The reaction mixture was stirred vigorously and shaken with 4 ml of n-

butanol. The mixture was allowed to stand for 10 min and then centrifuged and the butanol layer was removed. The colour intensity of the chromogen in butanol was measured at 560 nm using a multimode plate reader.

3.2.10. TrxR level

The assay of TrxR enzyme was based on the reduction of DTNB with NADPH to TNB to produce a yellow product that was measured at 407 nm. The TrxR activities of the cells from all experimental groups were determined as per the Cayman protocol. After respective treatments the cells were collected by centrifugation (2000×g) for 10 min at 4 °C. The cell pellets were homogenized in cold buffer (50 mM potassium phosphate, pH 7.4, containing 1 mM EDTA) and centrifuged at 10, 000×g for 15 min at 4 °C. For assay, 140 µl diluted assay buffer and 20 µl samples (supernatant) were added to wells. The reaction was initiated by adding 20 µl of NADPH and 20 µl of DTNB to all the wells and the plates were shaked for 10 seconds. The absorbance was read once in every min at 407 nm.

3.2.11. XO assay

XO activities of the cells from all experimental groups were assayed spectrophotometrically using the Cayman assay kit. The assay is based on enzymatic reaction in which XO first produces H_2O_2 during oxidation of hypoxanthine. In the presence of horse radish peroxidase (HRP), the H_2O_2 reacts with acetyl-3, 7-dihydroxyphenoxazine to produce the highly fluorescent resorufin. Resorufin fluorescence are analysed with an excitation wavelength of 520 nm and an emission wavelength of 585 nm. After respective treatments the cells were homogenized in cold buffer (100 mM Tris-HCl, pH 7.5) and centrifuged at 10,000×g for 15 min at 4 °C. Supernatant was used for assay. 50 µl of sample and 50 µl of standard were added to designated wells. 50 µl assay cocktail mixture (assay buffer (4.9 ml), detector (50 µl) and HRP (50 µl) were added to both sample and standard wells. The samples and standard were incubated for 45 min at 37 °C. The fluorescence was read at excitation wavelength of 520 nm and emission wavelength of 585 nm.

3.2.12. Protein carbonyl and lipid peroxidation assays

The protein carbonyl assay was based on the fact that DNPH reacts with protein carbonyls forming Schiff's base to produce corresponding hydrazone which can be

quantified at an absorbance between 370 nm. In this assay, the cells were collected by centrifugation (2000×g for 10 min at 4 °C) from respective groups. This was homogenized in cold buffer (50 mM MES, pH 6.7 containing 1 mM EDTA). The cells were again centrifuged at 10,000×g for 15 min at 4 °C. Supernatant was used for assay. 200 µl of sample (supernatant) was added to two tubes. One tube was the sample tube and the other control tube. To that 800 µl of DNPH was added and 800 µl of 2.5 M HCl to the control tube. The tubes were incubated in dark at room temperature for 1 h. The tubes were vortexed at every 15 min during incubation. After incubation 1 ml of 20% of TCA was added with 5 min incubation in ice. The tubes were centrifuged at 10,000×g for 10 min at 4 °C. The pellets were resuspended in 1 ml of (1:1) ethanol /ethyl acetate mixture and centrifuged at 10,000×g for 10 min at 4 °C. This step was repeated for 2 times. Then the protein pellets were resuspended in 500 µl of guanidine hydrochloride by vortexing. Again centrifuged at 10,000×g for 10 min at 4 °C and then 220 µl of supernatant from the samples and 220 µl of supernatant from control tubes were transferred to 96 well plates and the absorbance was read at 370 nm.

Lipid peroxidation was estimated for all experimental groups with TBARS assay kit (Cayman, USA). The absorbance of the colored product was measured at 530 nm. After respective treatments the cells were collected along with culture medium and it is sonicated for 5 seconds intervals. 100 µl of sample and 100 µl of standard were added to labelled tubes. To that 100 µl of SDS and 4 ml of colouring reagent were added. The tubes were boiled for 1 h and after 1 h it was placed in ice bath for 10 min to stop the reaction. After incubation it was centrifuged for 10 min at 1,600×g at 4 °C and incubated in room temperature for 30 min. From these 150 µl of samples were transferred to black well plate and absorbance was read at 530 nm in plate reader.

3.2.13. Nrf2 transcription factor assay

Nrf2 transcription factor assay and nuclear extraction was done using Nrf2 Cayman assay kit and Cayman nuclear extraction kit respectively. Nrf2 contained in nuclear extract samples were bound specifically to the Nrf2 response element immobilized in 96 well plate and was detected by addition of a specific Nrf2 antibody and a secondary antibody conjugated to HRP. The absorbance was read at 450 nm.

3.2.14. Detection of ROS by confocal/ flow cytometry

Intracellular ROS was determined by oxidative conversion of cell-permeable DCFH-DA to fluorescent 2'7' dichlorofluorescein (DCF). The increase in DCF fluorescence suggests H_2O_2 or hydroxyl radical generation. For this H9c2 cells were seeded in 96-well plate at a density of 5000 cells per well and was subjected to ischemia, I/R and treatment with different test materials (Se, GGN and SGG). Then cells were incubated with DCFH-DA at 37 °C for 20 min. After three washes, DCF fluorescence was measured by fluorimetry (excitation: 488 nm and emission: 525 nm) in multi well plate reader and fluorescent imaging was done to detect the difference in the intensity of fluorescence emitted using spinning disk facility (BD Pathway Bioimager System, BD Biosciences, USA). The same experiment was repeated with flow cytometry technique. For this the cells preincubated with DCFHDA was trypsinized, collected and centrifuged at 300×g for 5 min (Oyama *et al* 2009). The cell pellets were resuspended with PBS and analyzed using a flow cytometer (BD FACS Aria II flow cytometer, USA). Acquisition and analysis of flow cytometric data were carried out using BD FACS Diva software.

3.2.15. Activity of Ca^{2+}-ATPase

Activity of Ca^{2+}-ATPase was evaluated as per the previous method (Rooban *et al* 2010). After induction of ischemia and I/R and treatment with various experimental groups cell lysate was added to the reaction mixture composed of 0.4 M Tris HCl, 15 mM NaN_3, 0.2 mM EDTA, 120 mM $CaCl_2$, 20 mM $MgCl_2$ and 3 mM ATP (as substrate) and incubated for 30 min at 37 °C and the enzyme activity was stopped by adding 10% TCA. All the tubes were then centrifuged at 2,500 rpm for 10 min to collect supernatant. The protein-free supernatant was then analyzed for inorganic phosphate. For that the supernatant was treated with ammonium molybdate and 1-amino 2-naphthol 4-sulphonic acid (ANSA) and then the absorbance was measured at 680 nm after 20 min.

3.2.16. Detection of intracellular calcium

The total calcium content in the cell of various experimental groups was assayed with a kit from Cayman. The assay utilizes an optimized o-cresolphthalein-calcium reaction in which a vivid purple complex is formed in the presence of calcium that absorbs between 560 nm and 590 nm. The intensity of the colour is directly proportional to the concentration of calcium in the sample.

The level of intracellular calcium in different experimental groups is visualized with Fura 2-AM. For this, cells were treated with Fura 2-AM for 20 min at room temperature (excitation; 340 and 380 nm and emission; 510 nm) (Venkataraman *et al* 2012) and visualized under a fluorescent spinning disk microscope.

3.2.17. Statistical analysis

Results were expressed in mean and standard deviation (SD) of the control and treated cells from three independent experiments with duplicates (n=6). Data were subjected to one-way ANOVA followed by the Bonferroni test to calculate the statistical difference among the groups using SPSS for Windows, standard version 11.5.1 (SPSS, Inc.) and significance was accepted at $P \leq 0.05$.

3.3. Results

Preliminary studies with SGG showed that they are safe for H9c2 cardiomyoblasts. In this chapter we examined the comparative protective effect of various particles like Se, GGN and SGG against the cell based cardiac ischemia model.

3.3.1. Morphological analysis

It is interesting to note that ischemia induced more pathological alterations compared to reperfusion in all the parameters studied in this cell model of ischemia. Microscopic evaluation showed severe alterations in the morphology of cells on ischemia of 30 min (Figure.3.1.b). The cells had undergone severe morphological alterations like shrinkage, rounding up and membrane blebbing (Figure.3.1.b). The treatment with Se (Figure.3.1.d, e), GGN (Figure.3.1.f, g) and SGG (Figure.3.1.h, i) were effective in maintaining the normal cell morphology on ischemia. During I/R (Figure.3.1.c) most of the cells were able to revert back to normal morphology (Figure.3.1.a). In order to assess the beneficial effect of test materials, the effect of test materials were compared with I/R group in all the cases unless otherwise specified.

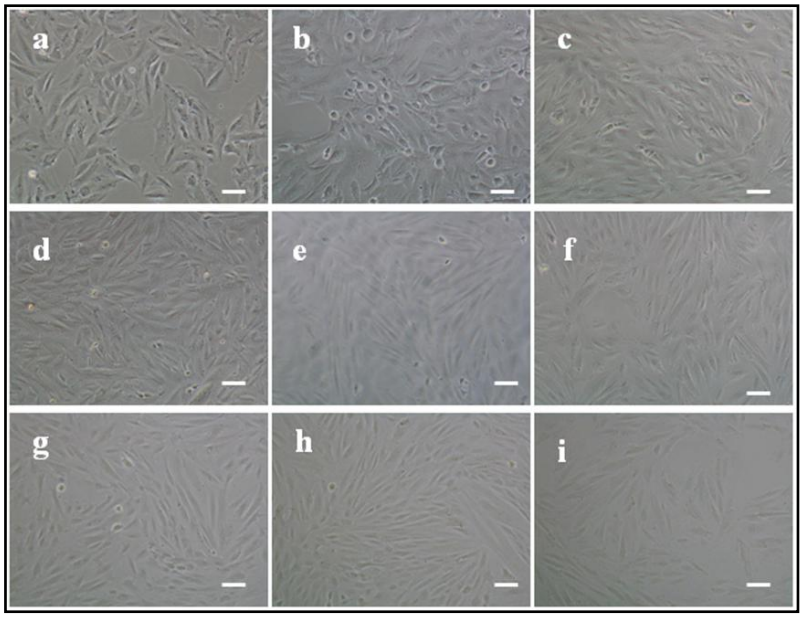

Figure 3. 1. Effect of Se, GGN and SGG on the morphology of H9c2 after I/R. Microscopic images of H9c2 cells from different experimental groups under phase contrast microscope (original magnification 10x). (a) control cells; (b) ischemic cells; (c) I/R cells; (d, e) cells treated with 5 nM and 25 nM Se; (f, g) cells treated with 60 µg and 300 µg of GGN; and (h, i) cells treated with 5 nM and 25 nM SGG. Scale bar corresponds to 100 µm.

3.3.2. Cell viability

The cell viability of SGG nanoparticles was evaluated by measuring the mitochondrial dehydrogenase activity using MTT assay. H9c2 cells with ischemia for 30 min caused 31.51% of cell death whereas I/R caused 25.09% that was statistically significant compared to control ($P \leq 0.05$). Application of higher concentrations of Se (25 nM), GGN (300 µg) and SGG (25 nM) for 1 h after ischemia reduced the cell death to 9.88%, 10.64% and 8.60% respectively, compared to I/R (Table 3.1).

3.3.3. LDH level

LDH activity is often determined as a biomarker of cell damage. In the present study, it was observed that in ischemia there was significant increase of LDH activity (141.05±1.20 µU/ml) when compared to the control (14.76±1.69 µU/ml). On the other hand in I/R, LDH release was reduced compared to the ischemic group (114.75±0.50 µU/ml). Treatment with all the test materials was significantly ($P \leq 0.05$) effective in reducing LDH release after I/R (Table 3.1). Statistical analysis revealed that SGG (5 nM

and 25 nM) was more effective compared to other test materials in bringing the LDH level to normal. (Table 3.1).

Table 3. 1. Effect of Se, GGN and SGG on cell viability after I/R.

	MTT(% toxicity)	LDH release (µU/ml)
Control	-	14.76 ± 1.69
Ischemia	31.51± 3.40*	141.05 ± 1.20*
I/R	25.09 ± 4.98*	114.75 ±0.50*
Se (nM)		
5	6.49 ± 0.34$	18.66 ± 0.36$
25	9.88 ± 0.96$	20.66 ± 2.44$
GGN (µg)		
60	9.47 ± 0.09$	21.90 ± 0.71$
300	10.64 ± 0.46$	19.32 ± 0.65$
SGG (nM)		
5	6.13 ± 0.68$	11.59±1.60$
25	8.60 ± 1.04$	14.09 ±1.90$

The Se, GGN and SGG groups were compared with I/R group. Each value represents mean ± SD (n=6). * Mean value was significantly different from the control cells (P≤0.05). $ Mean value was significantly different from I/R group (P≤0.05).

3.3.4. GSH level

Ischemia for 30 min caused a decrease in GSH level (0.143±0.004 mM) compared to control (0.267±0.001 mM). Statistical analysis revealed that all test materials were effective to bring back the GSH level to the normal (Table 3.2) but SGG was the best. Imaging study also showed same trend like fluorimetry results. GSH content had decreased from the basal level in ischemia and I/R cells (Figure3.2.b, c) compared to control (Figure.3.2.a) whereas SGG, Se and GGN (Figure. 3.2.d-i) treatment prevents the alteration of GSH content compared to in I/R cells (Figure. 3.2.c).

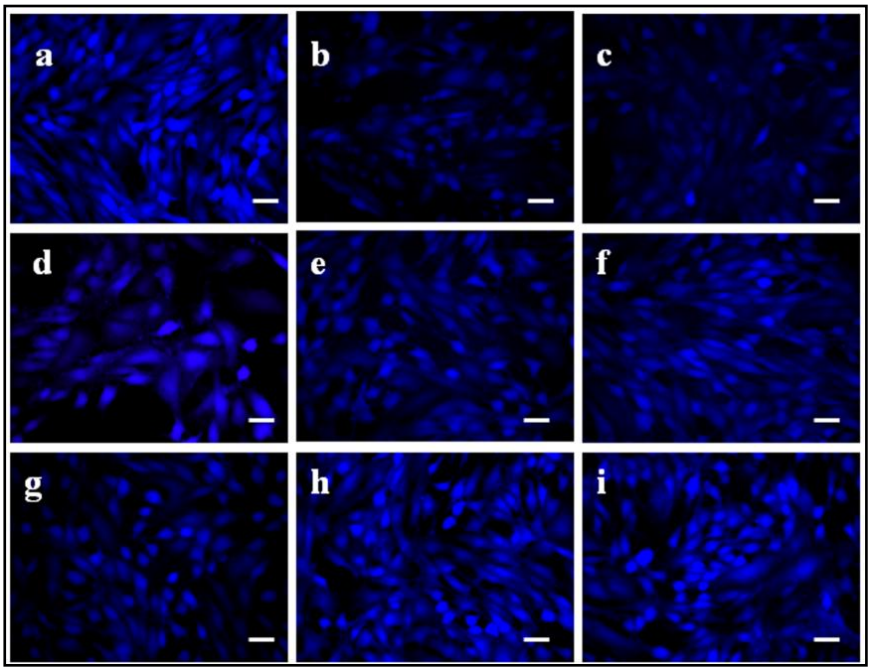

Figure 3. 2. Fluorescent microscopic images of H9c2 cells stained for glutathione evaluation (original magnification 20x). (a) control cells; (b) ischemic cells; (c) I/R cells; (d, e) cells treated with 5 nM and 25 nM Se; (f, g) cells treated with 60 µg and 300 µg of GGN; and (h, i) cells treated with 5 nM and 25 nM SGG. Scale bar corresponds to 100 µm.

3.3.5. Catalase and SOD activity

Herein, ischemia and I/R caused a decrease in catalase (0.033±0.002, 0.047±0.017 U/mg protein) and SOD (0.441±0.017, 0.524±0.107 U/mg protein) compared to control (0.908±0.003, 0.116±0.005). Among various test materials 5 nM (0.103±0.002, 0.873±0.003 U/mg protein) and 25 nM SGG (0.107±0.003, 0.940±0.012 U/mg protein) showed the best results to bring back the catalase and SOD level near to the normal (Table 3.2).

3.3.6. Level of GPx

GPx catalyses the peroxidation of H_2O_2 in the presence of reduced glutathione to form H_2O and oxidized glutathione (GSSG). Thus GPx play an important role as a H_2O_2 scavenger in the heart cell. Here also, Gpx activity was decreased in ischemia (0.228± 0.004 nmol/min/ml) and I/R group (0.249±0.006 nmol/min/ml) compared to control (0.341±0.001 nmol/min/ml). All the test materials were effective in bringing the antioxidant enzyme activities to normal. In case of GPx 25 nM SGG (0.339±0.013

nmol/min/ml) and 25 nM Se (0.336±0.002 nmol/min/ml) showed better activity compared to other test materials (Table 3.2).

Table 3. 2. Effect of Se, GGN and SGG on SOD, Catalase and GPx and GSH level after I/R.

	SOD (U/mg protein)	Catalase (U/mg protein)	GPx (nmol/ min/ml)	Glutathione (mM)
Control	0.908±0.003	0.116±0.005	0.341±0.001	0.267±0.004
Ischemia	0.441±0.017*	0.033±0.002*	0.228±0.004*	0.143±0.016*
I/R	0.524±0.107*	0.047±0.017*	0.249±0.006*	0.161±0.013*
Se (nM)				
5	0.760±0.009$	0.093±0.002$	0.312±0.007$	0.181±0.003$
25	0.867±0.003$	0.096±0.003$	0.336±0.002$	0.192±0.002$
GGN (µg)				
60	0.678±0.004$	0.091±0.004$	0.329±0.013$	0.187±0.009$
300	0.624±0.005$	0.093±0.001$	0.323±0.008$	0.196±0.001$
SGG (nM)				
5	0.873±0.003$	0.103±0.002$	0.333±0.003$	0.205±0.005$
25	0.940±0.012$	0.107±0.003$	0.339±0.013$	0.199±0.004$

The Se, GGN and SGG groups were compared with I/R group. Each value represents mean ±SD (n=6). * Mean value was significantly different from the control cells (P≤0.05). $ Mean value was significantly different from I/R group (P≤0.05).

3.3.7. TrxR level

Thioredoxins are key players in the cardiac defense against oxidative stress and cytoprotection against oxidative stress. Our result shows that TrxR level is decreased in ischemia (1.9±1.0 nmol/min/ml) and I/R (2.3±0.1 nmol/min/ml) compared to control 4.3±0.2 nmol/min/ml). TrxR level of 25 nM SGG (4.7±0.6 nmol/min/ml) and 25 nM Se (3.9±0.2 nmol/min/ml) showed better activity compared to other test materials. Reduced activities of TrxR in ischemia and I/R cells again is an indication of dysfunction of antioxidant status *via* excessive production of ROS (Table 3.3).

3.3.8. Total antioxidant level

Total antioxidant activity was decreased in ischemia (0.020±0.003 mM) and I/R group (0.025±0.002 mM) compared to control (0.050±0.002 mM). Surprisingly, total antioxidant activity was better with 300 µg GGN (0.050±0.001 mM) and 25 nM Se (0.054±0.003 mM) treated groups compared other groups (Table 3.3). There was a

significant inhibition of total antioxidant status during ischemia and I/R but administration of all test materials prevented inhibition of antioxidant parameters during ischemia and I/R.

3.3.9. Protein carbonyl and lipid peroxidation assays

Protein carbonyls are the products of protein oxidation and common marker of protein oxidation and an increased level of same reveals oxidative damage in the ischemic cells. Protein carbonyl showed an increasing trend ($P \leq 0.05$) during ischemia (9.301±0.093 nmol/ml) and I/R (7.182±0.137 nmol/ml) respectively compared to control (2.172±0.129 nmol/ml) (Table 3.3). In protein carbonyl assay 5 nM (2.441±1.042 nmol/ml) and 25 nM (1.851±0.135 nmol/ml) SGG treated groups showed better activity compared to Se (2.736±0.117 and 4.315±0.003 nmol/ml) and GGN (3.142±0.035 and 3.637±0.300 nmol/ml) in preventing the protein oxidation.

Likewise, MDA is a major lipid peroxidation product that reflect the degree of cellular injury. MDA level (Table 3.3) was increased in ischemia (1.568±0.104 nmol/ml) and I/R (1.30±0.027 nmol/ml) groups where treatment with 25 nM Se (0.745±0.023 nmol/ml) and 5 nM SGG (0.652±0.010 nmol/ml) showed protective effect in bringing the condition to normal compared to other treated groups.

Table 3. 3. Effect of Se, GGN and SGG on TrxR, Total antioxidant, Protein carbonyl and Lipid peroxidation after I/R

	TrxR (nmol/min/ml)	**Total antioxidant (mM)**	**Protein carbonyl (nmol/ml)**	**Lipid peroxidation (nmol/ml)**
Control	4.3±0.2	0.050± 0.002	2.172±0.129	0.714±0.011
Ischemia	1.9±1.0*	0.020±0.003*	9.301±0.093*	1.568±0.104*
I/R	2.3±0.1*	0.025±0.002*	7.182±0.137*	1.30±0.027*
Se (nM)				
5	2.9±0.1$^{\$}$	0.039±0.007$^{\$}$	2.736±0.117$^{\$}$	0.797±0.011$^{\$}$
25	3.9±0.2$^{\$}$	0.054±0.003$^{\$}$	4.315±0.003$^{\$}$	0.745±0.023$^{\$}$
GGN (µg)				
60	2.5±0.4$^{\$}$	0.044±0.006$^{\$}$	3.142±0.035$^{\$}$	0.860±0.025$^{\$}$
300	3.4±0.6$^{\$}$	0.050±0.001$^{\$}$	3.637±0.300$^{\$}$	0.881±0.028$^{\$}$
SGG (nM)				
5	3.9±0.8$^{\$}$	0.047±0.003$^{\$}$	2.441±1.042$^{\$}$	0.652±0.010$^{\$}$
25	4.7±0.6$^{\$}$	0.055±0.002$^{\$}$	1.851±0.135$^{\$}$	0.558±0.055$^{\$}$

The Se, GGN and SGG groups were compared with I/R group. Each value represents

mean ±SD (n=6). * Mean value was significantly different from the control cells (P≤0.05). $ Mean value was significantly different from I/R group (P≤0.05).

3.3.10. XO assay

In this study, we found ischemia (148.82%) and I/R (132.62%) induces surplus generation of XO compared to control (100%) (Figure.3.3). All the test materials were effective to bring down the enzyme activity. But 5 nM SGG (95.73%) and 25 nM Se (92.47%) showed significant (P≤0.05) protective effect (Figure.3.3) compared to other test materials.

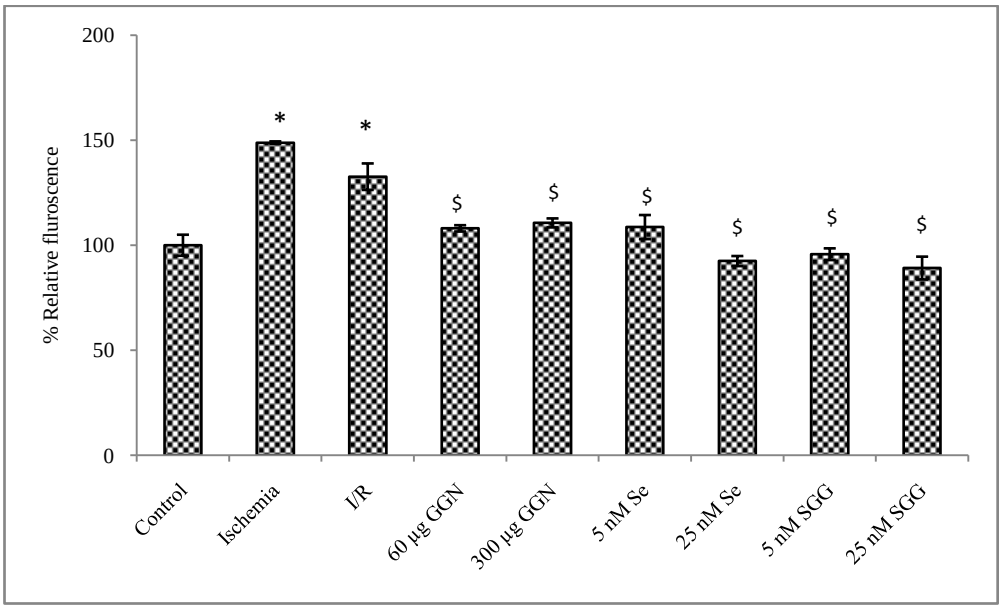

Figure 3. 3. Activity of XO in control and treated H9c2 cells after I/R. Values are means, with standard deviations represented by vertical bars (n=6). The ischemic and I/R groups were compared with the control group. The Se, GGN and SGG treated groups were compared with I/R group. * Indicates that the mean value was significantly different from the control cells (P≤0.05). $ Indicates mean value was significantly different from the I/R cells (P≤0.05).

3.3.11. Nrf2 transcription factor assay

Nrf2 transcription activity was expressed as optical density (OD at 450 nm). Ischemia (0.3865±0.012) and I/R (0.3504±0.016) resulted in increase of Nrf2 levels in nuclear fractions compared to control (0.1140±0.013) (Figure.3.4). 5 nM (0.3324±0.010) and 25 nM (0.4201±0.016) SGG showed the upregulation of Nrf2 levels in nuclear fraction compared to other treatment groups (Figure.3.4).

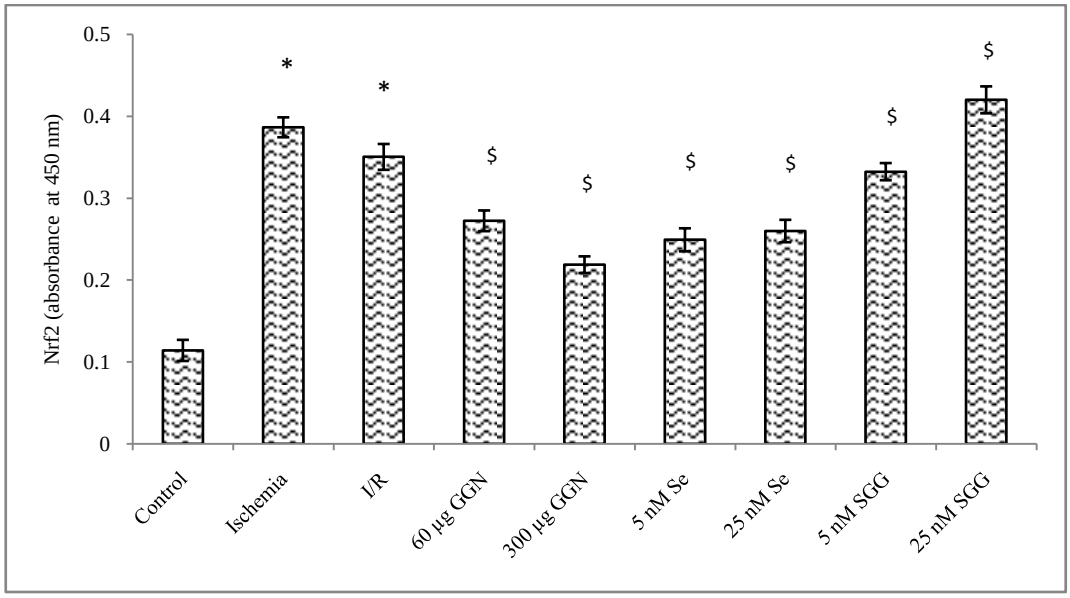

Figure 3. 4. Activity of Nrf2 in control and treated H9c2 cells after I/R. Values are means, with standard deviations represented by vertical bars (n= 6). The ischemic and I/R groups were compared with the control group. The Se, GGN and SGG treated groups were compared with I/R group. * indicates that the mean value was significantly different from the control cells ($P \leq 0.05$). $ indicates that the mean value was significantly different from I/R cells ($P \leq 0.05$).

3.3.12. Effect of SGG on ROS generation

Evaluation of ROS both by flow and confocal images revealed surplus generation of ROS during ischemia (14969±384.4 relative fluorescence) and I/R (12647±698.02 relative fluroscence) (Figure.3.5A.b, c) compared to control (10386.33±380.52 of relative fluorescence) (Figure.3.5A.a). 300 µg GGN and 25 nM Se was significantly ($P \leq 0.05$) effective for preventing ROS generation compared to other test materials (Figure.3.5A.g, e). This was also confirmed with flow cytometry data (Figure.3.5B.a- g).

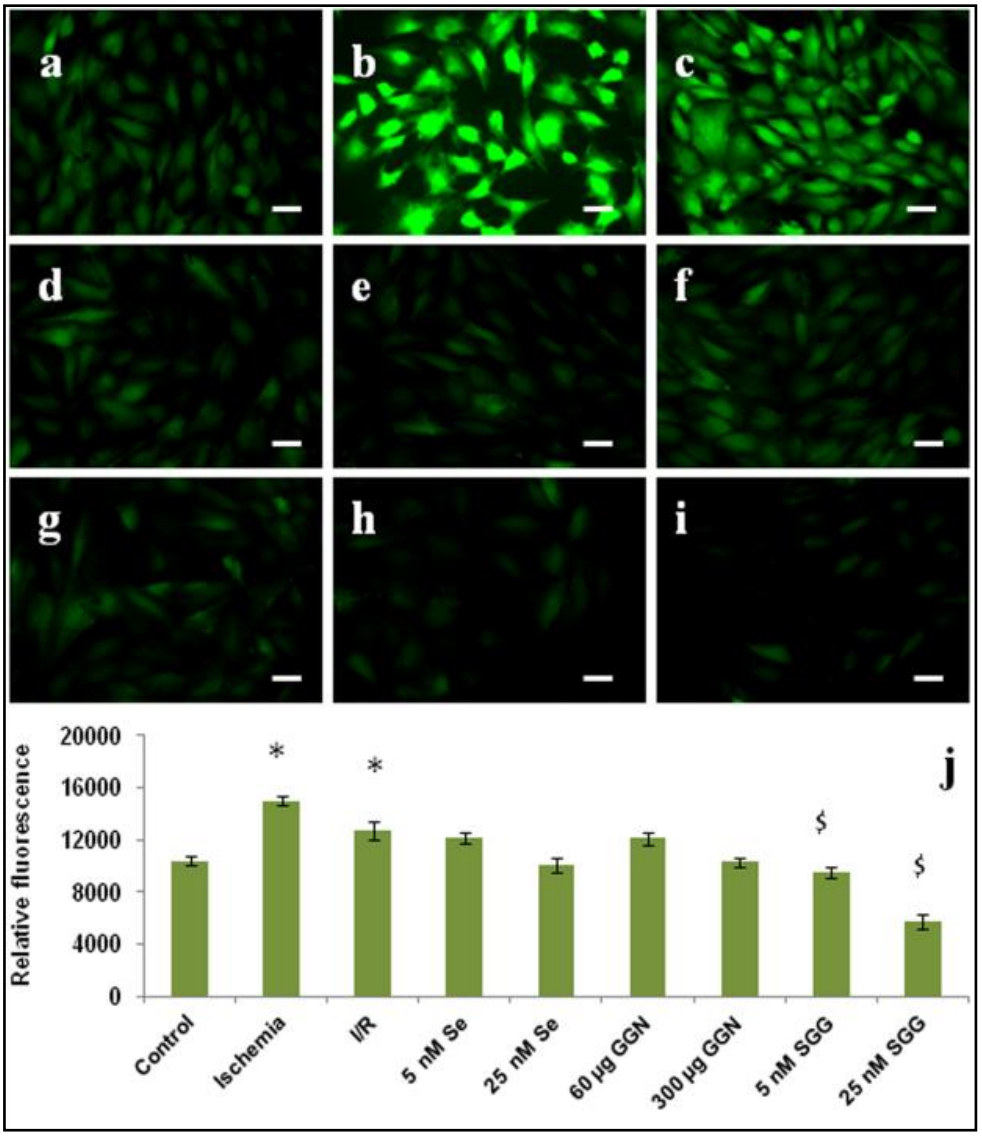

Figure 3. 5A. Effect of Se, GGN and SGG on ROS generation in I/R induced H9c2 cells. Fluorescent microscopic images of H9c2 cells stained with DCFHDA (original magnification 20 x). (a) control cells; (b) ischemic cells; (c) I/R; (d, e) cells treated with 5 nM and 25 nM Se; (f, g) cells treated with 60 µg and 300 µg of GGN and (h, i) cells treated with 5 nM and 25 nM SGG; and (j) relative fluorescence intensity analysis. The Se, GGN and SGG treated groups were compared with I/R group. The ischemic and I/R groups were compared with the control group. * Indicates that the mean value was significantly different from the control cells ($P \leq 0.05$). $ Indicates mean value was significantly different from I/R cells ($P \leq 0.05$). Scale bar corresponds to 100 µm.

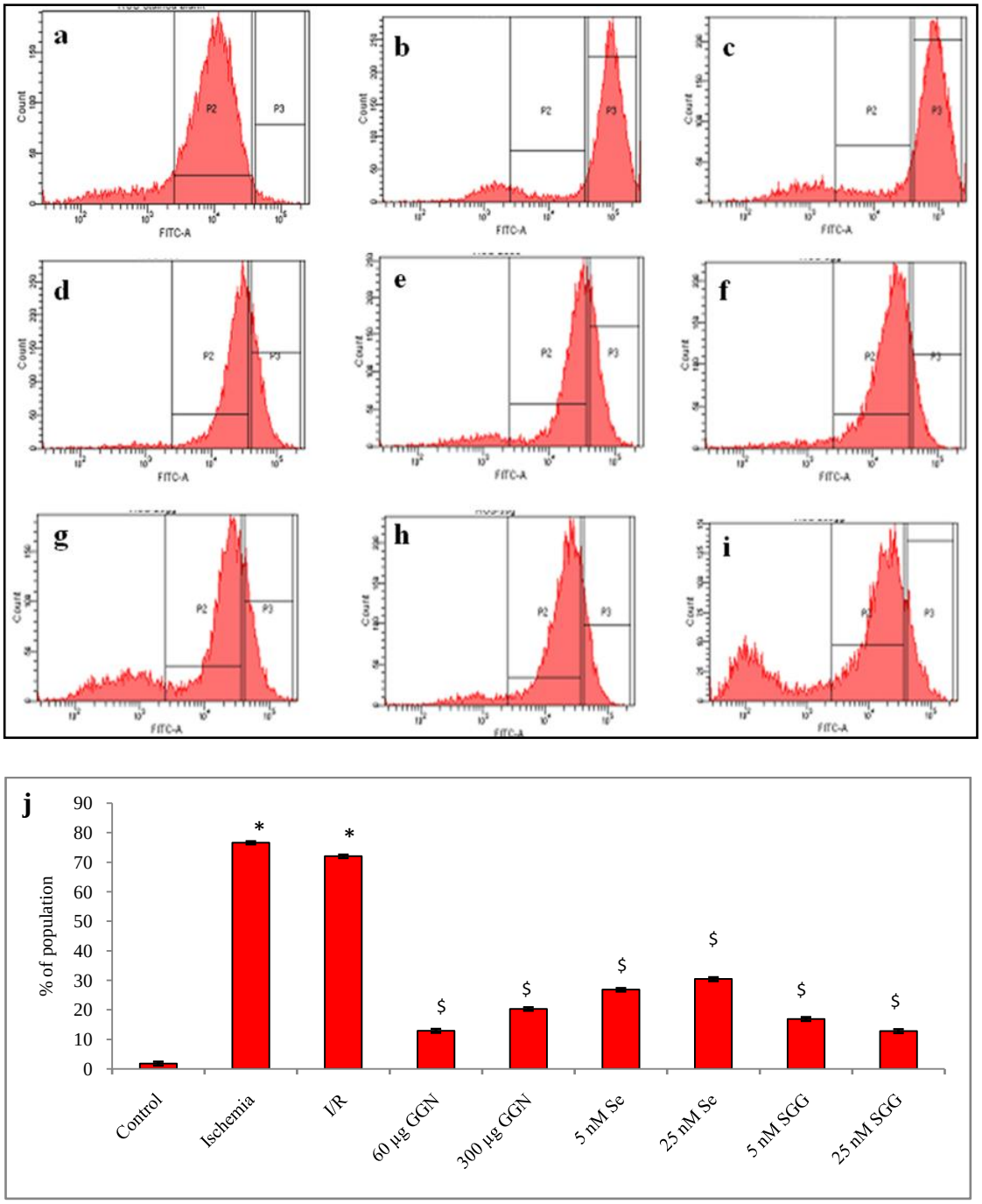

Figure 3. 5B. Flow cytometric analysis of intracellular ROS generation in different groups. Analysis of intracellular ROS using fluorescent probe, DCFH-DA reveals significant increase in ROS generation by ischemia and I/R. (a) control cells; (b) ischemic cells; (c) I/R cells; (d, e) cells treated with 5 nM and 25 nM Se (f, g) cells treated with 60 µg and 300 µg of GGN and (h, i) cells treated with 5 nM and 25 nM SGG (j) statistical analysis of flow cytometry data. Population P3 represents the ROS. Results expressed as mean ±SD; n=6 and the significance accepted at ($P \leq 0.05$).

3.3.13. Effect of SGG on maintaining calcium homeostasis

To study the effect of test materials in maintaining calcium homeostasis during I/R, the activity of Ca^{2+}-ATPase and level of intracellular calcium were evaluated. Activity of Ca^{2+}-ATPase were significantly reduced in ischemia (0.046±0.006 µmoles inorganic phosphate/mg protein), as well as in I/R (0.103±0.012 µmoles inorganic phosphate/mg protein) groups (Table 3.4) compared to the control (0.187±0.005 µmoles inorganic phosphate/mg protein). Application of all test materials showed protective trend in dose dependent manner. Among this 300 µg GGN (0.190±0.005 µmoles inorganic phosphate/mg protein), 5 nM SGG (0.199±0.009 µmoles inorganic phosphate/mg protein) and 25 nM Se (0.199±0.004 µmoles inorganic phosphate/mg protein) showed better activity in reverting the enzyme concentration to normal (Table 3.4).

The total calcium in ischemic group (3.344±0.095 mg/dl) and I/R group (3.060 ±0.048 mg/dl) had been increased significantly compared to control (1.881±0.069 mg/dl) (Table 3.4). Here also all test materials showed protection. Among these, 300 µg GGN (2.186±0.074 mg/dl) and 25 nM SGG (2.107±0.024 mg/dl) brought back the calcium concentration towards normal.

Table 3. 4. Effect of Se, GGN and SGG on calcium homeostasis.

	Ca^{2+}-ATPase (µmoles inorganic phosphate/mg protein)	**Calcium (mg/dl)**
Control	0.187 ±0.005	1.881 ± 0.069
Ischemia	0.046 ±0.006*	3.344 ± 0.095*
I/R	0.103 ±0.012*	3.060 ±0.048*
Se (nM)		
5	0.179 ±0.006$	2.523 ±0.111$
25	0.199 ±0.004$	2.213±0.092$
GGN (µg)		
60	0.154 ±0.005$	2.423 ±0.073$
300	0.190 ±0.005$	2.186 ±0.074$
SGG (nM)		
5	0.199 ±0.009$	2.260 ±0.073$
25	0.214 ±0.009$	2.107 ±0.024$

The Se, GGN and SGG groups were compared with I/R group. Each value represents mean ±SD (n=6). * Mean value was significantly different from the control cells (P≤0.05). $ Mean value was significantly different from I/R cells (P≤0.05).

There was significant calcium overload during I/R which was evident from Fura-2 AM fluorescence imaging as well as quantification assay compared to control (Figure.3.6.a, b). All the test materials showed protection against calcium overload in a dose dependent manner (Figure.3.6.d-i). The fluorescent imaging revealed that 5 nM SGG and 25 nM SGG was effective in normalizing the calcium overload compared to other test materials.

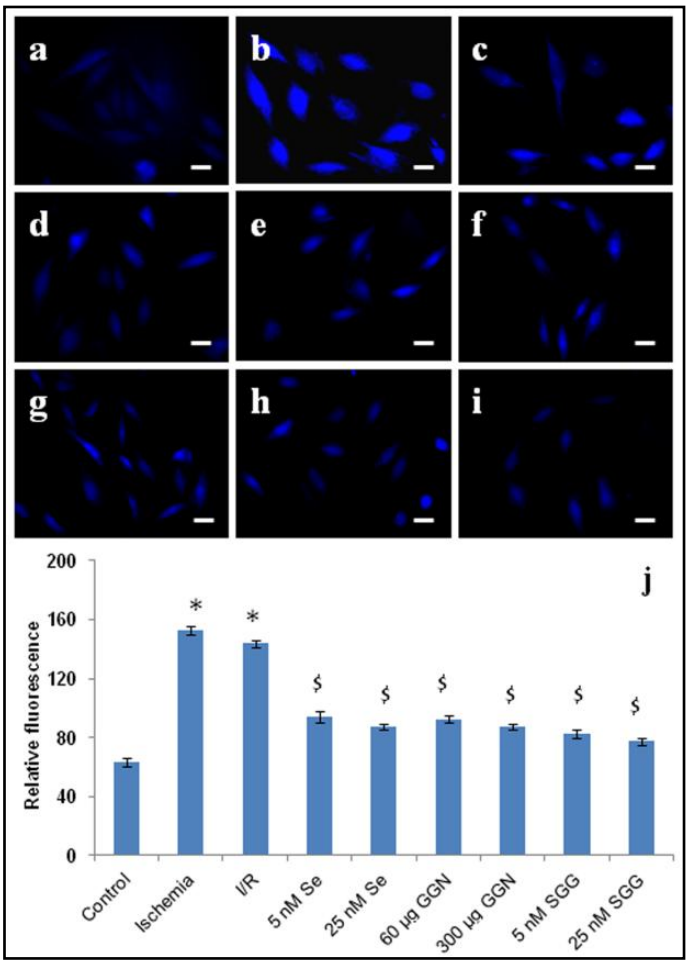

Figure 3. 6. Intracellular calcium overload in H9c2 with Se, GGN and SGG treatment. Images of H9c2 cells stained with Fura-2 AM (original magnification 20x). (a) control cells; (b) ischemic cells; (c) I/R cells; (d, e) cells treated with 5 nM and 25 nM Se; (f, g) cells treated with 60 µg and 300 µg of GGN; (h, i) cells treated with 5 nM and 25 nM SGG; and (j) relative fluorescence intensity analysis. The Se, GGN and SGG treated groups were compared with I/R group. The ischemic and I/R groups were compared with the control group. * Indicates that the mean value was significantly different from the control cells ($P \leq 0.05$). $ indicates mean value was significantly different from the I/R cells ($P \leq 0.05$). Scale bar corresponds to 100 µm.

3.4. Discussion

Nanomedicine is an emerging field that utilizes nanotechnology concepts for advanced therapy and diagnostics. Nanomedicine promises to enhance the ability of clinicians to address some of the serious challenges responsible for cardiovascular mortality, morbidity and numerous societal consequences (Lanza *et al* 2006). By taking advantage of the unique physicochemical properties of nanoparticles, nanomedicine where drugs are blended into nanomaterials readily offers a wide range of applications in the tracing, diagnosis and treatment of diseases. Recently, there has been increasing interest in the synthesis of nanoparticles using biologic systems, leading to the development of various biomimetic approaches (Mohampuria *et al* 2008). The SeNPs also have biologic activity and good adsorptive ability due to interaction between the nanoparticles and NH, C=O, COO–, and C–N functional groups of proteins (Zhang *et al* 2004). Ball and Garwin (1992) pointed out that the physical, chemical and biological properties of most nanochemical compounds have a size effect. Huang *et al* (2003) also reported that there was a potential size dependent effect on scavenging various free radicals by nano-Se. The present study demonstrates for the first time that SGG nanoparticles attenuate I/R induced oxidative stress in H9c2 cardiomyoblasts. Previous chapter revealed protective properties of SGG on H9c2 cells during oxidative stress. The present study describes the potential therapeutic capabilities of SGG against the cell based cardiac ischemia and I/R model mediated *via* its antioxidant associated properties.

Antioxidants have gained increasing interest due to its potential to prevent the detrimental effects of free radicals in human body. In addition, there is a preference for antioxidants from natural sources due to low adverse effects and high tolerance in the human body. Under abnormal conditions the antioxidant mechanism is disturbed and ROS induced tissue damage can takes place. Such injury occurs during I/R where a shortage of blood supply to a region of the heart tissue for a certain period is followed by reflow of blood supply. Recent studies showed that cardiomyocyte damage induced by heart I/R has been evidenced to be largely due to the generation of ROS (Venardos *et al* 2007; Zhao 2004; Saini *et al* 2004). This suggested that changes in the redox state of cardiac proteins play an important role in the formation of myocardial I/R injury. Cell

based assays were conducted to characterize the efficacy of various particles to protect innate antioxidant systems like GSH, GPx, TrxR, SOD, catalase, total antioxidant activity during I/R.

To determine the cell membrane integrity and to assess cytotoxicity, LDH assay were carried out. LDH is a soluble cytosolic enzyme that is released into the culture medium following the loss of membrane integrity, resulting from either apoptosis or necrosis. Wang *et al* (2013) reported the nano Se had the potential size dependent characteristic on the regulation of LDH activity. Here also, in ischemia and I/R cells the LDH release was increased and all the treatments were effective in decreasing the LDH release. Among all, SGG showed better effect compared to other treatment groups.

GSH is an important antioxidant in heart (Singh *et al* 1989) and cofactor for GPx. GSH has an important role in providing protection against myocardial injury after a short period of ischemia. Ischemia and I/R have caused severe alterations in the cellular antioxidant defense mechanisms. The reduced form of glutathione may act as a first line of defense against oxidative stress during I/R (Shin *et al* 2011). A recent investigation has reported a depletion of endogenous antioxidants in the ischemic heart upon reperfusion; this change was dependent upon the severity of I/R (Haramaki *et al* 1998). GSH can also reduce the generation of ROS such as hydroxyl radical and peroxynitrite. Changes in GSH status provide information on cellular oxidative events with accumulation or release of GSSG being an index of oxidative stress (Ferrari *et al* 1985; Ferrari *et al* 1986; Curello *et al* 1986; Kaul *et al* 1993). There was a significant decrease in GSH content in ischemia and reperfusion. SGG protects the H9c2 cells from GSH depletion and thus maintains the antioxidant status.

The heart is more susceptible to oxidative stress than other organs (Di Meo *et al* 1996; Odom *et al* 1992; Bordoni *et al* 2003). Excessive formation of free radicals may overwhelm antioxidant heart defense capacity and damage myocardial cells. Se is an essential component of GPx, which plays a critical role in protecting aerobic organisms from oxygen radical initiated injury. GPx catalyses the peroxidation of H_2O_2 in the presence of reduced GSH to form H_2O and GSSG. Thus GPx plays an important role as a H_2O_2 scavenger in the heart cell. Low Se status results in decreased GPx activity and Se

deficiency has been known to cause extensive oxidative damage in the myocardium in which SOD and GPx are the most active antioxidant enzymes. Therefore, any significant modification of Se status would lead to changes in the activity of the GPx and leads to oxidative stress. Bordoni *et al* (2003) suggested that the Se supplementation can protect the cardiomyocytes from hypoxia reoxygenation damage by improving the activities of antioxidant enzyme. In this study also the activity of GPx is decreased in ischemia and I/R whereas the all the test materials were effective in maintaining the level of GPx during ischemia and I/R. SGG was better among the groups.

There are reports to show the importance of catalase and SOD in protecting myocardium against I/R injury (Chen *et al* 1998; Woo *et al* 1998). Together with GSH system, it controls the redox state of cysteine residues of proteins and thus maintains the cellular process. It plays an important role in protecting against oxidative injury, cell growth and transformation and recycling of ascorbate. SOD catalyses the dismutation of superoxide anion ($O_2^{\cdot -}$) to H_2O_2 and subsequently reduced to H_2O and O_2 by peroxidases such as GPx and catalase. SOD is present in the cytoplasm with either copper or zinc and in the mitochondria with manganese (Ohta *et al* 1994). Analysis of results revealed significant inhibition of all these during ischemia and I/R but administration of SGG prevented inhibition of antioxidant parameters during ischemia and I/R. This clearly reveals the involvement of the redox antioxidant status during cardiac I/R in H9c2 cells.

In addition, we also found that lipid peroxidation indicators like MDA, protein carbonyl content and XO are getting increased. ROS damage the cellular membrane by causing lipid peroxidation. MDA is a major lipid peroxidation product and may reflect the degree of cellular injury. Protein carbonyls are the products of protein oxidation and common markers of protein oxidation (Dhalla *et al* 2000). An increased level of MDA and protein carbonyls revealed oxidative damage in the ischemic cells. One of the main enzymatic sources that generate the superoxide anion in the myocardium is XO and previous studies have shown that the activity of XO is higher in cardiac dysfunction (Hajjar and Leopold 2006). Here also we found that ischemia and I/R induce surplus generation of XO. The mitochondrial electron transport chain, NADPH oxidase and XO are reported to be the main sources of ROS in the cardiomyocyte during the

pathophysiology process (Rodrigo *et al* 2013). Thus, the two concentrations of SGG was able to upregulate several antioxidative enzymes and reduced the formation of oxidative stress and enhanced survival of cardiac myocytes upon the induction of oxidative stress.

Nrf2 which is a transcription factor that controls the expression of antioxidant genes and is ubiquitously expressed in cardiovascular system. It is a master regulator of cellular defenses against oxidative stress (Li *et al* 2009a). Activation of Nrf2 and its target genes provides mechanisms to protect the heart against pathological cardiac remodeling through suppressing oxidative stress (Li *et al* 2009b; Hu *et al* 2004; Lu *et al* 2008; Xing *et al* 2012). Nrf2-target genes for antioxidant enzymes and thus the upregulation of Nrf2 provide a protective mechanism against cellular and tissue damage in the cardiovascular system. Here SGG upregulates the Nrf2 expression significantly compared to other treatments.

Calcium ions are secondary messengers in numerous signaling pathways especially in cardiac myocytes. Oxidative stress results in cellular defects including a depression in the sarcolemmal calcium pump ATPase. These changes lead to decrease in calcium efflux and increased calcium influx. Oxidative stress has also been reported to lower the sarcoplasmic reticulum calcium pump ATPase thus inhibit calcium sequestration from cytoplasm in cardiac myocytes (Dixon *et al* 1992). The depression in the calcium regulatory mechanism by ROS ultimately results in intracellular calcium overloads and cell death. In addition, ROS have been reported to increase the activity of the Na^+/H^+ exchanger, thereby leading to an increase in cytosolic calcium *via* a reversal of the Na^+/Ca^+ antiporter (Day *et al* 2007). Calcium overload is an important feature of tissue ischemia and infarction, and increased calcium activates a number of phosphatases, proteases, and nucleases (Lemasters *et al* 2009). We also found depletion of Ca^{2+}-ATPase and significant intracellular calcium overload during ischemia as well as I/R. All the test materials were effective to block intracellular accumulation of calcium as well as keep maintenance of Ca^{2+}-ATPase activity in normal range during cardiac ischemia and I/R. Here also SGG was better among the groups.

Conclusions

Ischemia and I/R significantly altered the innate antioxidant defence system like GSH, antioxidant enzymes and Nrf2 transcription factor including calcium homeostasis.

But overall results revealed that SGG protect the cardiomyoblast from depletion of innate antioxidant defence system and calcium overload and the protection is slightly superior to Se and GGN. We conclude from this *in vitro* study that SGG is a safe nanomaterial with greater antioxidant potential and can be used for therapeutic application for cardiac disorders.

References

1. Ball P, Garwin L (1992) Science at the atomic scale. *Nature* 355: 761-766.
2. Battin EE, Brumaghim JL (2008) Metal specificity in DNA damage prevention by sulfur antioxidants. *J Inorg Biochem* 102: 2036-2042.
3. Battin EE, Perron NR, Brumaghim JL (2006) The central role of metal coordination in selenium antioxidant activity. *Inorg Chem* 45: 499-501.
4. Bordoni A, Biagi PL, Angeloni C, Leoncini E, Muccinelli I, Hrelia S (2003) Selenium supplementation can protect cultured rat cardiomyocytes from hypoxia/reoxygenation damage. *J Agric Food Chem* 51: 1736-1740
5. Bradford MA (1976) A rapid and sensitive method for the quantitation of microgram quantities of protein utilizing the principle of protein-dye binding. *Anal Biochem* 72: 248-254.
6. Burk RF (1989) Recent developments in trace element metabolism and function: newer roles of selenium in nutrition. *J Nutr* 119: 1051-1054.
7. Burton GW, Traber MG (1990) Vitamin E: antioxidant activity, biokinetics, and bioavailability. *Annu Rev Nutr* 10: 357-382.
8. Chen Z, Siu B, Ho YS, Vincent R, Chua CC, Hamdy RC, Chua BH (1998) Overexpression of MnSOD protects against myocardial ischemia/reperfusion injury in transgenic mice. *J Mol Cell Cardiol* 30: 2281-2289.
9. Cohen G, Dembiec D, Marcus J (1970) Measurement of catalase activity in tissue extracts. *Anal Biochem* 34: 30-38.
10. Curello S, Ceconi C, Cargnoni A, Medici D, Ferrari R (1986) Oxidative stress during myocardial ischemia and reperfusion: experimental and clinical evidence. *J Appl Cardiol* 1: 311-327.
11. Day SM, Westfall MV, Metzger JM (2007) Tuning cardiac performance in ischemic heart disease and failure by modulating myofilament function. *J Mol Med* 85: 911-921.
12. Depre C, Taegtmeyer H (2000) Metabolic aspects of programmed cell survival and cell death in the heart. *Cardiovasc Res* 45: 538-548.
13. Dhalla NS, Elmoselhi AB, Hata T, Makino N (2000) Status of myocardial

antioxidants in ischemia-reperfusion injury. *Cardiovasc Res* 47: 446-456.

14. Di Meo S, Venditti P, De Leo T (1996) Tissue protection against oxidative stress. *Experientia* 52: 786-794
15. Dixon IMC, Hata T, Dhalla NS (1992) Sarcolemmal Na^+-K^+-ATPase activity in congestive heart failure due to myocardial infarction. *Am J Physiol* 262: 664-671.
16. Ferrari R, Ceconi C, Curello S, Cargnoni A, Medici D (1986) Oxygen-free radicals and reperfusion injury: the effects of ischemia and reperfusion on the cellular ability to neutralize oxygen toxicity. *J Mol Cell Cardiol* 18: 67-69.
17. Ferrari R, Ceconi C, Curello S, Guarnieri C, Caldarera CM, Albertini A, Visioli O (1985) Oxygen-mediated myocardial damage during ischemia and reperfusion: role of the cellular defenses against oxygen toxicity. *J Mol Cell Cardiol* 17: 937-945.
18. Hajjar RJ, Leopold JA (2006) Xanthine oxidase inhibition and heart failure. *Circ Res* 98: 169-171.
19. Halmosi R, Deres P, Toth A, Berente Z, Kalai T, Sumegi B, Hideg K, Toth K (2002) 2, 2, 5, 5-tetramethyl pyrroline based compounds in prevention of oxyradical induced myocardial damage. *J Cardiovasc Pharmacol* 40: 854-867.
20. Halmosi R, Berente Z, Osz E, Toth K, Literati-Nagy P, Sumegi B (2001) Effect of poly ADP ribose polymerase inhibitors on the ischemia reperfusion induced oxidative cardiac injury and mitochondrial metabolism in langendroff heart perfusion system. *Mol Pharmacol* 59: 1497-1505.
21. Haramaki N, Stewart DB, Aggarwal S, Ikeda H, Reznick AZ, Packer L (1998) Netwo rking antioxidants in the isolated rat heart are selectively depleted by ischemia–reperfusion. *Free Radic Biol Med* 25: 329-339.
22. Hu CM, Chen YH, Chiang MT, Chau LY (2004) Heme oxygenase-1 inhibits angiotensin II-induced cardiac hypertrophy in vitro and in vivo. *Circulation* 110: 309-316.
23. Huang B, Zhang J, Hou J, Chen C (2003) Free radical scavenging efficiency of nano-Se in vitro. *Free Radic Biol Med* 35: 805-813.
24. Kakkar P, Das B, Viswanathan PN (1984) A modified spectrophotometric assay of superoxide dismutase. *Indian J Biochem Biophys* 21: 130-132.
25. Kaul N, Siveski-Iliskovic N, Hill M, Slezak J, Singal PK (1993) Free radicals and the

heart. *J Pharmacol Toxicol Methods* 30: 55-67.

26. Koyama T, Temma K, Akera T (1991) Reperfusion-induced contracture develops with a decreasing [Ca^{2+}] in single heart cells. *Am J Physiol* 261: 1115-1122.
27. Lanza GM, Winter PM, Caruthers SD, Hughes MS, Cyrus T, Marsh JN, Neubauer AM, Partlow KC, Wickline SA (2006) Nanomedicine opportunities for cardiovascular disease with perfluorocarbon nanoparticles. *Nanomedicine* 1: 321-329.
28. Lemasters JJ, Theruvath TP, Zhong Z, Nieminen AL (2009) Mitochondrial calcium and the permeability transition in cell death. *Biochim Biophys Acta* 1787: 1395-1401.
29. Li J, Ichikawa T, Janicki JS, Cui T (2009a) Targeting the Nrf2 pathway against cardiovascular disease. *Expert Opin Ther Targets* 13: 785-794.
30. Li J, Ichikawa T, Villacorta L, Janicki JS, Brower GL, Yamamoto M, Cui T (2009b) Nrf2 protects against maladaptive cardiac responses to hemodynamic stress. *Arterioscler Thromb Vasc Biol* 29: 1843-1850.
31. Lu Z, Xu X, Hu X, Zhu G, Zhang P, van Deel ED, French JP, Fassett JT, Oury TD, Bache RJ, Chen Y (2008) Extracellular superoxide dismutase deficiency exacerbates pressure overload-induced left ventricular hypertrophy and dysfunction. *Hypertension* 51: 19-25.
32. Mates JM, Perez-Gomez C, Nunez de Castro I (1999) Antioxidant enzymes and human diseases. *Clin Biochem* 32: 595-603.
33. Mohampuria P, Rana N, Kumar Y (2008) Biosynthesis of nanoparticles: technological concepts and future applications. *J Nanopart Res* 10: 507-517.
34. Mugesh G, Singh HB (2000). Synthetic organoselenium compounds as antioxidants: glutathione peroxidase activity. *Chem Soc Rev* 29: 347-357.
35. Neve J (1996) Selenium as a risk factor for cardiovascular disease. *J Cardiovasc Risk* 3: 42-47.
36. Odom AL, Hatwig CA, Stanley JS, Benson AM (1992) Biochemical determinants of adriamycin toxicity in mouse liver, heart and intestine. *Biochem Pharmacol* 43: 831-836
37. Ohta H, Adachi T, Hirano K (1994) Internalization of human extracellular-superoxide dismutase by bovine aortic endothelial cells. *Free Radic Biol Med* 16: 501-507.
38. Oyama K, Takahashi K, Sakurai K (2009) Cardiomyocyte H9c2 cells exhibit

differential sensitivity to intracellular reactive oxygen species generation with regard to their hypertrophic vs death responses to exogenously added hydrogen peroxide. *J Clin Biochem Nutr* 45: 361-369.

39. Padayatty SJ, Katz A, Wang Y, Eck P, Kwon O, Lee JH, Chen S, Corpe C, Dutta A, Dutta SK, Levine M (2003) Vitamin C as an antioxidant: evaluation of its role in disease prevention. *J Am Coll Nutr* 22: 18-35.
40. Perron NR, Hodges JN, Jenkins M, Brumaghim JL (2008) Predicting how polyphenol antioxidants prevent DNA damage by binding to iron. *Inorg Chem* 47: 6153-6161.
41. Rodrigo R, Libuy M, Feliú F, Hasson D (2013) Oxidative stress-related biomarkers in essential hypertension and ischemia reperfusion myocardial damage. *Dis Markers* 35: 773-790.
42. Ramoutar RR, Brumaghim JL (2007a) Investigating the antioxidant properties of oxo-sulfur compounds on metal-mediated DNA damage. *Main Group Chem* 6: 143-153.
43. Ramoutar RR, Brumaghim JL (2007b). Effects of inorganic selenium compounds on oxidative DNA damage. *J Inorg Biochem* 101: 1028-1035.
44. Rice-Evans C, Miller N, Paganga G (1997) Antioxidant properties of phenolic compound. *Trends Plant Sci* 2: 152-159.
45. Rooban BN, Sasikala V, Sahasranamam V, Abraham A (2010) Vitex negundo modulates selenite-induced opacification and cataractogensis in rat pups. *Biol Trace Elem Res* 138: 282-292.
46. Saini HK, Machackova J, Dhalla NS (2004) Role of reactive oxygen species in ischemic preconditioning of subcellular organelles in the heart. *Antioxid Redox Signal* 6: 393-404.
47. Seifried HE, Anderson DE, Fisher EI, Milner JA (2007) A review of the interaction among dietary antioxidants and reactive oxygen species. *J Nutr Biochem* 18: 567-579.
48. Shin YJ, Seo JM, Chung TY, Hyon JY, Wee WR (2011) Effect of cysteamine on oxidative stress-induced cell death of human corneal endothelial cells. *Curr Eye Res* 36: 910-917.
49. Singh A, Lee KJ, Lee CY, Goldfarb RD, Tsan MF (1989) Relation between myocardial glutathione content and extent of ischemia-reperfusion injury. *Circulation* 80: 1795-1804.

50. Szabados E, Fischer GM, Gallyas F Jr, Kispal G, Sumegi B (1999) Enhanced ADP-ribosylation and its diminution of lipomide after ischemia-reperfusion in perfused rat heart. *Free Radic Biol Med* 27: 1103-1113.
51. Tanaka T, Kohno H, Murakami M, Kagami S, El-Bayoumy K (2000) Suppressing effects of dietary supplementation of the organoselenium 1,4 phenylenebis (methylene) selenocyanate and the citrus antioxidant auraptene on lung metastasis of melanoma cells in mice. *Cancer Res* 60: 3713-3716.
52. Tonfektsian MC, Boucher F, Pucheu S, Tamguy S, Ribuot C, Sanou D, Trsallet N, de Leiris J (2000) Effects of selenium deficiency on the response of cardiac tissues to ischemia and reperfusion. *Toxicology* 148: 125-132.
53. Valko M, Rhodes CJ, Moncol J, Izakovic M, Mazur M (2006) Free radicals, metals and antioxidants in oxidative stress-induced cancer. *Chem Biol Interact* 160: 1-40.
54. Venardos KM, Perkins A, Headrick J, Kaye DM (2007) Myocardial ischemia–reperfusion injury, antioxidant enzyme systems, and selenium: a review. *Curr Med Chem* 14: 1539-1549.
55. Venkataraman R, Holcomb MR, Harder R, Knollmann BC, Baudenbacher F (2012) Ratiometric imaging of calcium during ischemia-reperfusion injury in isolated mouse hearts using Fura-2. *Biomed Eng Online*. 19: 11-39.
56. Wang H, Zhang J, Yu H (2007) Elemental selenium at nano size possesses lower toxicity without compromising the fundamental effect on selenoenzymes: comparison with selenomethionine in mice. *Free Radic Biol Med* 42: 1524-1533.
57. Wang Y, Yan X, Fu L (2013) Effect of selenium nanoparticles with different sizes in primary cultured intestinal epithelial cells of crucian carp, Carassius auratus gibelio. *Int J Nanomedicine* 8: 4007-4013.
58. Woo YJ, Zhang JC, Vijayasarathy C, Zwacka RM, Englehardt JF, Gardner TJ, Sweeney HL (1998) Recombinant adenovirus mediated cardiac gene transfer of superoxide dismutase and catalase attenuates postischemic contractile dysfunction. *Circulation* 98: 255-260.
59. Xing Y, Niu T, Wang W, Li J, Li S, Janicki JS, Ruiz S, Meyer CJ, Wang XL, Tang D, Zhao Y, Cui T (2012) Triterpenoid dihydro-CDDO-trifluoroethyl amide protects

against maladaptive cardiac remodeling and dysfunction in mice: a critical role of Nrf2. *PLoS ONE* 7: ID e44899.

60. Zhang J, Wang X, Xu T (2008) Elemental selenium at nano size (nano-Se) as a potential chemopreventive agent with reduced risk of selenium toxicity: comparison with se-methylselenocysteine in mice. *Toxicol Sci* 101: 22-31.
61. Zhang JS, Gao XY, Zhang LD, Bao YP (2001) Biological effects of a nano red elemental selenium. *BioFactors* 15: 27-38
62. Zhang Y, Zhang J, Wang HY, Chen HY (2004) Synthesis of selenium nanoparticles in the presence of polysaccharides. *Mater Lett* 58: 2590-2594.
63. Zhao ZQ (2004) Oxidative stress-elicited myocardial apoptosis during reperfusion *Curr Opin Pharmacol* 4: 159-165.

Chapter 4

Effect of selenium incorporated guar gum nanoparticles against I/R induced alteration in mitochondrial functions

4.1. Introduction

Mitochondria play a very important role in cellular energy metabolism and intracellular signaling processes. About 30% of the volume of a single cardiomyocyte is made up of mitochondria (Hausenloy and Ruiz-Meana 2010). Mitochondria consume the greatest amount (85-90%) of oxygen in cells to allow oxidative phosphorylation, which is the primary metabolic pathway for ATP production. Beyond its function as the cellular powerhouse this complex organelle plays a variety of roles within the cardiomyocyte (Ha and Kim 2010). Mitochondria participates in a number of intracellular processes like initiation of mitochondrial signaling pathways, modulation of cytosolic metabolic pathways, modulation of cytosolic Ca^{2+} signals and determination of cell life or death. In addition, mitochondria are a continuous source of $O_2^{\bullet-}$ anions and their ROS products emerges as potential therapeutic targets especially for heart diseases (Stowe and Camara 2009; Camara *et al* 2010; Koopman *et al* 2010). For normal myocardial function mitochondria exist in a metabolic and cellular ion homeostatic condition. Oxidative damage to mitochondrial membranes, enzymes and electron transport chain (ETC) components leads to impaired mitochondrial ATP production which facilitates mPTP opening (Waldmeier *et al* 2003) that leads to cellular apoptosis and necrosis. Increase in mitochondrial calcium (mCa^{2+}) and ROS generation are two important fundamental factors in the CVD including heart failure, I/R injury and other vascular disease processes. Over the last few years, mitochondria re-emerged into the spotlight of experimental cardiologists; their interest in the potential role of mitochondria in the pathogenesis of cardiac diseases particularly of I/R, has markedly increased (Lesnefsky *et al* 2001). Several studies have attempted to treat heart failure associated with cardiomyopathy by targeting bioenergetic dysfunction (Desai *et al* 2001). The general strategy for primary mitochondrial genetic disorders is supplementation with cofactors, such as coenzyme Q, carnitine, riboflavin and thiamine or antioxidants such as ascorbate. In chapter 3, we had seen the protective effect of SGG towards antioxidant defence system as well as calcium homeostasis during ischemia and I/R. This part of thesis deals

with the beneficial effect of SGG, GGN and Se against various alterations in mitochondrial dynamics during ischemia and I/R. The functional markers of mitochondria like, mitochondrial membrane potential, mitochondrial permeability transition pore, mitochondrial superoxide, mitochondrial electron transport chain enzymes like complexes I, II, III and IV, oxygen consumption, ATP level, alteration in HSP 60 expression, aconitase activity, including hypoxia inducible factor 1 alpha **(**HIF-1α) and atrial natriuretic peptide (ANP) were studied.

4.2. Experimental methods

4.2.1. Materials

Menadione, rotenone, NADH, dichlorophenolindophenol (DCPIP), succinate, EDTA, malonate, oxidized cytochrome c, potassium cyanide (KCN), Tween-20, antimycin A, 3, 3′-diaminobenzidine tablets (DAB), mitoSOX™, calcein AM, cobalt chloride, JC-1 kit were purchased from Sigma Aldrich (St. Louis, USA). Heat shock protein 60 (HSP 60) primary antibody, glyceraldehyde 3 phosphate dehydrogenase (GAPDH) primary antibody and HRP conjugated secondary antibody were purchased from Santacruz USA. All cell based assay kits used were from Cayman, USA. ANP was measured using ELISA kit from Assaypro (St. Charles, USA).

The experimental groups were same as described in chapter 3.

4.2.2. Alteration in ΔΨm and integrity of mPTP

The cells were seeded in 96-well plate in 200 µl of culture medium and subjected to various treatments for ΔΨm and mPTP. The experiment was done as per the protocol provided with the kit (JC-1 kit, Sigma). After respective treatments the cells were stained with JC-1 stain for 20 min at 37 °C and wash with growth medium. The shift of fluorescence was visualized under spinning disk microscope and fluorescence intensity was measured in multiwell plate reader. In normal cells, the JC-1 dye concentrates in the mitochondrial matrix, where it forms red fluorescent aggregates because of the electrochemical potential gradient. Dissipation of ΔΨm prevents the accumulation of JC-1 in the mitochondria and thus it is dispersed throughout the cell, leading to a shift from red (J-aggregates) to green fluorescence (JC-1 monomers) (Javadov *et al* 2006). For JC-1 monomers, the fluorimeter was set at 490 nm excitation and 530 nm emission wavelengths and for J- aggregates, the fluorimeter was set at 525 nm excitation and 590 nm emission wavelengths.

Integrity of mPTP was detected by treating the cells with 0.25 µM calcein-AM in the presence of 8 mM cobalt chloride for 30 min to quench cytosolic and nuclear calcein loading. The calcein fluorescence is then compartmentalized within mitochondria until mPTP opening permits the distribution of cobalt inside mitochondria, which results in the quenching of calcein fluorescence in the mitochondrial matrix (Petronilli *et al* 1999). Images of the cells were observed at 488 nm excitation and 525 nm emission. Bongkrekic acid, an inhibitor of the adenine nucleotide translocase and mPTP opening, was used as negative control. Cells were exposed to bongkrekic acid (5 mM) for 20 min before loading calcein and cobalt chloride.

4.2.3. Mitochondrial superoxide generations and alterations in mitochondrial enzyme complexes

Mitochondrial superoxide productions in the cells were evaluated with fluorescent dye, mitoSOX™. This dye selectively detects $O_2^{\bullet-}$ in the mitochondria of live cells. The cells were spread in 96-well black plates at a density of 5×10^3 cells per well. After respective treatments, the cells were incubated with mitoSOX™ (5 mM) in the HBSS (Hank's balanced salt solution) and incubated for 20 min. For bioimaging the dye was excited at 514 nm as described earlier (Mukhopadhyay *et al* 2007).

For determining the alteration in mitochondria after respective treatments, mitochondria were isolated using a mitochondrial isolation kit (Sigma-Aldrich, USA). The cells were trypsinized and centrifuged for 5 min at 600×g and the pellets were washed in ice cold PBS and again centrifuged them for 5 min at 600×g at 4 °C. The supernatant was discarded. To that, 2 ml of the extraction buffer A was added and incubated on ice for 15 min. The cells were homogenized at -20 °C and the homogenized cells were centrifuged at 600×g for 10 min at 4 °C. The supernatants were transferred to a fresh tube and centrifuged at 11,000×g for 10 min at 4 °C. The supernatants were removed and the pellets were dissolved in 200 µl of CelLytic M Cell Lysis Reagent with Protease Inhibitor Cocktail [1:100 (v/v)] for the determination of protein.

The effect of Se, GGN and SGG on complex I-mediated electron transfer (NADH dehydrogenase) was studied using NADH as the substrate and menadione as electron acceptor. The reaction mixture containing 200 mM menadione and 150 mM NADH was prepared in phosphate buffer (0.1 M, pH 8.0). To this mitochondria (100 µg) was added, mixed immediately and observed quickly for change in the absorbance (ΔOD) at 340 nm

for 8 min (Paul *et al* 2007; Schulte and Weiss 1995).

Complex II mediated activity (succinate dehydrogenase) was measured spectrophotometrically at 600 nm using DCPIP as an artificial electron acceptor and succinate as substrate. The extent of decrease of absorbance (ΔOD) was considered as the measure of the electron transfer activity of complex II (Paul *et al* 2007; Robinson and Lemire 1995). The reaction mixture was prepared in 0.1 M phosphate buffer (pH 7.4) containing 10 mM EDTA, 50 mM DCPIP, 20 mM succinate and mitochondria (50 µg). The change in absorbance was observed immediately for 8 min at 30 °C.

Complex III (decylubiquinol cytochrome *c* oxidoreductase) activity was determined as per the method described previously (Spinazzi *et al* 2012). In brief mitochondrial protein (50 µg) was mixed with 730 µl distilled water, 50 µl of potassium phosphate buffer (0.5 M, pH 7.5), 75 µl of oxidized cytochrome *c*, 50 µl of KCN (10 mM), 20 µl of EDTA (5 mM, pH 7.5), 10 µl of Tween-20 [2.5% (vol/vol)] in a final volume of 1 ml. A parallel well was run with same quantity of reagents and 10 µl 1 mg/ml of antimycin A. The reaction was started by adding 10 µl of 10 mM decylubiquinol, mixed rapidly and then the increase in absorbance at 550 nm for 2 min was observed. Activity of complex III was calculated by subtracting total complex III activity (without antimycin A) and antimycin A-resistant activity (with antimycin A) and expressed as nmol/min/mg of total proteins.

Complex IV activity of mitochondria was assayed in control and treated cells using respective kits from Sigma Aldrich chemicals (USA) as per manufacturer's instructions. Briefly, 950 µl of 1X assay buffer was added to a cuvette and then 10 µg of mitochondrial suspension was added and brought the reaction volume to 1.05 ml with 1X enzyme dilution buffer. The reaction was initiated by the addition of 50 µl of ferrocytochrome c substrate solution. Absorbance was read at A_{550}/min. The activity of the sample was expressed in U/ml.

4.2.4. Oxygen consumption and ATP determination assay

Oxygen consumption rate in control and treated cells were assayed using Cayman's cell based oxygen consumption rate assay kit using antimycin A as standard inhibitor. Cayman's oxygen consumption rate assay kit utilizes phosphorescent oxygen probe to measure oxygen consumption rate. After respective treatments, the culture medium was removed and replaced with fresh medium. Blank wells were added with

culture medium alone. Then 10 µl MitoXpress®-Xtra solution was added to all wells except blank wells and then 100 µl of HS mineral oil over each well. The fluorescence was read at excitation; 380 nm and emission; 650 nm kinetically for 150 min.

ATP in control, ischemic, I/R and treated cells were assayed using ATP determination kit (Molecular Probes®, Life Technologies, USA). It is a bioluminescence assay for quantitative determination of ATP with recombinant firefly luciferase and its substrate D-luciferin. The assay is based on luciferase's requirement for ATP in producing light (emission maximum 560 nm at pH 7.8). Standard reaction solution was made as follows: the standard reaction mixture consisting of 8.9 ml distilled water, 0.5 ml 20X reaction buffer, 0.1 ml 0.1 M DTT, 0.5 ml of 10 mM D-luciferin, 2.5 µl of firefly luciferase (5 mg/ml stock solution) and 100 µl sample was mixed gently and the luminescence was read at 560 nm.

4.2.5. Alterations in HSP 60 protein in cardiac ischemia and I/R

Immunoblotting was conducted to see the variation in the level HSP 60 protein. For this, H9c2 cells were seeded in a T25 flask containing 5 ml of DMEM medium and treatments were carried out. At the end of the treatments, the H9c2 cells were harvested and lysed with ice-cold cell lysis solution (RIPA buffer containing a protease inhibitor cocktail) and the homogenate was centrifuged at 10,000×g for 15 min at 4 °C. Total protein in the supernatant was quantified using a BCA protein assay kit (Pierce, Rockford, IL USA). Total protein (40 µg) from each sample was separated by 10% SDS-PAGE at 55 V. 25 µl of experimental samples was loaded in each wells. The protein in the gel was transferred into polyvinylidene difluoride (PVDF) membrane using Trans-Blot Turbo™ (Bio-Rad). The membrane was blocked with BSA in TBST (Tris buffered saline-Tween 20) for 1 h at room temperature, and then incubated with the primary antibodies specific to HSP 60 (1:500), and GAPDH (1:500) with gentle agitation at 4 °C overnight. The incubation was followed by 3 times wash with TBST for 10 min in a shaker, followed by HRP-conjugated secondary antibodies (1:1000) in 0.25% BSA in TBST for 60 min at room temperature with continuous shaking. After three washes with TBST, the membranes were developed using DAB tablets (Sigma Aldrich, St Louis, MO, USA) and the relative intensity of bands were quantified using Bio-Rad Quantity One version 4.5 software in a Bio-Rad gel doc. The quantity of HSP 60 in cell lysate was normalized with the content of GAPDH.

4.2.6. Determination of aconitase activity

Activity of aconitase, was assayed in control and treated cells using kits from Cayman chemicals. This assay utilizes the coupled enzymatic reactions of citrate to isocitrate by aconitase and isocitrate to α-ketoglutarate by isocitrate dehydrogenase. The assay was based upon the measurement of formation of NADPH from $NADP^+$. NADPH reacts with the fluorescent substrate to yield a highly fluorescent product. The fluorescent product was analysed with an excitation wavelength of 535 nm and an emission wavelength of 590 nm. The rate of NADPH was proportional to aconitase activity. For performing the assay, 50 µl of activated aconitase was added to the aconitase positive wells and 50 µl of sample to the wells. Then 10 µl of 1X assay buffer, 50 µl of $NADP^+$ reagent, 50 µl of isocitric dehydrogenase, 10 µl of reconstituted enzyme mixture and 10 µl of reconstituted fluorometric detector were added to all the wells. The reaction was initiated by adding 50 µl of diluted substrate solution to all wells and the fluorescence was read once every minute using an excitation wavelength of 535 nm and an emission wavelength of 590 nm for 30 min at 37 °C.

4.2.7. HIF-1 α level

After respective treatments as described in chapter 3, the cells were collected by centrifugation and using Cayman's nuclear extraction kit, nuclear proteins were isolated. After nuclear extraction the HIF-1 α level was detected. Briefly a specific double stranded DNA sequence containing the HIF-1 α response element immobilised to the well was used in this procedure. The HIF transcription complex was detected by the addition of a HIF-1 α primary antibody (1:100) directed against HIF-1 α. The primary antibody was added to all wells except blank. After adding primary antibody the plate was incubated for 1 h at room temperature. Then the wells were emptied and washed 5 times with 200 µl 1X wash buffer. Then a secondary antibody conjugated to HRP (goat anti-rabbit HRP (1:100)) was added and incubated for 1 h at room temperature. Again it was emptied and the wells were washed 5 times with 200 µl 1X wash buffer. 100 µl of transcription factor developing solution were added to all the wells and again incubated the plates for 45 min at room temperature in dark. Finally, 100 µl of stop solution was added to all the tubes and the absorbance were read at 450 nm.

4.2.8. Determination of ANP

After respective treatments cell culture media were centrifuged at 2000×g for 10 min to remove debris and the supernatant was used to detect the concentration of ANP using ELISA kit (AssayPro USA). The assay employs a quantitative sandwich enzyme immunoassay technique that measures ANP in a relatively short time. A microplate coated with polyclonal antibody specific for ANP was used for analysis. The ANP in standards and samples were sandwiched by the immobilized antibody and biotinylated polyclonal antibody specific for ANP, which was recognized by a streptavidin-peroxidase conjugate. All unbound materials were then washed away and a peroxidase enzyme substrate (peroxidase chromogen substrate tetramethylbenzidine) was added. The colour development was stopped by using 0.5 N HCl and the intensity of the colour was measured at 540 nm.

4.2.9. Statistical analysis

Results were expressed in mean and standard deviation (SD) of the control and treated cells from three independent experiments with duplicate (n=6). Data were subjected to one-way ANOVA followed by the Bonferroni test to calculate the statistical difference among the groups using SPSS for Windows, standard version 11.5.1 (SPSS, Inc.) and significance was accepted at $P \leq 0.05$.

4.3. Results

4.3.1. Effect of SGG on ΔΨm and mPTP

Analysis of ΔΨm of mitochondria during ischemia and I/R revealed significant dissipation (depolarization) of the same during ischemia and I/R (Figure.4.1A.b, c) compared with control (Figure.4.1A.a). In normal cells the JC-1 dye concentrates in mitochondrial matrix and form red fluorescent aggregates due to the existence of electrochemical potential gradient. Alteration of ΔΨm prevents the accumulation of JC-1 in the mitochondria and gets dispersed throughout the cells leading to a shift from red (JC-1 aggregates) to green fluorescence (JC-1 monomers). The dissipation of ΔΨm was more severe with ischemia compared to I/R. All the doses of test materials were effective to prevent the dissipation of mitochondria compared to I/R. Among the test materials, SGG (Figure.4.1A.h, i) was found to be better compared to others in keeping ΔΨm intact (Figure.41A.d-g).

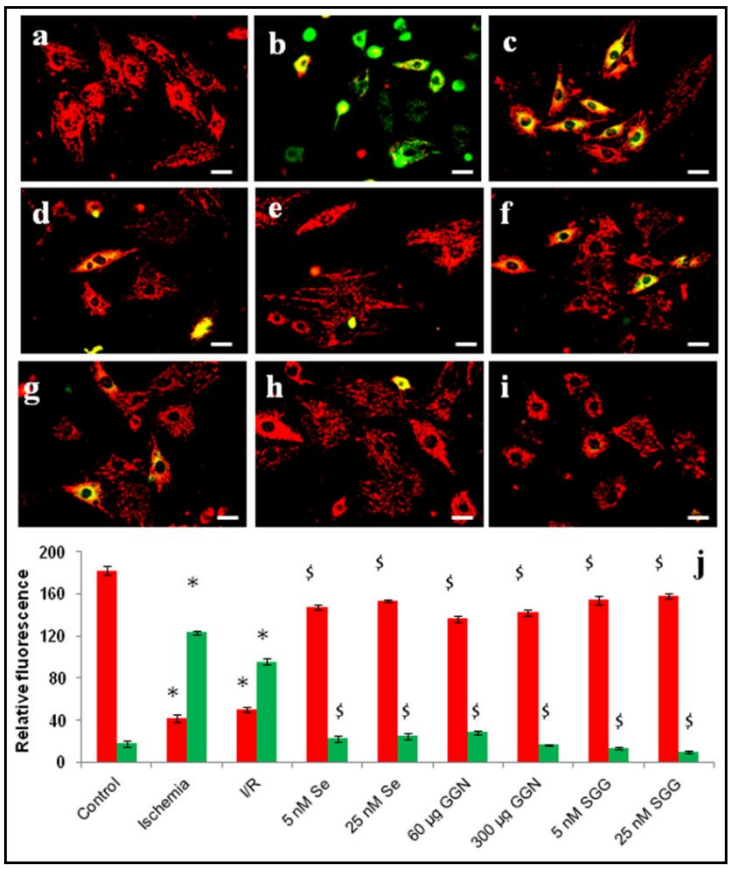

Figure 4. 1A. Mitochondrial transmembrane potential determined by JC-1 staining. The representative images are merged images of JC-1aggregates and JC-1 monomers. JC-1 aggregates are more in control cells revealing intact mitochondria and the formation of JC-1 monomers in ischemic and I/R cells shows dissipation of Δψm. (a) control cells; (b) ischemic cells; (c) I/R cells; (d, e) cells treated with 5 nM and 25 nM Se (f, g) cells treated with 60 µg and 300 µg of GGN; (h, i) cells treated with 5 nM and 25 nM SGG; and (j) relative fluorescence intensity analysis. The Se, GGN and SGG treated groups were compared with I/R group. The ischemic and I/R groups were compared with the control group. * Indicates that the mean value was significantly different from the control cells ($P \leq 0.05$). $ Indicates mean value was significantly different from I/R cells ($P \leq 0.05$). Scale bar corresponds to 100 µm.

Like Δψm, severe alteration in the integrity of mPTP was observed during ischemia and I/R which was evident in calcein AM-cobalt chloride staining. Cells stained with calcein showed punctiform fluorescence revealing the normal integrity of mPTP (closed state) *via* blocking diffusion of any materials (Figure.4.1B.a). But the loss of integrity of mPTP was clearly evident during ischemia and I/R with diffusion of calcein fluorescence to the mitochondria (Figure.4.1B.b, d). Loss of integrity of mPTP was also observed with bongkerkic acid (Figure.4.1B.c). Here also all the doses of test materials (Se, GGN and SGG) were effective to keep the integrity of mPTP intact. Among the test

materials SGG (Figure.4.1B.i, j) showed better protection in a dose dependent way.

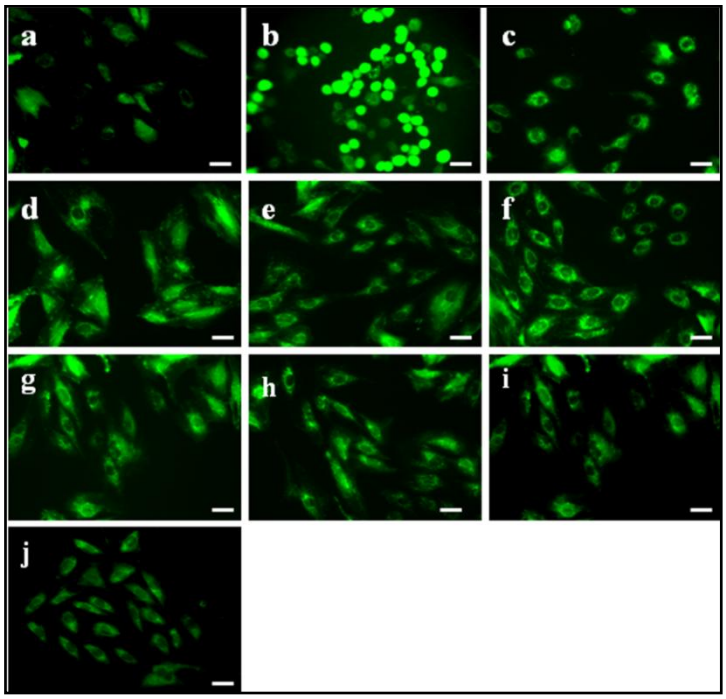

Figure 4. 1B. Integrity of permeability transition visualized by calcein AM and cobalt chloride staining: (a) control; (b) ischemic cells; (c) bongkrekic acid; (d) I/R cells; (e, f) cells treated with 5 nM and 25 nM Se; (g, h) cells treated with 60 µg and 300 µg of GGN; and (i, j) cells treated with 5 nM and 25 nM SGG. Scale bar corresponds to 100 µm.

4.3.2. Effect of SGG on mitochondrial superoxide production and respiratory enzyme complexes

$O_2^{\bullet-}$ production was detected by bioimaging with MitoSOX™ Red and found surplus generation of the same in ischemic and I/R groups (Figure.4.2.b, c) compared to the control cells (Figure.4.2.a). Fluorescence intensity analysis also showed increase of fluorescence in ischemia (34.5±0.866) and I/R (29.5±0.500) compared to control (15.67±0.577) indicating surplus $O_2^{\bullet-}$ generation. All the test materials (Se, GGN and SGG) showed protective effect in scavenging the generation of $O_2^{\bullet-}$ production (Figure.4.2.d-g). Among various groups SGG showed comparatively better result against $O_2^{\bullet-}$ generation (Figure.4.2.h-i).

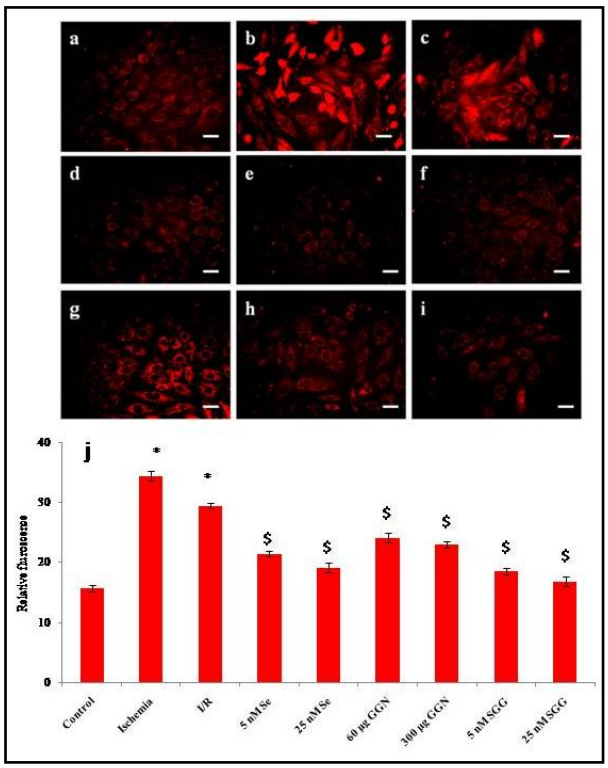

Figure. 4. 2. Fluorescent microscopic images of H9c2 cells stained with MitoSOX™ Red indicator to show mitochondrial superoxide generations in H9c2 on various treatments (original magnification 20x). (a) control cells; (b) ischemic cells; (c) I/R cells; (d, e) cells treated with 5 nM and 25 nM Se; (f, g) cells treated with 60 µg and 300 µg of GGN; and (h, i) cells treated with 5 nM and 25 nM SGG (j) relative fluorescence intensity analysis. The Se, GGN and SGG treated groups were compared with I/R group. The ischemic and I/R groups were compared with the control group. * Indicates that the mean value was significantly different from the control cells ($P \leq 0.05$). $ Indicates mean value was significantly different from I/R cells ($P \leq 0.05$). Scale bar corresponds to 100 µm.

The ETC is composed of NADH-ubiquinone oxidoreductase (complex I), succinate dehydrogenase (complex II), ubiquinol cytochrome C oxidoreductase (complex III), and cytochrome C oxidase (complex IV). Table 4.1 shows the activities of mitochondrial respiratory complexes in control and treated cells. The activities of respiratory chain complexes such as complexes I, III and IV were significantly decreased in ischemia and I/R groups compared to control groups ($P \leq 0.05$).

According to the bioenergetic principle a decrease in bioenergy transfer leads to the inhibition of respiration. Complex I substrate mediated respiration was measured from change in absorbance (ΔOD 340 nm) at 340 nm for 8 min. Normal cells are found to have high respiratory activity compared to ischemia and I/R groups. This was calculated from the change in absorbance in 8 min. Control group showed high rate of change in

absorbance indicating high rate of respiration compared to ischemia and I/R groups where change in absorbance was less due to the inhibition of complex I mediated respiration. Ischemia and I/R showed (0.060±0.002 and 0.064±0.002 ΔOD 340 nm) decrease in complex I activity compared to control (0.108±0.002 ΔOD 340 nm) whereas 5 and 25 nM SGG showed (0.101±0.002 and 0.094±0.002 ΔOD 340 nm) recovery of activity compared to I/R. The details of the activities of other test materials are given in Table 4.1. There was no significant change in complex II respiration with any of the groups. Respiration mediated by complex III (complex III activity) was measured by the difference between the sample without antimycin A and with antimycin A.

The complex III activity of ischemia and I/R was 5.207±0.109 and 6.801±0.114 nmol/min/mg protein respectively compared to control (9.699±0.054 nmol/min/mg protein). There was a significant ($P \leq 0.05$) inhibition of complex III activity with ischemia and I/R. Here also, all the test materials (Table 4.1) showed recovery of complex III activity. Among all, both doses of SGG (8.176±0.065, 9.082±0.188 nmol/min/mg protein) showed better result in maintaining the respiration unaltered.

The complex IV activity of ischemia and I/R was 0.594±0.004 and 0.656±0.027 µmol of ferrocytochrome c/min/ml respectively compared to control (0.907±0.037 µmol of ferrocytochrome c/min/ml). All the material was able to protect the depletion of complex IV during ischemia and I/R. Among the test materials 5 and 25 nM of SGG (0.800±0.011 and 0.885±0.036 µmol of ferrocytochrome c/min/ml) showed slightly better activity (Table 4.1).

Table 4. 1. Activities of mitochondrial respiratory complexes in control and treated cells.

	ComplexI(ΔOD 340 nm)	ComplexII(ΔOD 600 nm)	Complex III(nmol/min/mg protein)	Complex IV(µmolof ferrocytochrome c /min/ml)
Control	0.108 ± 0.002	0.001 ±0.0004	9.699±0.054	0.907±0.037
Ischemia	0.060 ± 0.002*	0.001 ±0.0003*	5.207±0.109*	0.594±0.004*
I/R	0.064 ± 0.004*	0.001±0.0004*	6.801±0.028*	0.656±0.027*
Se (nM)				
5	0.068 ± 0.003	0.001±0.0001	5.661±0.072$	0.721±0.037$
25	0.076 ± 0.001	0.001 ±0.0003	6.047±0.021$	0.736±0.032$
GG (µg)				
60	0.077 ± 0.002	0.001 ±0.0005	5.951±0.060$	0.705±0.036$
300	0.072 ± 0.003	0.001 ±0.0003	6.423±0.013$	0.818±0.027$
SGG (nM)				
5	0.101 ± 0.002$	0.001 ±0.0004	8.176±0.065$	0.800±0.011$
25	0.094 ± 0.002$	0.001 ± 0.0005	9.082±0.188$	0.885±0.036$

Each value represents mean ± SD (n=6). * Mean value was significantly different from the control cells (P≤0.05). $ Mean value was significantly different from I/R group (P≤0.05).

4.3.3. Oxygen consumption and ATP level in control and treated cells

Oxygen consumption rate in living cells were analyzed by observing change in fluorescence signal over time of two and half hours. More change in fluorescence indicates more consumption of oxygen by cells. This in turn shows better metabolic status of cells. Ischemia and I/R cells showed a reduced consumption of oxygen rate (55.39% and 58.28% compared to control). Treatment with Se, GGN and SGG showed improvement in oxygen consumption rate compared with I/R group (Figure.4.3). SGG group (85% with 5 nM and 81% with 25 nM) with better oxygen consumption seems to be more effective against mitochondrial dysfunction in ischemia and I/R.

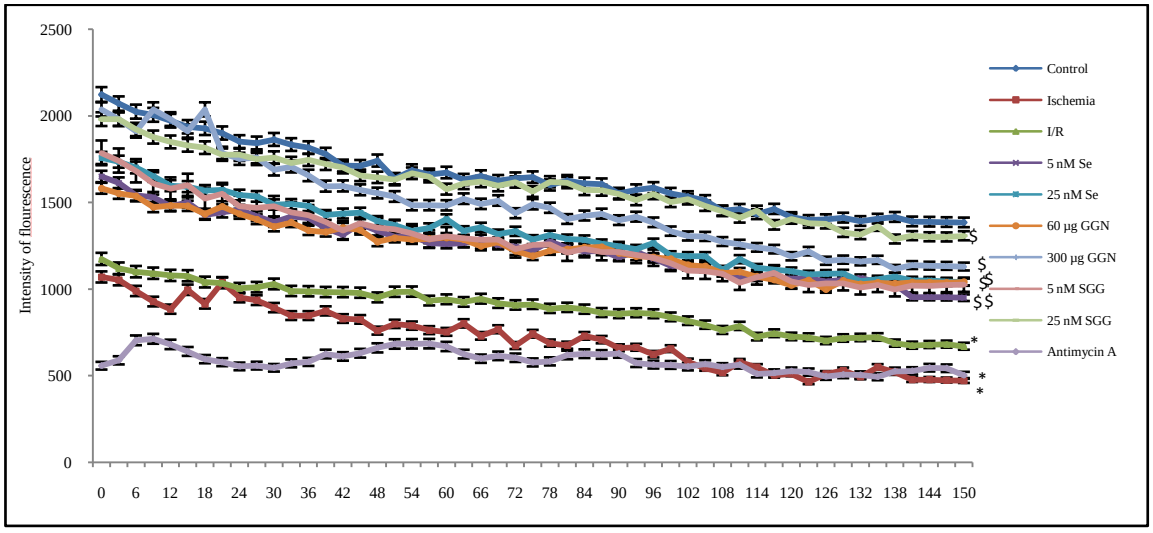

Figure 4. 3. Oxygen consumption rate in different groups. Reduction in fluorescence indicates lower oxygen consumption rate in the cells. Each value represents mean ±SD (n=6). The ischemic and I/R groups were compared with the control group. The Se, GGN and SGG treated groups were compared with I/R group. * Indicates that the mean value was significantly different from the control cells (P≤0.05). $ Indicates that the mean value was significantly different from I/R cells (P≤0.05).

The level of ATP was decreased in ischemia (4.59±0.14 picomoles) and I/R (4.66±0.12 picomoles) groups compared to control (6.62±0.13 picomoles). Like previous results, all the treatment groups showed protection from depletion of ATP over other test materials. In this case too, 5 nM (6.42±0.29 picomoles) and 25 nM (6.61±0.15 picomoles) SGG showed slightly better activity in maintaining the level of ATP nearer to control (Figure.4.4).

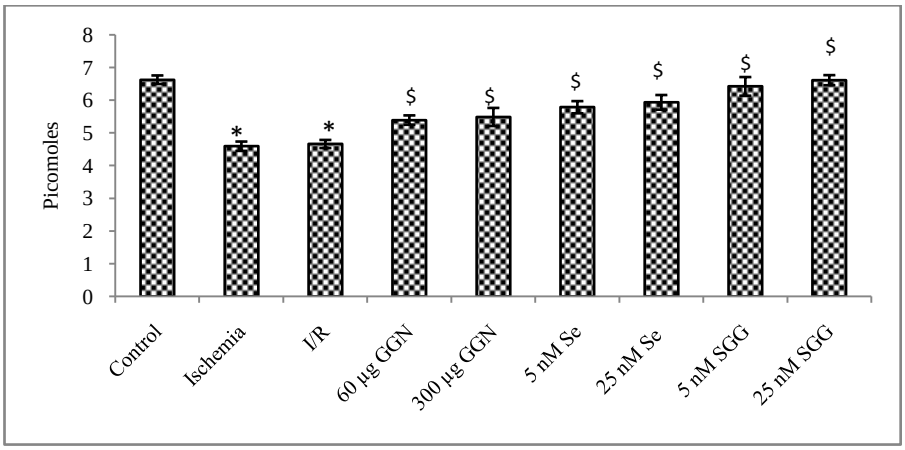

Figure 4. 4. ATP content in control and treated H9c2 cells after I/R. Values are means ±SD represented by vertical bars (n=6). The ischemic and I/R groups were compared with the control group. The Se, GGN and SGG treated groups were compared with I/R group. * Indicates that the mean value was significantly different from the control cells (P≤0.05). $ Indicates that the mean value was significantly different from I/R cells (P≤0.05).

4.3.4. Role of HSP 60 in I/R

The normal myocardium revealed a decreased but detectable baseline expression of HSP 60 (Figure.4.5.a). HSP 60 has been found to be correlated with mitochondria specific cell stress. Protein expression of HSP 60 was found to be increased in ischemia (200%) and I/R (190%). HSP 60 protectes rat neonatal cardiac myocytes (H9c2) cells against ischemia injury. The protein expression was decreased in SGG (130%) treated groups showing the protective role of SGG (Figure.4.5.f).

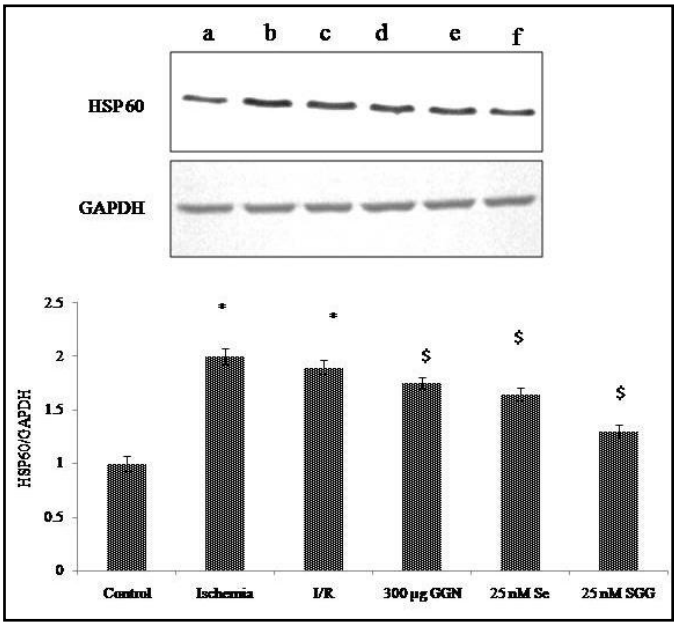

Figure 4. 5. HSP 60 expression in control and treated H9c2 cells after I/R. The amount of HSP 60 and GAPDH was detected with respective antibodies. The ischemic and I/R groups were compared with the control group. The Se, GGN and SGG treated groups were compared with I/R group. Lane a: control, b: ischemia, c: I/R d: GGN, e: Se, f: SGG. Results are representative of three independent experiments.* Indicates that the mean value was significantly different from the control cells ($P \leq 0.05$). $ Indicate mean value was significantly different from I/R cells ($P \leq 0.05$).

4.3.5. Aconitase activity

The aconitase activity was significantly reduced in ischemia (0.772±0.060 nm/min/ml) and I/R group (0.884±0.052 nm/min/ml) compared to control group (1.640±0.084 nm/min/ml). It is also worth to mention that all the test materials showed tendency to bring back the enzyme level to some extend of control level. 5 nM (1.564±0.063 nm/min/ml) and 25 nM (1.682±0.062 nm/min/ml) of SGG treatment significantly ($P \leq 0.05$) reversed the changes and brought back the activity near to normal (Figure.4.6).

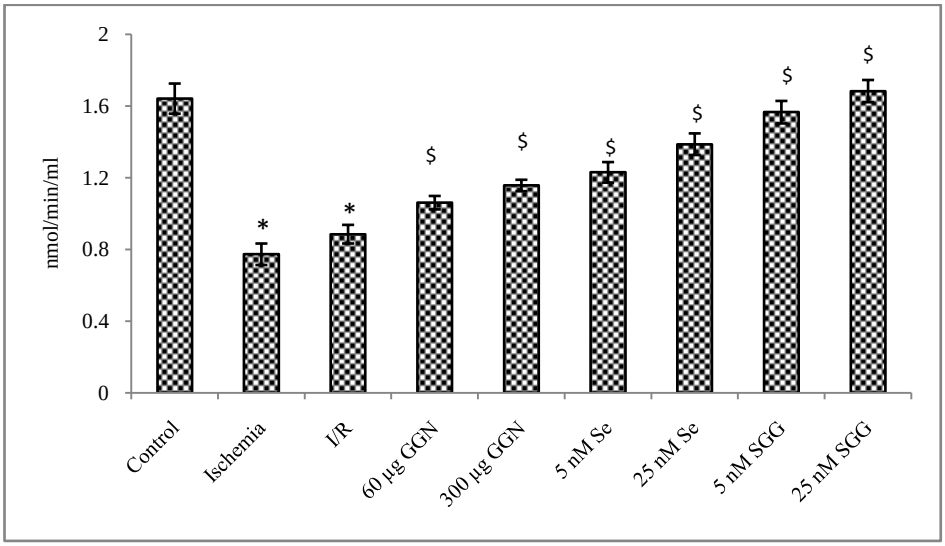

Figure 4. 6. Aconitase enzyme activities in different treated groups. Values are means ±SD represented by vertical bars (n=6). The ischemic and I/R groups were compared with the control group. The Se, GGN and SGG treated groups were compared with I/R group. * Indicates that the mean value was significantly different from the control cells (P≤0.05). $ Indicates that the mean value was significantly different from I/R cells (P≤0.05).

4.3.6. Effect of SGG on HIF-1 α activity

HIF-1 α activity was expressed as OD at 450 nm. There was a significant increase in HIF-1 α in ischemia (0.232±0.006) and I/R groups (0.195±0.005) compared to control (0.095±0.004). On the other hand treatments with all the test materials (Figure.4.7) reduced HIF-1 α expression. Analysis revealed that 5 nM (0.094±0.004) and 25 nM (0.085±0.004) SGG was more effective in reducing the expression compared to other test materials (Figure.4.7).

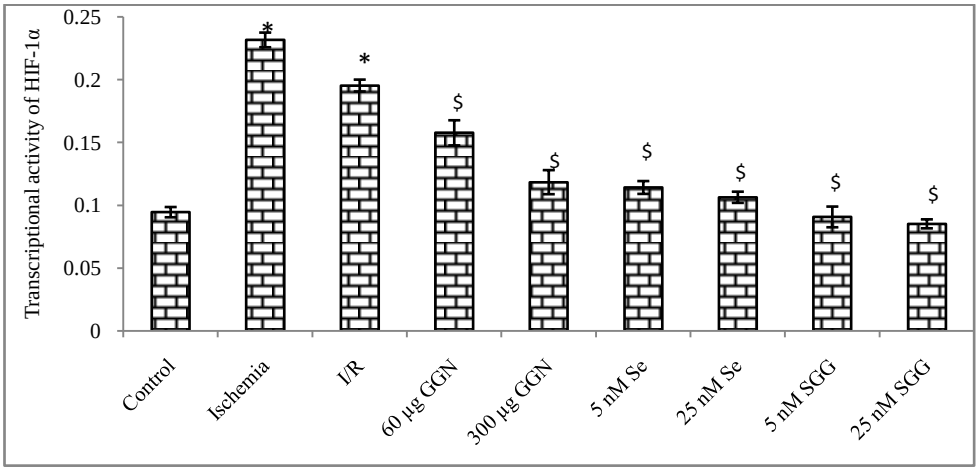

Figure 4. 7. HIF-1 α transcription factor in nuclear extract of control, ischemia, I/R and treated cells. Values are means ±SD represented by vertical bars (n=6). The ischemic and I/R groups were compared with the control group. The Se, GGN and SGG treated groups

were compared with I/R group. * Indicates that the mean value was significantly different from the control cells (P≤0.05). $ Indicates that the mean value was significantly different from I/R cells (P≤0.05).

4.3.7. Effect of SGG on ANP level

In this study the level of ANP is increased in ischemia (1.07±0.04 ng/ml) and I/R (0.995±0.03 ng/ml) groups compared to control (0.572± 0.025 ng/ml). The treatment with all the test materials shows protective effect to bringing back the ANP level towards normal (Figure.4.8). Among the groups 5 and 25 nM SGG (0.623±0.03 and 0.567±0.03 ng/ml) showed better activity in bringing back the ANP level toward to normal compared to other groups (Figure.4.8).

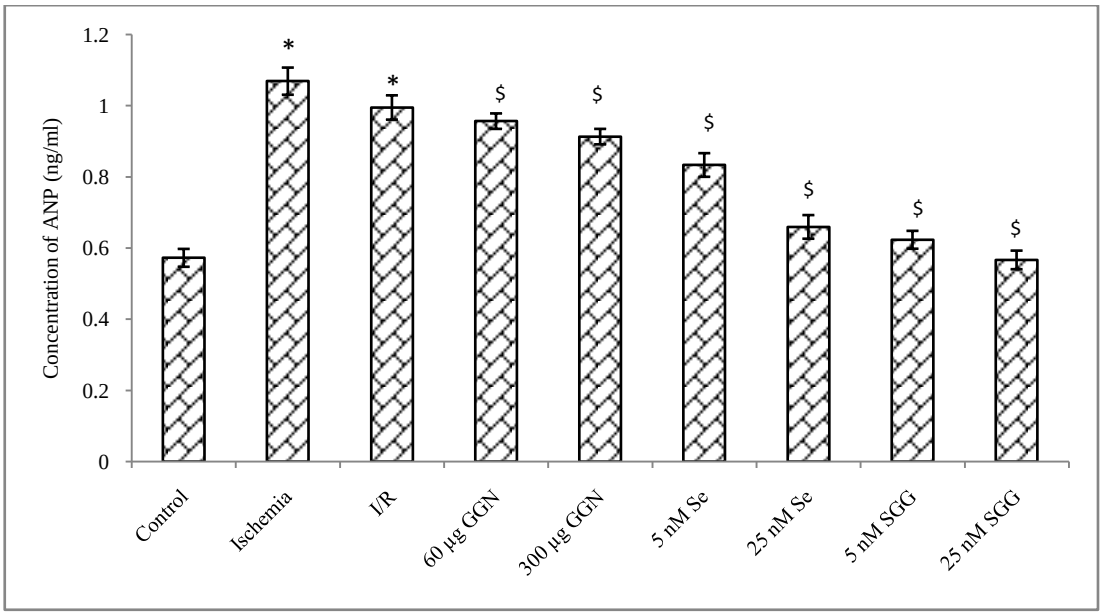

Figure 4. 8. Changes in ANP level in control, ischemia, I/R and treatment groups. Values are means ±SD represented by vertical bars (n=6). The ischemic and I/R groups were compared with the control group. The Se, GGN and SGG treated groups were compared with I/R group. * Indicates that the mean value was significantly different from the control cells (P≤0.05). $ Indicates that the mean value was significantly different from I/R cells (P≤0.05).

4.4. Discussion

Mitochondria are critical for cell survival because of their roles as metabolic energy producers and as regulators of programmed cell death. To protect cardiac myocytes from death, it is important to maintain mitochondrial integrity. Loss of mitochondrial membrane integrity is considered a point of no return so the preservation of mitochondrial integrity is of utmost importance in the design of cardioprotective

therapies. The normal performance and survival of cardiac cells depend on the maintenance of the mitochondrial membrane potential. ΔΨm represents an important marker of mitochondrial integrity. Measurement of ΔΨm is therefore essential for knowing the molecular mechanisms of the effect of test materials (Mathur *et al* 2000). Mitochondria are a major source of ROS, which are the by products of mitochondrial electron transfer activity. During oxidative stress, mitochondria may become susceptible to damage by ROS and ΔΨm is an important factor involved in the regulation of ROS production. Skarka and Ostadal (2002) had reported about I/R induced structural changes of cardiac mitochondria which is accompanied by an alteration of mitochondrial function. Kim *et al* (2003) had reported the protective effect of Se compounds in maintaining the ΔΨm in HepG2 cells. In this study, we observed dissipation of ΔΨm in ischemia and I/R cells on JC-1 staining and all the test materials prevent ΔΨm dissipation among them, SGG was found more specifically prevents mitochondrial depolarization and thereby preserve mitochondrial function.

Another important therapeutic target for knowing the mitochondrial integrity is mPTP opening. Mitochondria with reduced ability to support ΔΨm are more susceptible to mPTP because depolarization of ΔΨm directly increases the opening of mPTP. Prolonged oxidative stress causes decline in ΔΨm due to mild uncoupling and this leads to the opening of mPTP (Skarka *et al* 2002). Crompton *et al* (1987) were the first to state mPTP opening plays a crucial role in myocardial I/R injury. The mPTP is a voltage dependent high conductance channel allowing the rapid equilibration of metabolites and ions (Zoratti and Szabo1995). Under normal physiological conditions, the mitochondrial inner membrane is impermeable to almost all metabolites and ions. The compounds that enter or leave the mitochondria are generally transported *via* specific and controlled carriers. mPTP opening dramatically changes the properties of the inner membrane making it unspecifically permeable to molecules smaller than 1500 daltons (Zoratti and Szabo1995). The fate of the cell is then determined by the extent of mPTP opening. If minimal, the cell may recover and live; if moderate, the cell may undergo programmed cell death; if severe, the cell will die from necrosis due to inadequate energy production. In this study, mPTP opening was observed in ischemic groups and all the test materials were protective in preventing the mPTP opening. Among all, SGG was found to be better in keeping the integrity of mPTP.

During mitochondrial respiration, electrons are released from their normal transport pathway to molecular oxygen at complexes I and III (Jacobson 1996) resulting in formation of the $O_2^{\bullet-}$. $O_2^{\bullet-}$ is the primary ROS formed by monovalent reduction in the ETC. Elevated $O_2^{\bullet-}$ radical generation affects the normal functioning of mitochondria. The enzyme XO also plays significant role in cardiovascular pathology and these are the major enzymatic source of ROS in cardiovascular system (Kelley *et al* 2010). Increase in the activities of these enzyme leads to increased production of $O_2^{\bullet-}$ radicals that ultimately lead to cardiac dysfunction (Yokoyama *et al* 1990). In chapter 3, we reported the activity of XO was increased in ischemia and I/R groups and SGG protected the cells from the elevation of XO compared with other test materials effectively. This support the observation of surplus generation of $O_2^{\bullet-}$ generation with mitoSOX^{TM} staining. Ischemia and I/R groups showed increasing $O_2^{\bullet-}$ while treatment with test materials prevented the generation of $O_2^{\bullet-}$.

As there is an increased generation of $O_2^{\bullet-}$ radicals during ischemia and I/R and this may be due to the decreased activity of respiratory enzymes in ETC. So we checked the activities of respiratory enzymes. There are reports that the activities of mitochondrial electron transport chain complexes are decreased in CVD (Chen *et al* 2008). As discussed earlier, in mitochondria direct reduction of oxygen to $O_2^{\bullet-}$ occurs in the flavoprotein region of NADH dehydrogenase segment (complex I) of the respiratory chain (Arora *et al* 2002). Complex I is a multisubunit integral membrane complex of the mitochondrial electron transport chain that catalyzes electron transfer from NADH to ubiquinone. It is considered an important site of $O_2^{\bullet-}$ anion generation in mitochondria (Hansford *et al* 1997) and in normal condition the $O_2^{\bullet-}$ is scavenged by the mitochondrial enzyme SOD to produce H_2O_2. Thus, a defect of complex I activity can be considered a potential source of ROS in heart I/R. Here also the complex I activity was decreased in ischemic and I/R groups. The treatment with SGG showed better activity in retaining the activity of complex I. Mendelev *et al* (2012) reported that selenite treatment significantly increases mitochondrial respiration in murine hippocampal neuronal cells. In this study there was no significant activity in complex II enzyme.

The activity of complexes III was reduced in ischemic and I/R rat hearts. $O_2^{\bullet-}$ generation is enhanced at complex III during hypoxia *via*, auto-oxidation of ubiquinone on both sides of mitochondrial inner membrane. In this study, the complex III activity

was decreased in ischemia and I/R groups and all the treatment groups showed protective effect. Treatment with SGG showed better effect in maintaining the complex III activity. Indeed, published studies have reported that dietary Se protects against increase in the activities of mitochondrial respiratory chain complexes II, III, and IV (Desai *et al* 2001). Complex IV is the terminal enzyme of the ETC which catalyzes the final step of electron transfer from reduced cytochrome *c* to oxygen to make H_2O. Complex IV is also one of the three proton pumps along with complexes I and III that generate the proton gradient across the inner mitochondrial membrane leading to ATP synthesis. Cytochrome oxidase inhibition does not increase ROS production from complex IV (Babcock and Wikstro1992; Varotsis *et al* 1993) but leads to increased reduction of redox centers in complex I or complex III, enhancing electron leak and ROS generation from these complexes (Dawson *et al* 1993). Our results also support these findings that ischemia and I/R reduces the activity of complex IV enzymes. Here also, SGG brings better results in retaining the complex IV activity.

To determine the functional status of mitochondria, oxygen consumption rate has been used as an important parameter. For maintaining the normal cellular function consumption of oxygen is important and unhealthy cells with mitochondrial dysfunction shows a lower rate of oxygen consumption. Mehta *et al* (2012) reported about protective effects of Se against glutamate induced toxicity in murine neuronal HT22 cells and Se compounds showed better effect in maintaining the mitochondrial homeostasis. In this study, reduced oxygen consumption rate in I/R cells indicates the dysfunction of mitochondria and SGG treatment attenuated the reduction in oxygen consumption in H9c2 cells. Mitochondrial dysfunction as well as reduced oxygen consumption during ischemia and I/R causes loss of intracellular ATP. Indeed, our study indicated that all the test materials after ischemia and I/R preserved cellular ATP thereby preserving the cardiomyocyte energy supply during oxidative stress. Among all the groups SGG showed better activity and the increase of ATP level by SGG may be related to its protection of mitochondrial ETC function under ischemic insult.

Myocardial ischemia is a known potent inducer of the stress protein response. HSPs are a family of protective proteins expressed in all cells. They are found in the cytosol of normal heart and muscle cells. Myocardial stress proteins are upregulated by several stimuli which is activated in response to ischemia, such as hypoxia (Iwaki *et al*

1993; Benjamin *et al* 1999), decreased energy storage, particularly ATP levels (Williams *et al* 1993), acidic pH (Benjamin *et al* 1992), presence of denatured proteins (Ananthan *et al* 1986) and oxidative stress (Aucoin *et al* 1995; Donati *et al* 1990; Das *et al* 1995). Induction of the heat shock response supports the survival of myocardial cells (Williams *et al* 1993). Lin *et al* (2001) have reported the protective effects of HSP 60 on ATP levels in myocytes subjected to 8 h of simulated ischemia followed by 4 and 8 h of reoxygenation. To maintain the protein members of the oxidative phosphorylation cascade in a normal folding state a specific set of mitochondrial HSPs, especially HSP 60 and HSP 10, is used to form the chaperonin complex for efficient protein folding. In contrast, little is known about the HSP 60 response although recent studies show upregulation of myocardial HSP 60 expression in response to ischemia (Heads *et al* 1995; Marber *et al* 1993) suggesting signaling *via* adenosine receptor activation (Heads *et al* 1995) as well as a protective effect of HSP 60 overexpression from ischemia-induced injury (Lau *et al* 1997). In this study there was an upregulation of HSP 60 in ischemic and I/R groups. This may be due to the self adaptive mechanism of the cells towards the stressed conditions. Here also, SGG showed better protection compared to other groups.

The mitochondrial source of $OH^{\cdot}$ has been identified to be the aconitase, which is involved in the TCA cycle (Vasquez-Vivar *et al* 2000). There are reports that aconitase is susceptible to oxidative inactivation *in vitro* (Humphries and Szweda 1998a; Humphries *et al* 1998b; Nulton-Persson and Szweda 2001; Nulton-Persson *et al* 2003; Bulteau *et al* 2003; Vasquez-Vivar *et al* 2000; Verniquet *et al* 1991; Gardner 2002; Beinert *et al* 1996) and have been reported to decline in activity during *in vivo* cardiac I/R (Sadek *et al* 2002). The generation of ROS that inactivates the aconitase activity is commonly used as a biomarker of oxidative damage (Vasquez-Vivar *et al* 2000; Verniquet *et al* 1991; Gardner 2002; Beinert *et al* 1996). Aconitase is capable of participating in redox regulation thus a potential target of oxidative damage. As described above this enzyme has an iron-sulfur centre in its active site which is responsive to oxidation and loss of iron. There are reports that HSPs indirectly regulate the redox chemistry of aconitase in cellular systems (Ilangovan *et al* 2006). In this study the activity of aconitase is reduced in ischemia and I/R whereas, SGG treatment improves the activity of aconitase by preventing the oxidation and loss of iron from iron-sulphur centre.

Mammalian tissues are characterized by aerobic metabolism and require

uninterrupted oxygen supply. Accordingly, availability of oxygen in tissues plays a critical role in the pathophysiology of the organism (Dyson *et al* 2007). Mechanisms of oxygen sensing by the individual tissues and cells are more diverse and are often debated (Nauseef 2006). Diverse types of proteins/enzymes like potassium channels, mitochondrial complex III and IV, NADPH oxidases, prolyl hydroxylases and heme oxygenases have been described as oxygen sensors in various cellular contexts (Acker *et al* 2006). Under a number of pathophysiological conditions like coronary artery occlusion and anaemia myocardium might undergoe hypoxia (or anoxia) (Essop 2007; Sen *et al* 2006). Under hypoxic conditions, the availability of oxygen in various parts of the myocardium might remain uneven (Kupriyanov *et al* 2004) and leads to the expression of HIF-1. Originally, HIF-1 was identified as the activator of erythropoietin gene transcription under hypoxic condition (Wang and Semenza 1993a; Wang and Semenza 1993b). It is a heterodimeric transcription factor comprising of two polypeptide subunits i.e, α and β. HIF-1 elicits hypoxic response through the hypoxia response element (HRE) located in the regulatory regions of hypoxia responsive genes. The role of mitochondrial ROS in the activation of HIF-1 was first revealed in late nineties (Chandel *et al* 1998; Chandel *et al* 2000; Haddad and Land 2001; Enomoto *et al* 2002; Dada *et al* 2003; Sanjuan-Pla *et al* 2005). Studies on the activation of HIF-1α under hypoxia have created an excellent framework of understanding the role of ROS in hypoxic signaling. As in other tissues**,** HIF-1 also plays a major role in eliciting hypoxic response of the mammalian myocardium (Shohet and Garcia 2007; Qutub and Popel 2007) and it has been recently reported that acetylcholine can independently but additively (to hypoxia) activate HIF-1 in cardiac myocytes (Kakinuma *et al* 2005). Here also in ischemia and I/R groups the HIF-1α level is increased due to disturbed ETC and leads to the generation of superoxides. HIF-1α then dimerize with HIF-1β, binding to its target HRE and activating a battery of hypoxia responsive genes, while SGG treatment showed better activity in maintaining HIF-1α level.

The quantity ANP is elevated in the ischemic ventricular tissues, suggesting the role of ANP in the myocardial adaptation to ischemia (Drexler *et al* 1989, Loennechen *et al* 2001). Chun *et al* (2003) reported that HIF-1 α is responsible for the hypoxic induction of the ANP gene in ventricular myocytes and the hypoxic activation of ANP promoter was observed only in myocytes. However, factors other than HIF-1 α may be required for

the induction of ANP following ischemia (Loennechen *et al* 2001; Drexler *et al* 1989). The most potent stimuli for ANP secretion is ischemia which is an important homeostatic mechanism since ANP can produce cardiac vasodilatation to increase blood flow and oxygen delivery to the heart as well as peripheral vasodilatation to reduce arterial pressure (Ahmed *et al* 2012). Here also ischemia and I/R increase the ANP level while Se, GGN and SGG prevent the elevation of ANP level in myocytes. Among the test materials, SGG showed higher protection in preventing the release of ANP.

Conclusion

Overall results reveal that ischemia and I/R induces alterations in mitochondrial function in H9c2 cells and SGG protects mitochondria from the deleterious effects by reducing transmembrane potential, keeping the integrity of mitochondrial permeability transition pore, maintaining superoxide levels and enhancing the activities of mitochondrial ETC complexes, aconitase level, reducing HIF-1α level and ANP level. The outcome of this study shows the possibilities of using nanoparticles as nanomedicines for CVD which is a major health issue of the present century.

References

1. Acker T, Fandrey J, Acker H (2006) The good, the bad and the ugly in oxygen-sensing: ROS, cytochromes and prolyl-hydroxylases. *Cardiovasc Res* 71: 195-207.
2. Ahmed F, Tabassum N, Rasool S (2012) Regulation of atrial natriuretic peptide (ANP) and its role in blood pressure. *Int Curr Pharm J* 1: 176-179.
3. Ananthan J, Goldberg AL, Voellmy R (1986) Abnormal proteins serve as eukaryotic stress signals and trigger the activation of heat shock genes. *Science* 232: 522-524.
4. Arora A, Sairam RK, Srivastava GC (2002) Oxidative stress and antioxidative system in plants. *Curr Sci India* 82: 1227-1238.
5. Aucoin MM, Barhoumi R, Kochevar DT, Granger HJ, Burghardt RC (1995) Oxidative injury of coronary venular endothelial cells depletes intracellular glutathione and induces HSP70 mRNA. *Am J Physiol* 268: H1651-H1658.
6. Babcock GT, Wikstro M (1992) Oxygen activation and the conservation of energy in cell respiration. *Nature* 356: 301-309.
7. Beinert H, Kennedy MC, Stout CD (1996) Aconitase as iron minus sign sulfur protein, enzyme, and iron-regulatory protein. *Chem Rev* 96: 2335-2374.
8. Benjamin IJ, Horie S, Greenberg ML, Alpern RJ, Williams RS (1992) Induction of stress proteins in cultured myogenic cells: molecular signals for the activation of heat shock protein transcription factor during ischemia. *J Clin Invest* 89: 1689-1695.
9. Benjamin IJ, Horie S, Greenberg ML, Alpern RJ, Williams RS (1999) Induction of stress proteins in cultured myogenic cells. Molecular signals for the activation of heat shock transcription factor during ischemia. *J Clin Invest* 89: 1685-1689.
10. Bulteau AL, Ikeda-Saito M, Szweda LI (2003) Redox dependent modulation of aconitase activity in intact mitochondria. *Biochemistry* 42: 14846-14855.
11. Camara AK, Lesnefsky EJ, Stowe DF (2010) Potential therapeutic benefits of strategies directed to mitochondria. *Antioxid Redox Signal* 13: 279-347.
12. Chandel NS, McClintock DS, Feliciano CE, Wood TM, Melendez JA, Rodriguez AM, Schumacker PT (2000) Reactive oxygen species generated at mitochondrial

complex III stabilize hypoxia-inducible factor-1alpha during hypoxia: a mechanism of O_2 sensing. *J Biol Chem* 275: 25130-25138.

13. Chandel NS, Maltepe E, Goldwasser E, Mathieu CE, Simon MC, Schumacker PT (1998) Mitochondrial reactive oxygen species trigger hypoxia-induced transcription. *Proc Natl Acad Sci U S A* 95: 11715-11720.
14. Chen Q, Moghaddas S, Hoppel CL, Lesnefsky EJ (2008) Ischemic defects in the electron transport chain increase the production of reactive oxygen species from isolated rat heart mitochondria. *Am J Physiol Cell Physiol* 294: C460-C466.
15. Chun YS, Hyun JY, Kwak YG, Kim IS, Kim CH, Choi E, Kim MS, Park JW (2003) Hypoxic activation of the atrial natriuretic peptide gene promoter through direct and indirect actions of hypoxia-inducible factor-1. *Biochem J* 370: 149-157.
16. Crompton M, Costi A, Hayat L (1987) Evidence for the presence of a reversible Ca^{2+}-dependent pore activated by oxidative stress in heart mitochondria. *Biochem J* 245: 915-918
17. Dada LA, Chandel NS, Ridge KM, Pedemonte C, Bertorello AM, Sznajder JI (2003) Hypoxia-induced endocytosis of Na^+, K^+-ATPase in alveolar epithelial cells is mediated by mitochondrial reactive oxygen species and PKC-zeta. *J Clin Invest* 111: 1057-1064.
18. Das DK, Maulik N, Moraru II (1995) Gene expression in acute myocardial stress induction by hypoxia, ischemia, reperfusion, hyperthermia and oxidative stress. *J Mol Cell Cardiol* 27: 181-193.
19. Dawson TL, Gores GJ, Nieminen AL, Herman B, Lemasters JJ (1993) Mitochondria as a source of reactive oxygen species during reductive stress in rat hepatocytes. *Am J Physiol* 264: C961-C967
20. Desai VG, Casciano D, Feuers RJ, Aidoo A (2001) Activity profile of glutathione-dependent enzymes and respiratory chain complexes in rats supplemented with antioxidants and treated with carcinogens. *Arch Biochem Biophys* 394: 255-264.
21. Donati YRA, Slosman DO, Polla BS (1990) Oxidative injury and heat shock response. *Biochem Pharmacol* 40: 2571-2577.
22. Drexler H, Hanze J, Finckh M, Lu W, Just H, Lang RE (1989) Atrial natriuretic peptide in a rat model of cardiac failure. Atrial and ventricular mRNA, atrial content, plasma levels, and effect of volume loading. *Circulation* 79: 620-633.

23. Dyson A, Stidwill R, Taylor V, Singer M (2007) Tissue oxygen monitoring in rodent models of shock. *Am J Physiol Heart Circ Physiol* 293: H526-H533.
24. Enomoto N, Koshikawa N, Gassmann M, Hayashi J, Takenaga K (2002) Hypoxic induction of hypoxia-inducible factor-1alpha and oxygen regulated gene expression in mitochondrial DNA-depleted HeLa cells. *Biochem Biophys Res Commun* 297: 346-352.
25. Essop MF (2007) Cardiac metabolic adaptations in response to chronic hypoxia. *J Physiol* 584: 715-726.
26. Gardner PR (2002) Aconitase: sensitive target and measure of superoxide. *Methods Enzymol* 349: 9-23.
27. Ha SJ, Kim W (2010) Mechanism of ischemia and reperfusion injury to the heart: from the viewpoint of nitric oxide and mitochondria. *Chonnam Med J* 46: 129-139.
28. Haddad JJ, Land SC (2001) A non-hypoxic, ROS-sensitive pathway mediates TNF-alpha-dependent regulation of HIF-1alpha. *FEBS Lett* 505: 269-274.
29. Hansford RG, Hogue BA, Mildaziene V (1997) Dependence of H_2O_2 formation by rat heart mitochondria on substrate availability and donor age. *J Bioenerg Biomembr* 29: 89-95.
30. Hausenloy DJ, Ruiz-Meana M (2010) Not just the powerhouse of the cell: emerging roles for mitochondria in the heart. *Cardiovasc Res* 88: 5-6.
31. Heads RJ, Latchmann DS, Yellon DM (1995) Differential stress protein mRNA expression during early ischemic preconditioning in the rabbit heart and its relationship to adenosin receptor function. *J Mol Cell Cardiol* 27: 2133-2148.
32. Humphries KM, Szweda LI (1998a) Selective inactivation of α-ketoglutarate dehydrogenase: Reaction of lipoic acid with 4-hydroxy-2-nonenal. *Biochemistry* 37: 15835-15841.
33. Humphries KM, Yoo Y, Szweda LI (1998b) Inhibition of NADH-linked mitochondrial respiration by 4-hydroxy-2-nonenal. *Biochemistry* 37: 552-557.
34. Ilangovan G, Venkatakrishnan CD, Bratasz A, Osinbowale S, Cardounel AJ, Zweier JL, Kuppusamy P (2006) Heat shock-induced attenuation of hydroxyl radical generation and mitochondrial aconitase activity in cardiac H9c2 cells. *Am J Physiol Cell Physiol* 290: C313-C324.

35. Iwaki K, Chi SH, Dillmann WH, Mestril R (1993) Induction of HSP 70 in cultured rat neonatal cardimyocytes by hypoxia and metabolic stress. *Circulation* 87: 2023-2032.
36. Jacobson MD (1996) Reactive oxygen species and programmed cell death. *Trends Biochem Sci* 21: 83-6.
37. Javadov S, Baetz D, Rajapurohitam V, Zeidan A, Kirshenbaum LA, Karmazyn M (2006) Antihypertrophic effect of Na^+/H^+ exchanger isoform 1 inhibition is mediated by reduced mitogen-activated protein kinase activation secondary to improved mitochondrial integrity and decreased generation of mitochondrial-derived reactive oxygen species. *J Pharmacol Exp Ther* 317: 1036-1043.
38. Kakinuma Y, Ando M, Kuwabara M, Katare RG, Okudela K, Kobayashi M, Sato T (2005) Acetylcholine from vagal stimulation protects cardiomyocytes against ischemia and hypoxia involving additive non-hypoxic induction of HIF-1alpha. *FEBS Lett* 579: 2111-2118.
39. Kelley EE, Khoo NKH, Hundley NJ, Malik UZ, Freeman BA, Tarpey MM (2010) Hydrogen peroxide is the major oxidant product of xanthine oxidase. *Free Radic Biol Med* 48: 493-498.
40. Kim TS, Yun BY, Kim IY (2003) Induction of the mitochondrial permeability transition by selenium compounds mediated by oxidation of the protein thiol groups and generation of the superoxide. *Biochem Pharmacol* 66: 2301-2311.
41. Koopman WJ, Nijtmans LG, Dieteren CE, Roestenberg P, Valsecchi F, Smeitink JA, Willems PH (2010) Mammalian mitochondrial complex I: biogenesis, regulation, and reactive oxygen species generation. *Antioxid Redox Signal* 12: 1431-1470.
42. Kupriyanov VV, Nighswander-Rempel S, Xiang B (2004) Mapping regional oxygenation and flow in pig hearts *in vivo* using near infrared spectroscopic imaging. *J Mol Cell Cardiol* 37: 947-957.
43. Lau S, Patnaik N, Sayen R, Mestril R (1997) Simultaneous overexpression of two stress proteins in rat cardiomyocytes and myogenic cells confers protection against ischemia-induced injury. *Circulation* 96: 2287-2294.
44. Lesnefsky EJ, Moghaddas S, Tandler B, Kerner J, Hoppel CL (2001) Mitochondrial dysfunction in cardiac disease: ischemia-reperfusion, aging, and

heart failure. *J Mol Cell Cardiol* 33: 1065-1089.

45. Lin KM, Lin B, Lian IY, Mestril R, Scheffler IE, Dillmann WH (2001) Combined and individual mitochondrial HSP 60 and HSP 10 expression in cardiac myocytes protects mitochondrial function and prevents apoptotic cell deaths induced by simulated ischemia-reoxygenation. *Circulation* 103: 1787-1792.
46. Loennechen JP, Stoylen A, Beisvag V, Wisloff U, Ellingsen O (2001) Regional expression of endothelin-1, ANP, IGF-1, and LV wall stress in the infracted rat heart. *Am J Physiol Heart Circ Physiol* 280: H2902-H2910.
47. Marber MS, Latchmann DS, Walker JM, Yellon DM (1993) Cardiac stress protein elevation 24 h after brief ischemia or heat stress is associated with resistance to myocardial infarction. *Circulation* 88: 1264-1272.
48. Mathur A, Hong Y, Kemp BK, Barrientos AA, Erusalimsky JD (2000) Evaluation of fluorescent dyes for the detection of MMP changes in cultured cardiomyocytes. *Cardiovasc Res* 46: 126-138.
49. Mehta SL, Kumari S, Mendelev N, Li PA (2012) Selenium preserves mitochondrial function, stimulates mitochondrial biogenesis, and reduces infarct volume after focal cerebral ischemia. *BMC Neurosci* 13: 1-12.
50. Mendelev N, Mehta SL, Idris H, Kumari S, Li PA (2012) Selenite stimulates mitochondrial biogenesis signaling and enhances mitochondrial functional performance in murine hippocampal neuronal cells. *PLoS ONE* 7: e47910.
51. Mukhopadhyay P, Rajesh M, Yoshihiro K, Hasko G, Pacher P (2007) Simple quantitative detection of mitochondrial superoxide production in live cells. *Biochem Biophys Res Commun* 358: 203-208.
52. Nauseef WM (2006) Acute oxygen-sensing mechanisms. *N Engl J Med* 354: 975-977.
53. Nulton-Persson AC, Starke DW, Mieyal JJ, Szweda LI (2003) Reversible inactivation of α-ketoglutarate dehydrogenase in response to alterations in the mitochondrial glutathione status. *Biochemistry* 42: 4235-4242.
54. Nulton-Persson AC, Szweda LI (2001) Modulation of mitochondrial function by hydrogen peroxide. *J Biol Chem* 276: 23357-23361.
55. Paul MK, Patkari M, Mukhopadhyay AK (2007) Existence of a distinct concentration window governing daunorubicin-induced mammalian liver

mitotoxicity-implication for determining therapeutic window. *Biochem Pharmacol* 74: 821-830.

56. Petronilli V, Miotto G, Canton M, Brini M, Colonna R, Bernardi P, Lisa FD (1999) Transient and long-lasting openings of the mitochondrial permeability transition pore can be monitored directly in intact cells by changes in mitochondrial calcein fluorescence. *Biophys J* 76: 725-734.
57. Qutub AA, Popel AS (2007) Three autocrine feedback loops determine HIF1alpha expression in chronic hypoxia. *Biochim Biophys Acta* 1773: 1511-1525.
58. Robinson KM, Lemire BD (1995) Flavinylation of succinate: ubiquinone oxidoreductase from *Saccharomyces cerevisiae*. *Methods Enzymol* 260: 34-51.
59. Sadek HA, Humphries KM, Szweda PA, Szweda LI (2002) Selective inactivation of redox sensitive mitochondrial enzymes during cardiac reperfusion. *Arch Biochem Biophys* 406: 222-228.
60. Sanjuán-Pla A, Cervera AM, Apostolova N, Garcia-Bou R, Víctor VM, Murphy MP, McCreath KJ (2005) A targeted antioxidant reveals the importance of mitochondrial reactive oxygen species in the hypoxic signaling of HIF-1alpha. *FEBS Lett* 579: 2669-2674.
61. Schulte U, Weiss H (1995) Generation and characterization of NADH: ubiquinone oxido reductase mutants in *Neurospora crassa*. *Methods Enzymol* 260: 3-14.
62. Sen CK, Khanna S, Roy S (2006) Perceived hyperoxia: oxygen-induced remodeling of the reoxygenated heart. *Cardiovasc Res* 71: 280-288.
63. Shohet RV, Garcia JA (2007) Keeping the engine primed: HIF factors as key regulators of cardiac metabolism and angiogenesis during ischemia. *J Mol Med (Berl)* 85: 1309-1315.
64. Skarka L, Ostadal B (2002) Mitochondrial membrane potential in cardiac myocytes. *Physiol Res* 51: 425-434.
65. Spinazzi M, Casarin A, Pertegato V, Salviati L, Angelini C (2012) Assessment of mitochondrial respiratory chain enzymatic activities on tissues and cultured cells. *Nat Protoc* 7: 1235-1246.
66. Stowe DF, Camara AK (2009) Mitochondrial reactive oxygen species production in excitable cells: modulators of mitochondrial and cell function. *Antioxid Redox Signal* 11: 1373-1414.

67. Varotsis C, Zhang Y, Appelman EH, Babcock GT (1993) Resolution of the reaction sequence during the reduction of O_2 by cytochrome oxidase. *Pro Natl Acad Sci USA.* 90: 237-241.
68. Vasquez-Vivar J, Kalyanaraman B, Kennedy MC (2000) Mitochondrial aconitase is a source of hydroxyl radical an electron spin resonance investigation. *J Biol Chem* 275: 14064-14069.
69. Verniquet F, Gaillard J, Neuburger M, Douce R (1991) Rapid inactivation of plant aconitase by hydrogen peroxide. *Biochem J* 276: 643-648.
70. Waldmeier PC, Zimmermann K, Qian T, Tintelnot-Blomley M, Lemasters JJ (2003) Cyclophilin D as a drug target. *Curr Med Chem* 10: 1485-1506.
71. Wang GL, Semenza GL (1993a) Characterization of hypoxia-inducible factor 1 and regulation of DNA binding activity by hypoxia. *J Biol Chem* 268: 21513-21518.
72. Wang GL, Semenza GL (1993b) General involvement of hypoxia inducible factor 1 in transcriptional response to hypoxia. *Proc Natl Acad Sci USA* 90: 4304-4308.
73. Williams RS, Thomas JA, Fina M, German Z, Benjamin IJ (1993) Human heat shock protein 70 (HSP 70) protects murine cells from injury during metabolic stress. *J Clin Invest* 92: 503-508.
74. Yokoyama Y, Beckman JS, Beckman TK, Wheat JK, Cash TG, Freeman BA, Parks DA (1990) Circulating xanthine oxidase: potential mediator of ischemic injury. *Am J Physiol* 258: G564-G570.
75. Zoratti M, Szabo I (1995) The mitochondrial permeability transition. *Biochim Biophys Acta* 1241: 139-176.

Chapter 5

Anti-inflammatory and anti-apoptotic potential of selenium incorporated guar gum nanoparticles against I/R

5.1. Introduction

Inflammation and associated complications are considered as the major cause of I/R injury in cardiomyocytes (Marchant *et al* 2012). Reperfusion is generally associated with an inflammatory cascade that perpetuates damage to cardiac tissue after a period of ischemia. The effects of reperfusion lead to inflammatory responses damaging viable tissue around the infarct and results increased apoptosis in cardiomyocytes (Jayachandran *et al* 2007). This leads to a loss in cardiomyocytes and an increased infarct size (Zhong *et al* 2012). One of the central players in this cascade is the transcription factor nuclear factor kappa B **(**NF-$_K$B), known to play a vital role in regulating inflammatory signal transduction and cytokine production. Many effector genes including those encoding cytokines such as Tumor necrosis factor (TNF-α) and Interleukin-6 (IL-6) are activated by NF-$_K$B (Li *et al* 2011) to enhance the expression of pro-inflammatory cytokines. Interestingly, TNF-α act both as the target gene and inducer of NF-$_K$B (Pahl 1999) and its production was suppressed early in ischemia (Shames *et al* 2002). Apoptosis of cardiomyocytes has recently been recognized as a cellular mechanism of ischemia in the heart. Apoptosis was originally defined by its morphological characteristics, which include cell shrinkage, chromatin condensation, DNA fragmentation, membrane blebbing, and formation of apoptotic bodies. Hypoxia and TNF-α have been shown to induce apoptosis in cardiomyocytes (Long *et al* 1997; Haudek *et al* 2007; Sun *et al* 2013). Taken together, in cardiomyocytes different stimuli are capable for producing apoptosis most of which are expressed in advanced heart failure. So, a single proapoptotic stimulus leads to the activation of pathways which are involved in apoptosis. The prospective for the development of cardioprotective agents based on the prevention of apoptosis is emerging. This chapter deals with the beneficial effect of various test materials (Se, GGN and SGG) against inflammation and apoptosis during ischemia and I/R and the molecular mechanisms involved. Various markers of inflammation like IL-6, Interleukin-2 (IL-2), monocyte chemoattractant protein-1 (MCP-1), interferon-γ (INF-γ), TNF-α, NF-$_K$B(p65), serine/threonine-protein kinase (TNNI3K) and apoptotic markers like caspase 3,

annexin/FITC, cytoskeletal integrity and mRNA expression of genes involved in apoptosis like ERK-1 and ERK-2, insulin-like growth factor 1 (IGF-1), GATA-4, Raf-1 were studied in different experimental groups. In addition, western blot analysis of Bax/Bcl-2, Raf-1, ERK1/2 proteins and their role in preventing apoptosis were also conducted for detailed information.

5.2. Experimental methods

5.2.1. Materials

Phalloidin texas red and 4', 6-diamidino-2-phenylindole (DAPI) were from Sigma Aldrich (St. Louis, Mo, USA). ELISA kits for TNF-α were from Millipore, USA. IL-6, IL-2, MCP-1 and INF-γ kits were from BD Biosciences, USA. Kits for NF-$_K$B (p65) expression, caspase 3 assay and annexin/FITC assay were from Cayman chemicals (USA). TNNI3K were from MyBioSource, USA. Primers for PCR were from Hysel India Pvt Ltd, India. Antibodies for western blotting (ERK1/2, p-ERK1/2, Bax, Bcl-2, GAPDH) and HRP conjugated secondary antibodies were from Santacruz, USA.

5.2.2. ELISA analysis for inflammatory cytokines

After respective treatments inflammatory cytokines TNF-α, IL-6, IL-2, MCP-1 and INF-γ were estimated using ELISA kits. For performing these assays, 100 µl diluted capture antibody was added to the wells and incubated overnight at 4 °C. After incubation the supernatents was aspirated and the wells were washed 3 times with 300 µl wash buffer. 200 µl blocking buffer were added to all wells and the wells were incubated for 1 h at room temperature. After incubation the wells were washed 3 times. 100 µl of samples from different groups were added to the wells and incubated for 2 h at room temperature and the washing step was repeated. 100 µl working detector were added to all the wells and incubated for 1 h at room temperature and repeated the washing step with wash buffer. 100 µl of substrate solution was added and incubated for 30 min in dark. To that 50 µl stop solution was added and the absorbance was read at 450 nm. This procedure was common for MCP-1, IL-6, IL-2 and IFN-γ. For performing TNF-α ELISA, the wells were washed with 300 µl wash buffer and after that 50 µl samples were added to the wells. The plates were incubated for 2 h at room temperature with shaking at 200 rpm. The contents of the plate were discarded and the plates were washed with 1X wash buffer. 100 µl of TNF-α detection antibody was added to the wells and incubated the plates for 1

h at room temperature. Again the plates were washed with wash buffer. After washing 100 µl of avidin-HRP A solution was added to all wells and incubated for 30 min at room temperature. The contents of the plate were discarded and again washing step was repeated. 100 µl substrate solutions were added to all the wells and incubated in dark for 15 min. After 15 min, 100 µl stop solution were added and the absorbance was read at 450 nm.

5.2.3. NF-$_K$B (p65) expression

NF-$_K$B (p65) transcription factor assay is a non-radioactive sensitive method for detecting specific transcription factor DNA binding activity in nuclear extracts. NF-$_K$B contained in the nuclear extract, binds specifically to the NF-$_K$B response element. After respective treatments the cells were collected by centrifugation and using Cayman's nuclear extraction kit, nuclear proteins were isolated. After nuclear extraction the NF-$_K$B (p65) level was detected. 10 µl samples containing NF-$_K$B were added to the wells and incubated overnight at 4 °C. All the wells were washed with 200 µl 1X wash buffer. Then to all the wells except blank, 100 µl NF-$_K$B (p65) primary antibodies were added and incubated for 1 h at room temperature. The washing step was repeated with 1X wash buffer and to all the wells except blank 100 µl diluted goat anti-rabbit secondary antibody was added and incubated for 1 h at room temperature. After incubation it was washed with 1X wash buffer. Then to all wells 100 µl developing solution was added and incubated for 30 min with gentle agitation. 100 µl of stop solution was added to all the wells and the absorbance was read at 450 nm.

5.2.4. Role of TNNI3K in ischemia and I/R

TNNI3K, a novel cardiac specific and cardiac troponin I (cTnI)-interacting kinase, is emerging as a molecular therapeutic agent for heart disease. TNNI3K is a cardiac-specific gene that was undetectable in other tissues. This assay employs the quantitative sandwich enzyme immunoassay technique. TNNI3K was assayed according to the manufacturer's protocol. After respective treatments, the medium was removed and the cells were rinsed with ice-cold PBS, scraped off and the suspension was mixed with 1XPBS (pH 7.2-7.4). The cells were freeze-thawed to break up the cell membranes and the cell lysates were centrifuged for 5 min at 5000×g at 4 °C. The supernatant was collected after centrifugation and the assay was performed by adding 100 µl of standard

and sample per well and it was incubated for 2 h at 37 °C. After 2 h, the supernatant was removed from each well and 100 µl of biotin-antibody (1X) was added to each well. The wells were incubated for 1 h at 37 °C. After incubation the wells were washed for 3 times with wash buffer (200 µl). 100 µl of avidin-HRP (1X) was added to each well and it was incubated for 1 h at 37 °C. The washing process was repeated for five times and 90 µl of TMB substrate was added to each well and incubated for 30 min at 37 °C. 50 µl of stop solution was added to each well to stop the reaction and the optical density was measured at 450 nm.

5.2.5. Caspase 3 activity assay

Caspase 3 activity was spectrofluorimetrically estimated using a Cayman assay kit (Cayman, USA). The active caspase 3 cleaves the caspase 3 substrate (N-Ac-DEVD-N'-MC-R110) and it generates a highly fluorescent product that can be measured using excitation and emission wavelengths of 485 nm and 535 nm respectively. After respective treatments, 200 µl of caspase-3 assay buffer was added to each well and the plates were centrifuged for 800×g for 5 min. The supernatant was removed after centrifugation and 100 µl of cell based assay lysis buffer was added and incubated for 30 min at room temperature and again centrifuged for 800×g for 10 min. After that 90 µl of the supernatant was transferred from each well to a new black well plate. To that, 10 µl of caspase 3 assay buffer and 100 µl of caspase 3 substrate solution was added and the wells were incubated at 37 °C for 30 min. The fluorescent intensity of each well was read at an excitation of 485 nm and emission of 535 nm.

5.2.6. Annexin V FITC/ propidium iodide assay

Annexin V FITC is used to quantitatively determine the percentage of cells undergoing apoptosis. In apoptotic cells, the membrane phospholipid phosphatidylserine is translocated from the inner leaflet of the plasma membrane to the outer leaflet, thereby exposing phospholipid phosphatidylserine to the external environment. Annexin V is a Ca^{2+}-dependent phospholipid binding protein that has a high affinity for phospholipid phosphatidylserine and is useful for identifying apoptotic cells with exposed phospholipid phosphatidylserine. Propidium iodide (PI) is used to distinguish viable from non-viable cells. Viable cells with intact membranes exclude PI, whereas the membranes of dead and damaged cells are permeable to PI.

Briefly, after respective treatments the cells were trypsinized and resuspended in serum free medium. The cells were centrifuged at 400×g for 5 min and supernatant were removed. The cells were resuspended in 2 ml diluted assay binding buffer and centrifuged at 400×g for 5 min and supernatant was discarded. Then the cells were again resuspended in 250 µl of Annexin V FITC/ PI staining solution and incubated in dark for 10 min at room temperature and centrifuged at 400×g for 5 min and again the supernatant was discarded. Using 2 ml of the diluted assay binding buffer the cells were washed and centrifuged the cells at 400×g for 5 min. The cells were again resuspended in 1 ml of diluted assay binding buffer and were analysed for apoptosis immediately on FACS Aria II (BD Bioscience, USA).

5.2.7. Effect of SGG in maintaining cytoskeleton integrity

For determining the cytoskeletal integrity after ischemia and I/R the cells from experimental groups after respective treatments were washed with PBS. Then cells were fixed in 20 µl 4% paraformaldehyde in PBS for 10 min, permeabilized (20 µl 0.5% Triton X-100) and dehydrated with cold 100% acetone for 5 min. Phalloidin texas red stain (in PBS) was added and kept at room temperature for 20 min. Nucleus was counterstained with DAPI and visualized in spinning disk fluorescent microscope (BD Pathway™ Bioimager system, USA).

5.2.8. Alterations in various cardiac specific genes

Cellular mRNA expression of GATA-4, IGF-1, ERK-1, ERK-2 and Raf-1 was examined by RT-PCR. Total RNA was isolated from cells using TRIzol (Biochem Life Science, India). Subsequently, superscript III 1st strand synthesis system (Life technologies, Bangalore, India) kit was utilised for the reverse transcription (RT) of the samples. The samples were incubated in a Bio-rad CFX96™ Real-Time system at 25 °C for 10 min, 50 °C for 50 min, 85 °C for 5 min and then at 4 °C for 5 min. The specific PCR primers were synthesized based on nucleotides. Glyceraldehyde 3-phosphate dehydrogenase (GAPDH) mRNA was used as an internal reference. The amplification included the following reaction stages: stage I (initial denaturation), which involved an incubation at 94 °C for 3 min; stage II (30 cycles of PCR amplification), which involved 30 cycles of incubation at 94 °C for 10 s, 55 °C for 30 s, and 72 °C for 45 s; and stage III (melting curve analysis), which involved an incubation at 72 °C for 5 min followed by an

incubation at 16 °C for 10 min. The primers for various genes were designed using the Primer 3, a free online tool to design and analyze primers for PCR and real time PCR experiments and synthesised by Hysel India Pvt Ltd. In particular, the following specific primers were synthesised: GAPDH,F:5′-AGACAGCCGCATCTTCTTGG-3′,R:5′-TTGAGGTCAATGAAGGGGTC-3′;GATA binding protein 4 (GATA-4),F:5′-CTTTGTGATCCTAGAGTGGC-3′,R:5′-GAGTCAGATCAGGTATGGGA-3′;IGF-1,F:5′-CTACAAAGTCAGCTCGTTCC-3′,R:5′-CTGTAGGTCTTGTTTCCTGC-3′;Raf-1,F:5′-GGACATGCAGTTGGGAACTT-3′,R:5′-TGGAAGACAGATTCAGCGTG-3′;ERK-1, F:5′-TCCAAGGGCTACACCAAATC-3′,R:5′-AGGTAGTTTCGGGCCTTCAT-3′;ERK-2,F:5′-GAAGTTGAACAGGCTCTGGC-3′,R:5′-ACGGCTCAAAGGAGTCAAGA-3′.
Based on the amplification results, the comparative C_T method (ΔΔCT) was used to calculate the relative multiple of the starting copy number that existed in the template from each experimental group. The normalized gene expression was calculated.

5.2.9. Western blotting

Immunoblotting was used to analyze the presence of Bax, Bcl-2, Raf-1, ERK1/2 and GAPDH protein expression in ischemia and I/R. H9c2 cells were seeded in a T25 flask containing 5 ml of DMEM medium and treatments were carried out. At the end of the treatments, the H9c2 cells were harvested and lysed with ice-cold cell lysis solution (RIPA buffer containing a protease inhibitor cocktail) and the homogenate was centrifuged at 10,000×g for 15 min at 4 °C. Total protein in the supernatant was quantified using a BCA protein assay kit (Pierce, Rockford, IL USA). Total protein (40 µg) from each sample was separated by 10 % SDS-PAGE at 55 V. 25 µL of experimental samples was loaded in each wells. The protein in the gel was transferred into polyvinylidene difluoride (PVDF) membrane using Trans-Blot Turbo™ (Bio-Rad). The membrane was blocked with BSA in TBST (Tris buffered saline-Tween 20) for 1 h at room temperature, and then incubated with the primary antibodies (1:500) specific to Bax, Raf-1, ERK1/2 and GAPDH with gentle agitation at 4 °C overnight. The incubation was followed by 3 times wash with TBST for 10 min in a shaker followed by HRP-conjugated secondary antibodies (1:1000) in 0.25% BSA in TBST for 60 min at room temperature with shaking. After three washes with TBST, the membranes were developed using DAB tablets (Sigma Aldrich, St Louis, MO, USA) and the relative intensity of

bands were quantified using Bio-Rad Quantity One version 4.5 software in a Bio-Rad gel doc. The quantity of Bax, Bcl-2, Raf-1, ERK1/2 and GAPDH in cell lysate was normalized with the content of GAPDH.

5.2.10. Statistical analysis

Results were expressed in mean and standard deviation (SD) of the control and treated cells from three independent experiments with duplicate (n=6). Data were subjected to one-way ANOVA followed by the Bonferroni test to calculate the statistical difference among the groups using SPSS for Windows, standard version 11.5.1 (SPSS, Inc.) and significance was accepted at $P \leq 0.05$.

5.3. Results

5.3.1. Inflammatory markers in ischemia and I/R

The level of IL-2 and IL-6 (Figure.5.1A, B) were increased significantly ($P \leq 0.05$) in ischemia (104.86±3.37 and 139.98±3.45 pg/ml) and I/R (90.60±2.43 and 127±4.12 pg/ml) groups compared to control (29.38±4.68 and 35.16±1.52 pg/ml) (Figure.5.1A, B). All the treatment groups showed protection against the increase of IL-2 and IL-6 in ischemia and I/R groups. Among all the treated groups, 5 nM (47.28±4.9 and 35.19±2.16 pg/ml) and 25 nM of SGG (42.57±2.80 and 34.89±1.76 pg/ml) showed better protection in preventing the release of IL-2 and IL-6 to the medium ($P \leq 0.05$).

The level of MCP-1 and IFN-γ levels were significantly ($P \leq 0.05$) increased in ischemia (108.44±3.92 and 238.49±4.16 pg/ml) and I/R groups (101.29±1.92 and 236.19±4.19 pg/ml) compared to control (55.06±3.73 and 72.23±5.33 pg/ml) (Figure.5.1.C, D). All the test materials are effective in controlling the release of MCP-1 and IFN- γ. Among various test materials, SGG was found to be superior in reducing the level of MCP-1 and IFN-γ and the result showed that 5 nM (58.61±2.85 and 70.77±4.62 pg/ml) and 25 nM SGG (56.32±2.41 and 75.07±4.49 pg/ml) brought back the level of these cytokines to that of control cells (Figure.5.1.C, D). The level of TNF-α was significantly ($P \leq 0.05$) increased in ischemia (125.43±2.68 pg/ml) and I/R (122.18±5.11 pg/ml) groups compared to control (39.59±3.65 pg/ml). Here also, all the treatments were significantly effective in reducing the TNF-α release to the medium. Among these, 300 µg GGN (37.44±3.46 pg/ml) and 25 nM SGG (41.42±1.12 pg/ml) showed better activity in controlling the TNF-α release compared to I/R (Figure.5.1.E) and thus preventing the

inflammation induced by ischemia and I/R.

(A)

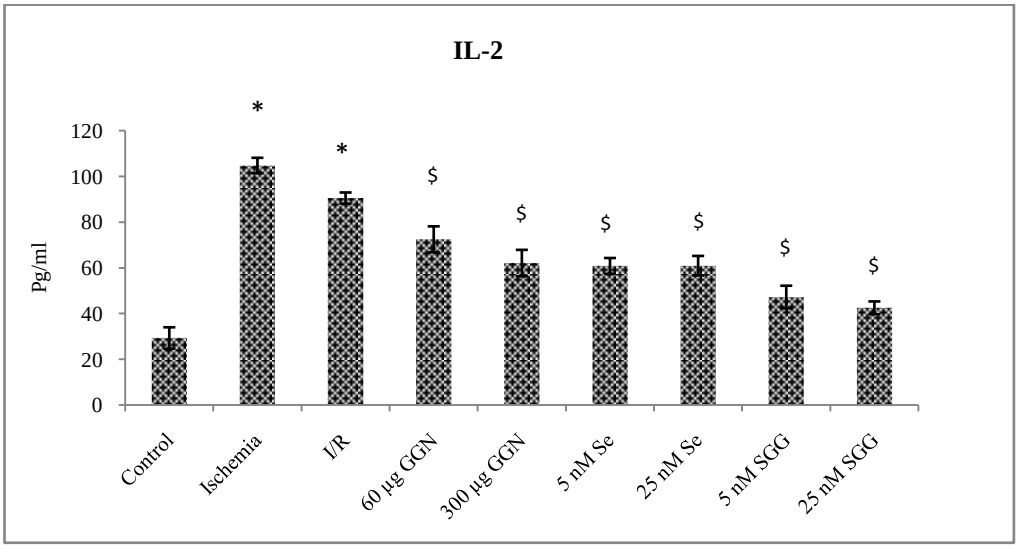

(B)

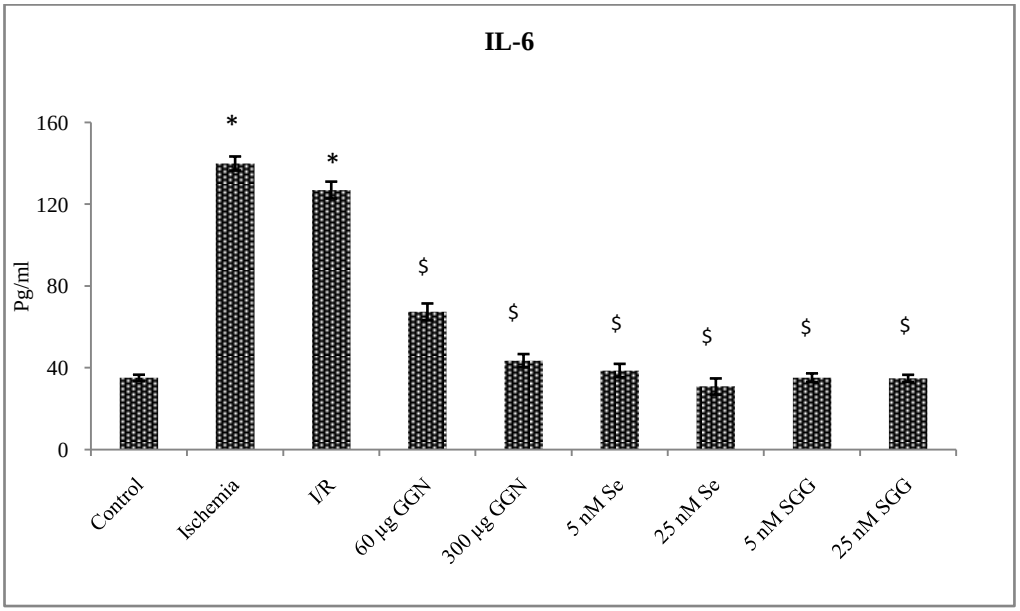

(C)

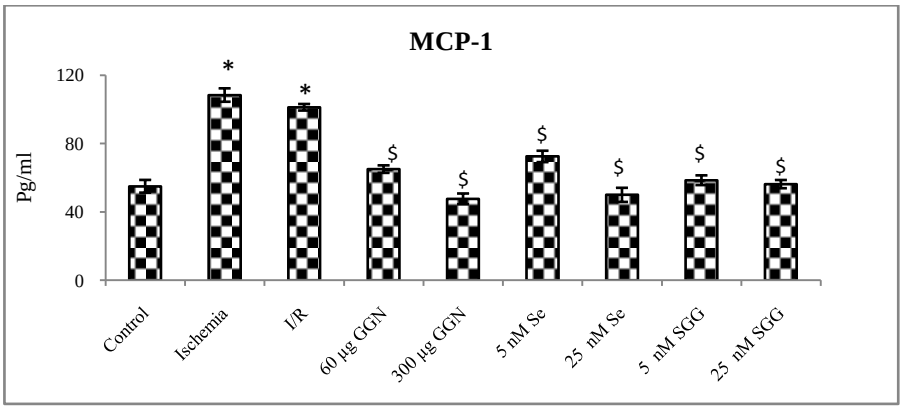

(D)

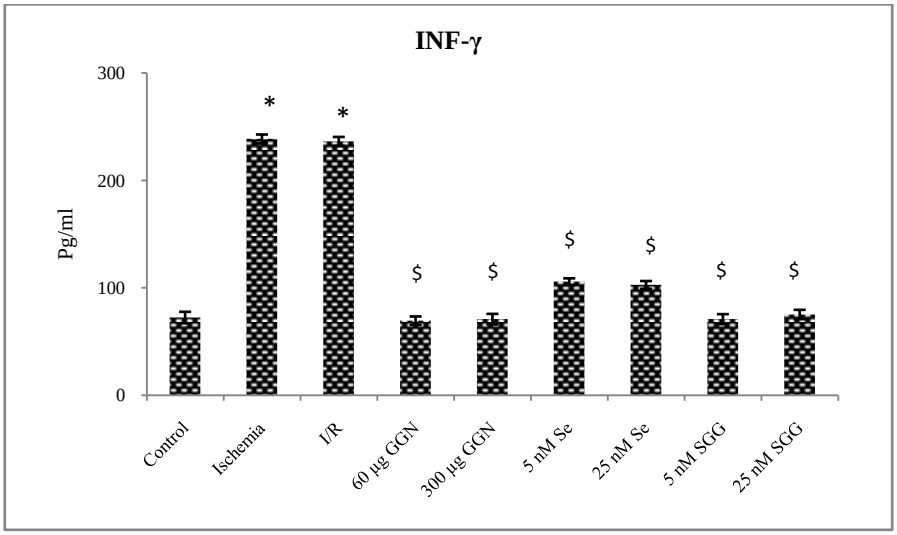

(E)

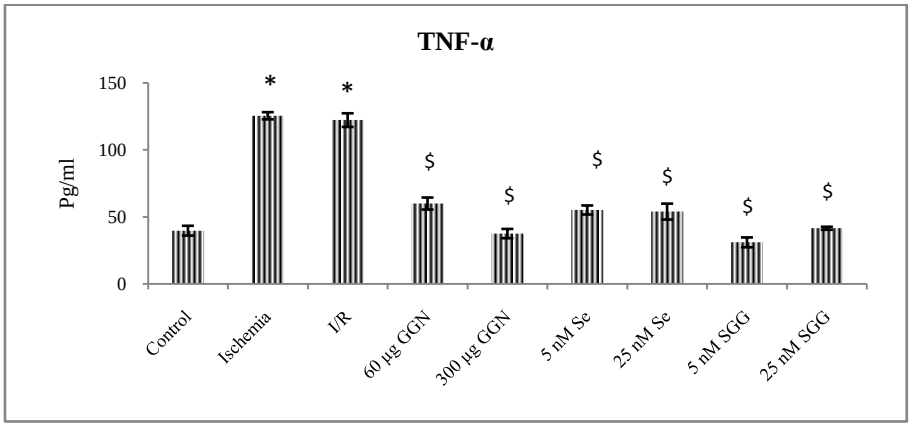

Figure 5. 1. Estimation of inflammatory cytokines release by ELISA in control, ischemia, I/R and treatment groups. (A) IL-2 (B) IL-6 (C) MCP-1 (D) IFN-γ (E) TNF-α. Values are means ±SD represented by vertical bars (n=6). * Mean value is significantly different

from the control cells (P≤0.05). $ Mean values are significantly different from I/R cells (P≤0.05).

5.3.2. Effect of SGG on NF-$_K$B (p65) expression

The level of NF-$_K$B (p65) in nuclear fraction was increased in ischemia (0.367±0.008 OD at 450 nm) and I/R (0.329±0.008 OD at 450 nm) groups compared to control (0.157±0.01 OD at 450 nm). All treatment groups showed protection in preventing the over expression of NF-$_K$B (p65) to nucleus (Figure.5.2). Here too, 5 nM (0.150±0.007 OD at 450 nm) and 25 nM (0.156±0.007 OD at 450 nm) SGG was found to be significantly (P≤0.05) effective in preventing the increase of NF-$_K$B (p65) compared to I/R groups.

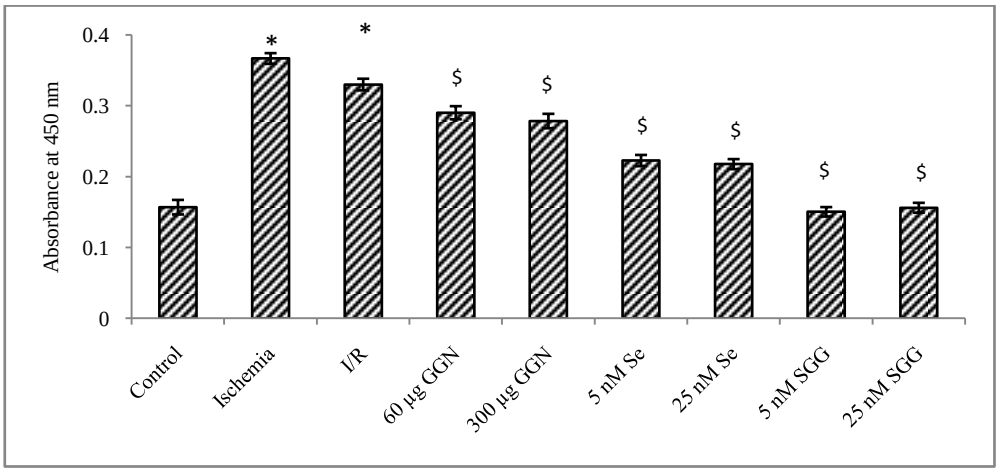

Figure 5. 2. Estimation of NF-$_K$B (p65) level in control and treated cells after I/R. Values are means ±SD represented by vertical bars (n=6). The ischemic and I/R groups were compared with the control group. * Indicates that the mean value was significantly different from the control cells (P≤0.05). $ Indicates mean value was significantly different from I/R cells (P≤0.05).

5.3.3. Effect of SGG onTNNI3K level

TNNI3K overexpression improves cardiac performance and attenuate ischemia-induced ventricular remodeling. The TNNI3K level was significantly (P≤0.05) decreased in ischemia (152.47±2.91 pg/ml) and I/R (169±5.39 pg/ml) compared to control (440.53±5.97 pg/ml). 5 nM (191.93±4.39 pg/ml) and 25 nM (204.98±5.5 pg/ml) SGG increased the TNNI3K level revealing SGG has protective effect (Figure.5.3).

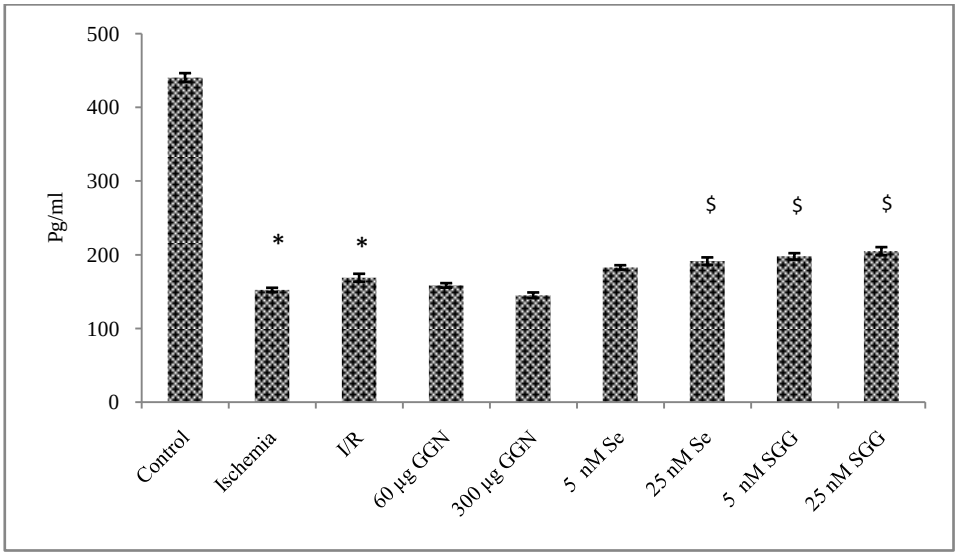

Figure 5. 3. Estimation of TNNI3K level in control and treated cells after I/R. Values are means ±SD represented by vertical bars (n=6). The ischemic and I/R groups were compared with the control group. * Indicates that the mean value was significantly different from the control cells (P≤0.05). $ Indicate mean value was significantly different from I/R groups (P≤0.05).

5.3.4. Activity of caspase 3

In ischemic (308.59%) and I/R (286.49%) groups there was an increase in caspase 3 activity compared to control. Application of all the test materials prevented the increase of caspase 3 activity (Figure.5.4). Among these 25 nM Se (102.92%) and 60 µg GGN (94.29%) were significantly effective in reducing the caspase 3 activity compared to other treated groups.

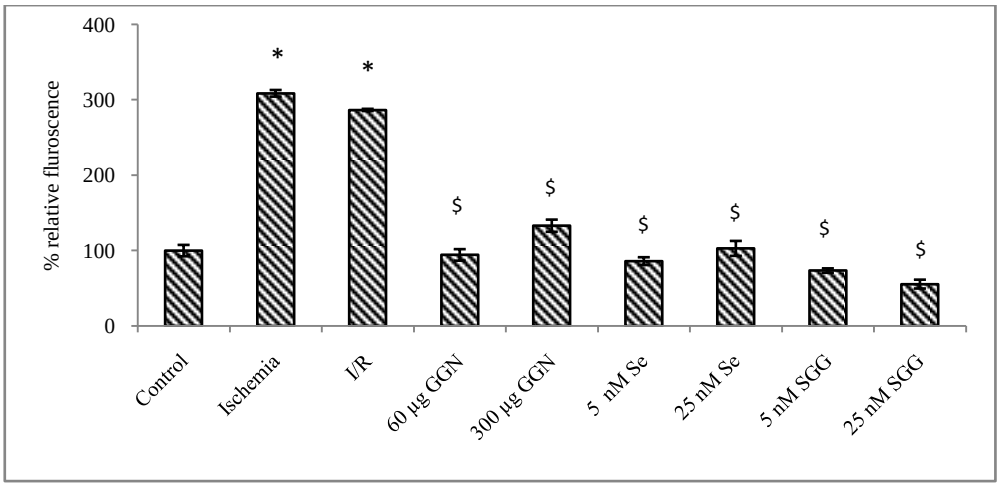

Figure 5. 4. Activity of caspase 3 in the control and treated cells after I/R. Values are means ±SD represented by vertical bars (n=6). The ischemic and I/R groups were compared with the control group. * Indicates that the mean value was significantly

different from the control cells ($P \leq 0.05$). $ Indicate mean value was significantly different from I/R cells ($P \leq 0.05$).

5.3.5. Effect of SGG on apoptosis

By staining cells with annexin V-FITC and PI, FACS was used to distinguish and quantitatively determine the percentage of dead, viable, apoptotic and necrotic cells after ischemia and treatment with GGN and SGG. The cytogram shows the early apoptotic cells in the lower right quadrant being Annexin V positive and PI negative; late apoptotic or necrotic cells are in the upper right quadrant being PI positive and Annexin V positive; live cells in the lower left quadrant being negative for both fluorescent probes and dead /advanced apoptotic cells in the upper left quadrant being PI positive and Annexin negative.

The biparametric analysis of Annexin V FITC green fluorescence (X axis) versus PI red fluorescence (Y axis) of control cells represent a cytogram in which the majority of cells (90.3%) remains alive showing only a background level of PI and Annexin V staining. In ischemia the percentage of dead cells increased from 9.4% in the control cells to 37.3% with corresponding decrease in live cells to 62.5%. The percentage of early apoptotic cells and the proportion of the late apoptotic/necrotic cells were insignificant. In I/R group also the percentage of dead cells (25%) was significantly higher than the control cells but lower than in ischemia. The percentage of dead cells was reduced in GGN, Se, and SGG treatment of which SGG 25nM showed a better protective effect. 5nM and 25 nM GGN reduced the cell death to 21.5 % and 22.3% respectively while 5nM and 25 nM Se reduced the cell death to 22.5% and 22%. In 5nM SGG treatment the dead cell percentage was lowered to 21.6% with a live cell percentage of 78.1. The number of dead cells was significantly reduced to 18.3% with corresponding increase in live cell percentage to 81.4 by SGG 25 nM treatment. These results indicate that the SGG was highly effective in protecting H9c2 cells from ischemia induced apoptosis.

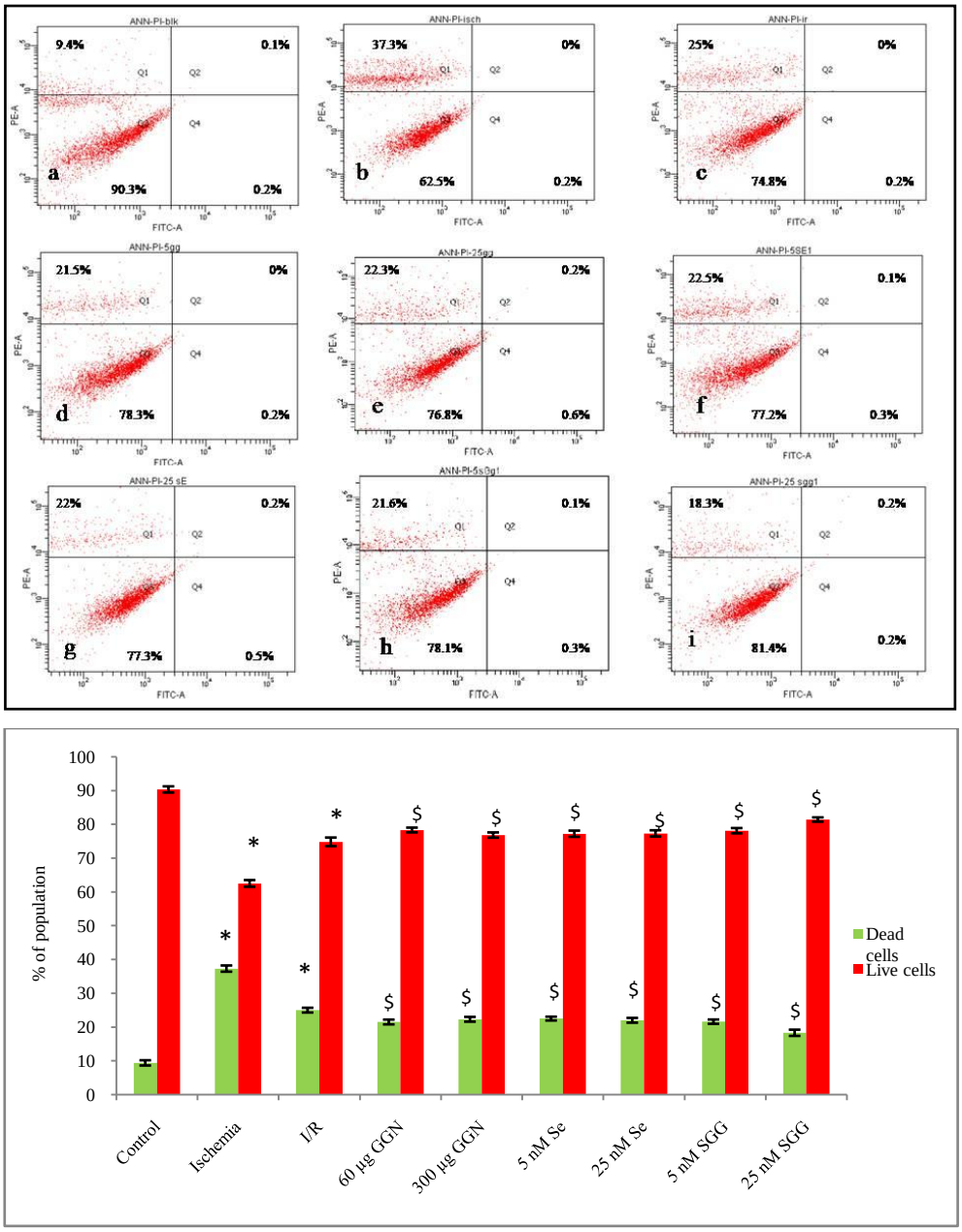

Figure 5. 5. Effects of Se, GGN and SGG on rate of apoptosis. Dot plot of H9c2 cells stained FITC (fluorescein-isothiocyanate) annexin V and PI (propidium iodide). (a) control cells; (b) ischemic cells (c) I/R cells; (d, e) cells treated with 60 µg GGN and 300 µg GGN; (f, g) cells treated with 5 nM and 25 nM Se; (h, i) cells treated with 5 nM and 25 nM SGG; (j) statistical analysis of flow cytometry data. Values are means ±SD represented by vertical bars (n=6). The ischemic and I/R groups were compared with the control group. * Indicates that the mean value was significantly different from the control cells (P≤0.05). $ Indicates mean value was significantly different from I/R cells (P≤ 0.05).

5.3.6. Effect of SGG in maintaining cytoskeleton integrity

Staining with F-actin revealed the alteration of contractile protein in ischemia and

I/R. In this experiment, the cytoskeleton of control cells (Figure.5.6.a) had an intact filamentous network, while cells with ischemia and I/R showed disruption of filamentous network (Figure.5.6.b, c). SGG was significantly effective in holding intact the mesh-like architecture of the cells among other treatment groups (Figure.5.6.h, i).

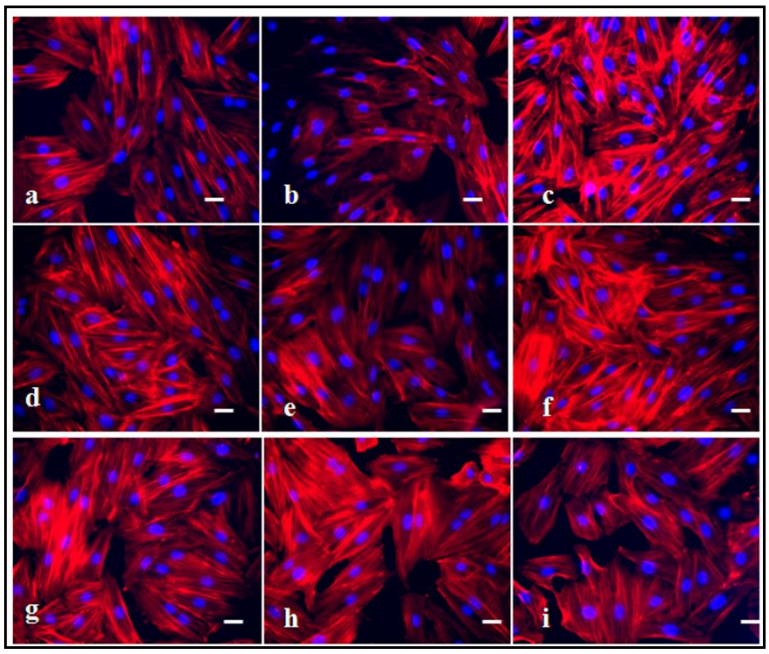

Figure 5. 6. Effect of SGG on ischemia and I/R induced cytoskeleton disorganization. After the end of the experiments, cells were fixed and stained for F-actin by phalloidin and nuclear staining by DAPI. (a) control cells; (b) ischemic cells; (c) I/R cells ; (d, e) cells treated with 60 µg and 300 µg of GGN (f, g) cells treated with 5 nM and 25 nM Se and (h, i) cells treated with 5 nM and 25 nM SGG.

5.3.7. SGG modulates the expression of genes involved in ischemia and I/R

The alteration in expression levels of genes related to protection from apoptosis were detected in H9c2 cells in ischemia and I/R. The genes studied include GATA-4, IGF-1, Raf-1, ERK-1 and ERK-2. The mRNA expression of IGF-1 was found to be decreased in ischemia and I/R groups and all the treatments were effective in upregulating the expression of IGF-1when compared with I/R cells (Figure.5.7). Likewise the expression of Raf-1, ERK-1 and ERK-2 were decreased in ischemia and I/R groups and treatment with SGG significantly increased the expression of these genes for preventing apoptosis compared with I/R. While there was no change in the expression of GATA-4 gene expression (data not shown).

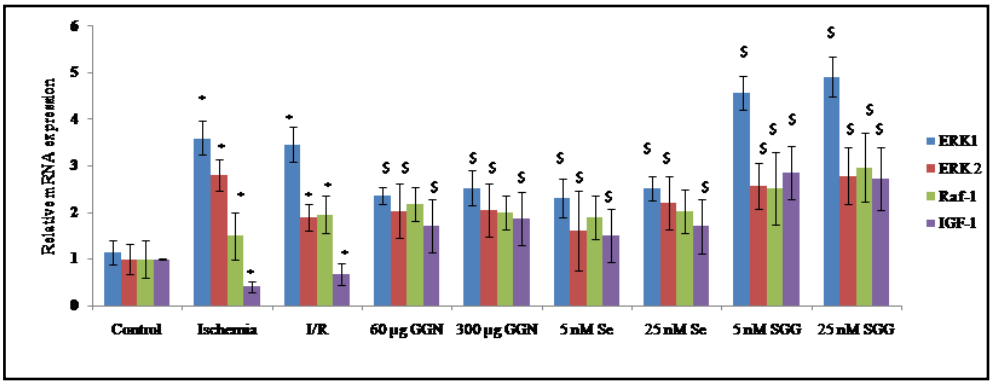

Figure 5. 7. SGG upregulates mRNA levels of IGF-1, Raf-1, ERK-1 and ERK-2. The mRNA results are expressed as difference in fold change in treated cells compared to I/R. Values are means ±SD represented by vertical bars (n=6). The ischemic and I/R groups were compared with the control group. * Indicates that the mean value was significantly different from the control cells (P≤0.05). $ Indicates mean value was significantly different from I/R cells (P≤ 0.05).

5.3.8. Bax and Bcl-2 expression after myocardial ischemia and I/R

Interaction of Bax and Bcl-2 played an important role in the regulation of apoptosis. Compared with control, ischemia and I/R had resulted in an increase in Bax (Figure.5.8.a) and corresponding decrease in expression of Bcl-2 protein (Figure.5.8.b). All treatment groups showed protection. But SGG showed better protection against apoptosis in preventing the alteration in the expression of Bax and Bcl-2 and thus preventing apoptosis.

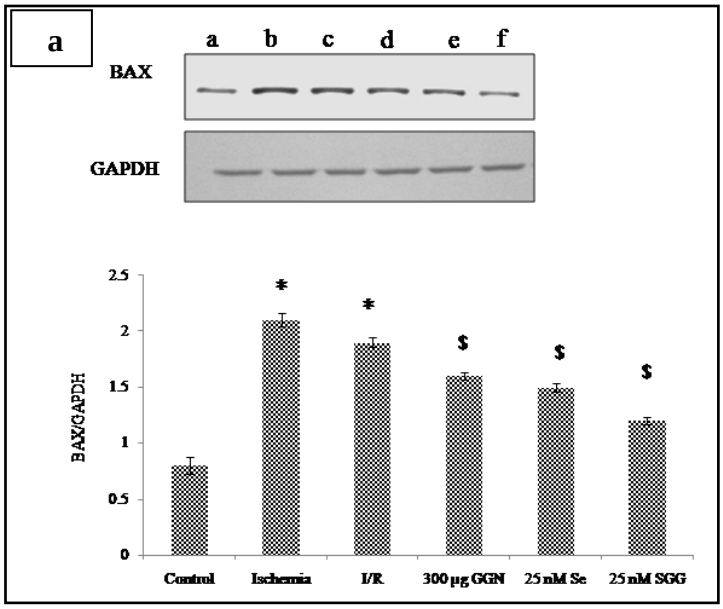

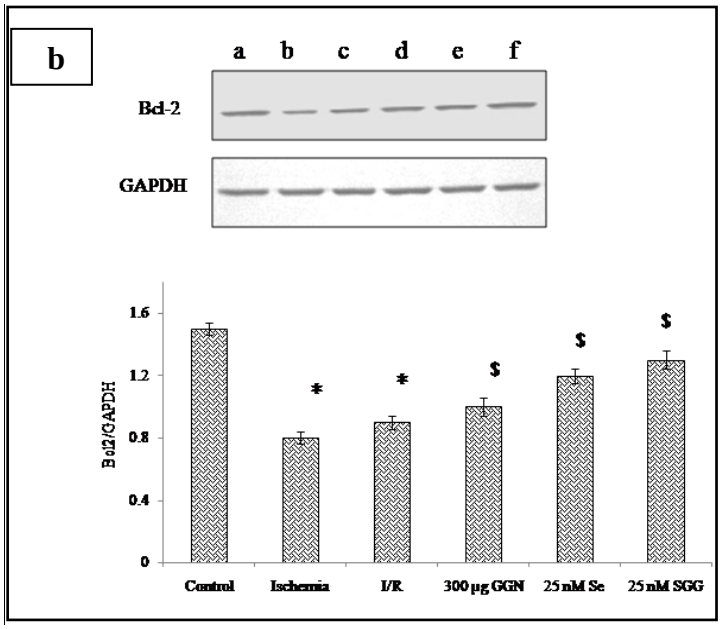

Figure 5. 8. Expression of (a) Bax and (b) Bcl-2 protein ischemia and I/R subjected to SDS-PAGE. The amount of Bax, Bcl-2 and GAPDH was detected with antibodies against Bax, Bcl-2 and GAPDH, respectively. The relative intensity of each band was quantified with GAPDH. The ischemic and I/R groups were compared with the control group. Lane a: control, b: ischemia, c: I/R d: GGN, e: Se, f: SGG. Results are representative of three independent experiments.* Indicates that the mean value was significantly different from the control cells ($P \leq 0.05$). $ Indicates mean value was significantly different from I/R cells ($P \leq 0.05$).

5.3.9. Expression of Raf-1and ERK1/2 after myocardial ischemia and I/R

After ischemia and I/R, western blotting was used to detect the alteration in the extent of expression of Raf-1 and phosphorylation of ERK1/2. Ischemia and I/R caused a decrease in the protein expression of Raf-1 as well as the phosphorylation of ERK1/2 (Figure.5.9.a, b). The expression of phoshorylated ERK1/2 and Raf-1 were increased on SGG treatment.

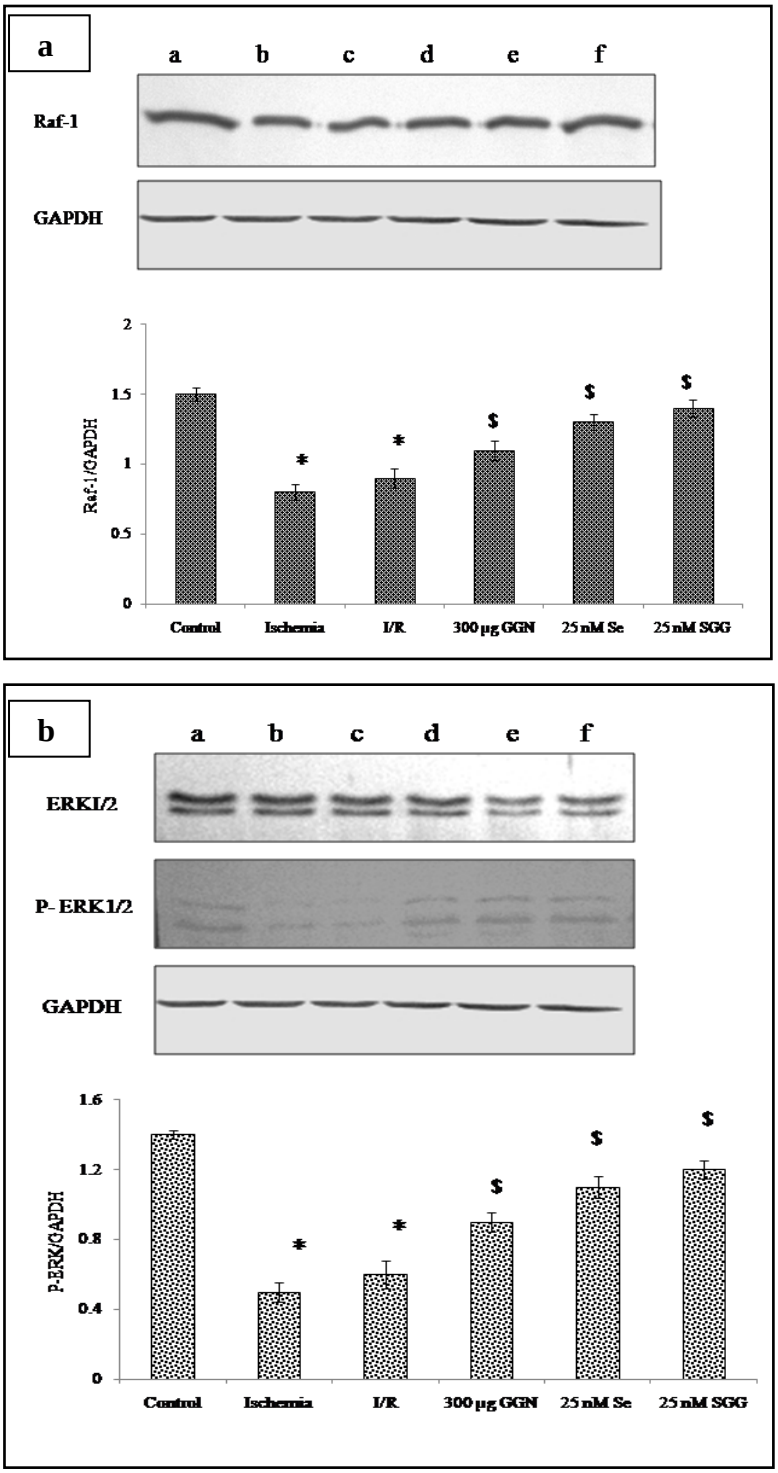

Figure 5. 9. Expression of (a) Raf-1 and (b) ERK1/2 and p-ERK1/2 protein in ischemia and I/R subjected to SDS-PAGE. The amount of Raf-1, ERK1/2, p-ERK1/2 and GAPDH was detected with antibodies against Raf-1, ERK1/2, p-ERK1/2 and GAPDH, respectively. The relative intensity of each band was quantified with GAPDH. The ischemic and I/R groups were compared with the control group. Lane a: control, b: ischemia, c: I/R d: GGN, e: Se, f: SGG. Results are representative of three independent

experiments.* Indicates that the mean value was significantly different from the control cells (P≤0.05). $ Indicate mean value was significantly different from I/R cells (P≤0.05).

5.4. Discussion

Myocardial infarction is associated with inflammatory reactions. There are reports that inflammatory processes are involved in cardiovascular injury resulting from I/R, thrombosis and infection and leads to cardiomyocyte necrosis, as well as apoptosis. Mizia-stec *et al* (2002) reported that patients with CAD have higher serum levels of pro-inflammatory and anti-inflammatory cytokines than control subjects. These mediators mainly include TNF-α, transforming growth factor-beta (TGF-β) and interleukins such as IL-2, IL-6, IL-8 and IL-12. The initial experimental evidence suggests that inflammation can extend myocardial injury and anti-inflammatory strategies are found to reduce I/R induced injury in the heart (Libby *et al* 1973). Oxidative stress causes injury to cardiac myocytes and vascular cells and triggering inflammatory cascades through the induction of cytokines (Dhalla *et al* 2000; Granger 1988). IL-6, TNF-α, IL-10 showed to be good predictors of cardiovascular events. The IL-6 is an important immune cell activator and can participate in the destabilization of the atherosclerotic plaque (Hamdy 2011). Yamauchi-Takihara *et al* (1995) reported the induction of IL-6 in isolated cardiomyocytes exposed to hypoxia followed by reoxygenation. Kukielka *et al* (1995) demonstrated induction of IL-6 in ischemic myocardium of dogs.

In normal conditions immunologic response does not show IL-2 within circulation. IL-2 has a central role in the development of cell-mediated immunity and also it serves as an important factor in the induction of a complex network of cytokines. The level of IL-2 is increased in patients with CAD (Ding *et al* 2013). MCP-1 is believed to play a crucial role in heart failure and is known to be involved in apoptosis. Many lines of experimental evidence from animal models also provide strong evidence for a critical role for MCP-1 in the development of CVD. Younce *et al* (2010) reported that MCP-1 cause cell death in H9c2 cells via MCPIP (MCP-1-induced protein) induction, ROS production, ER stress and autophagy. Shanu *et al* (2013) reported that Se supplementation improves the kidney redox status by inhibiting MCP-1 production in renal tissues.

Among the different cytokines IFN-γ plays relevant role in ischemic heart diseases. IFN-γ is highly expressed in atherosclerotic lesions and has emerged as an

important factor in the development and progression of CVD (Schroecksnadel *et al* 2006). IFN-γ is the main trigger for production and release of ROS in endothelium (Garcia-Bermudez *et al* 2012). In addition, IFN-γ has an important role in atherosclerosis and plaque disruption by enhancing expression of adhesion molecules on endothelial cells (Hansson and Libby 2006). It can also recruit macrophages and T cells into plaque, contributing to production of ROS, inhibiting collagen production, stimulating matrix metalloproteinases, and inducing tissue factor expression. In this study, the levels of IL-6, IL-2, MCP-1 and IFN-γ were found to be high in ischemia and I/R groups, whereas all test materials were found to be protective *via* preventing the release of these cytokines.

There is increasing evidence that cytokines in general and TNF-α in particular plays an important role in CVD. Recently, it was found that TNF-α is expressed and released from the rat and human myocardium after I/R injury (Meldrum *et al* 1998a; Shames *et al* 2002; Meldrum *et al* 1998b). TNF-α is also associated with the induction of apoptosis in cardiomyocytes. Additionally, TNF-α has been indicated to be an initiator of a cytokine cascade, which results in the production of IL-6 and eventually, augment the adverse alterations induced by I/R. Ferrari (1999) reported that the increased levels of TNF-α have been implicated in the pathophysiology of I/R injury. There are reports that the Se treatment reduces the TNF-α mediated activation of NF-κB in Jurkat and Esb-LT lymphocytes (Makropoulos *et al* 1996; Kim and Stadtman 1997). Increased amounts of TNF-α has been reported to be synthesized upon activation of NF-κB in I/R and Ca^{2+}paradox hearts (Cain *et al* 1999; Zhang *et al* 2005). They showed that improvement of cardiac function by Se treatment in I/R hearts may be due to the reduction in the formation of TNF-α. Thus, the results presented here suggest that SGG showed better protection in reducing TNF-α compared to Se and GGN because of its nanosize and combined effect of Se and GG. This may ultimately improve the recovery of cardiac function by attenuating the activation of NF-κB. The protective effect of SGG may be due to its beneficial effect in reducing oxidative stress and thereby reduction in intracellular Ca^{2+} overload as discussed in chapter 3.

To determine whether TNNI3K level has a role in apoptosis we checked TNNI3K in ischemia and I/R. It is a cardiac-specific gene that is undetectable in other tissues (Lai 2009). TNNI3K is a novel molecular target for cardiac diseases. It contains a central

kinase domain, flanking by an ankyrin repeat domain in the amino terminus and a serine-rich domain in the carboxyl terminus. TNNI3K is a functional kinase and directly interacts with cardiac troponin I (cTnI) (Zhao *et al* 2003). TNNI3K induces cardiomyocyte hypertrophy *in vitro* (Wang *et al* 2011) and enhances cardiac performance and protects the myocardium from ischemic injury *in vivo*, (Lai *et al* 2008) while others have shown that over expression of TNNI3K can accelerate disease progression in mouse models of heart failure. The study of Lai (2009) indicates that TNNI3K promotes cardiomyogenesis, enhances cardiac performance, and protects the myocardium from ischemic injury by suppressing p38/JNK-mediated apoptosis. Recent investigations suggest that, modulation of TNNI3K activity was reported to be a useful therapeutic approach for ischemic cardiac disease. There are reports that TNNI3K promotes cardiomyogenesis by; (i) suppressing apoptosis formation by inhibiting the phosphorylation of p38 and JNK and (ii) decreasing the annexin V-positive cells and suppressing Bax protein expression. This results in a decrease of cell death. The results from our study showed that in ischemia and I/R, TNNI3K activity was decreased and SGG treatment increased the level TNNI3K and thereby prevents the cell from apoptosis.

To date, some experiments and clinical studies have suggested that cell apoptosis may be an important link during the pathogenesis of myocardial I/R. In clinical studies, myocardial apoptosis was also observed in patients with acute coronary syndrome (ACS), even after percutaneous coronary intervention (PCI) treatment. These results further confirmed that ischemia could cause myocardial apoptosis, indicating that cell apoptosis is closely correlated to myocardial I/R (Xu *et al* 2012). During myocardial I/R due to the production of large quantity of free radicals promote the development of lipid and protein destructive molecular chain reactions. Moreover, the mitochondrial functions are significantly changed during I/R, including decreasing $\Delta\Psi m$ and energy synthesis (discussed in chapter 4). Besides, the cellular Ca^{2+} content increase leads to calcium overload (discussed in chapter 4). During I/R, Ca^{2+} is mostly accumulated in the mitochondria, leads to mPTP opening that facilitates the release of cytochrome c into the cytoplasm, followed by caspase activation and apoptosis (Xu *et al* 2012). In our study also, these changes were happening in ischemia and I/R which was discussed in previous chapters, led to the activation of apoptotic cascade which was evident from caspase 3

activity assay. These results were confirmed with annexin/PI staining for the detection of apoptosis.

It has been reported that cellular apoptosis leads to F-actin remodelling facilitation (Okada *et al* 2005). Therefore, we evaluated the effect of test materials on actin cytoskeleton organization in cell subjected to simulated ischemia and I/R. Phalloidin/ DAPI staining for actin cytoskeleton showed a well-organized intact fibre of actin filaments. The loss of intact fibers, appeared like broken filaments caused by simulated ischemia and I/R was consistent with the previous finding (Wachtel *et al* 2002). Treatment with all the test materials preserved the cytoskeleton, which was observed by the increased intact fibers compared with ischemia and I/R. Interestingly, treatment with SGG gave higher intact fibers.

IGF-1 plays an important role in the regulation of myocardial structure and function and it improves cardiac performance and muscle survival in heart subjected to I/R (Davani *et al* 2003; Buerke *et al* 1995). IGF-1 promotes cell survival in a number of cell types, but the effect of IGF-1 on the oxidative stress has not been elucidated in cardiac muscle cells. Therefore, we examined the role of IGF-1 signaling pathway in cell survival against I/R induced apoptosis in H9c2 cardiac myoblasts. SGG significantly increased the expression of IGF-1. IGF-1 confers cardiac protection from reperfusion injury *via* mitochondria dependent mechanisms. There are reports that IGF-1 not only inhibits necrosis *via* preservation of mitochondrial function, specifically by inhibiting membrane permeability and cytochrome c release in mitochondria, but also it reduces apoptosis through the inhibition of death signals generated by mitochondria (Yamamura *et al* 2001).

Apoptosis is carried out by a number of regulatory genes through apoptosis signals. Among them, the Bcl-2 family of proteins constitutes a central checkpoint. The Bcl-2 family consists of both cell death promoters and cell death preventers (Oltvai *et al* 1993; Chao and Korsmeyer 1998; Adams and Cory 1998). The ratio of anti- to pro-apoptotic molecules such as Bcl-2/Bax determines the response to a death signal. Bcl-2 has been shown to suppress cytochrome c (cyt c) efflux from mitochondria, inhibit calcium release from the endoplasmic reticulum (Adams and Cory 1998; Youssefi *et al* 2000; Zhang *et al* 2000). Whereas Bax which is a pro-apoptotic protein normally resides

in the cytosol, translocates to mitochondria when triggered by certain stimuli, enables its active configuration as a dimerized integral mitochondrial membrane protein (Khaled *et al* 1999; Murphy *et al* 1999; Putcha *et al* 1999; Wolter *et a*l 1997). Translocated Bax has been shown to induce cytochrome c release and leads to the activation of caspase. Expression of Bax was increased in ischemia and I/R. In the present study, it was shown that the SGG attenuated the expression of Bax and decrease the expression of Bcl-2 and thus it prevented the activation of caspases regulating the level of apoptosis.

We checked the gene expression of Raf-1 activation, which is the member of mitogen-activated protein kinase (MAPK) cascade. Recently, Raf-1 activation of the MEK-ERK pathway has been associated with inhibition of apoptosis, leading to cell survival (Cleveland *et al* 1994; Xia *et al* 1995; Erhardt *et al* 1999; Le Gall *et al* 2000). Gene expression studies showed that SGG up-regulated the Raf-1 expression significantly than other test materials and this leads to the activation of MEK and ERK pathway. The mRNA expression studies with ERK-1 and EKR-2 also gave consistent results about the protective effect of SGG and role in preventing apoptosis.

In stressed conditions, including I/R a family of MAPKs proteins like p38 MAPK, ERK1/2, and JNK are expressed (Engelbrecht *et al* 2004; Ma *et al* 1999; Saurin *et al* 2000; Strohm *et al* 2000; Yue *et al* 1998). Studies demonstrated that ERK1/2 is activated in the first few minutes of reperfusion and offers cardioprotection against oxidative stress by blocking apoptosis (Fryer *et al* 2001; Hausenloy *et al* 2005; Hausenloy and Wellon 2004; Liu *et al* 2004; Yue *et al* 2000). There are reports that Se has a role in suppressing smooth muscle cell calcification and ERK activation (Liu *et al* 2010). Activation of ERKs is important in protecting cardiomyocytes from oxidative stress-induced apoptosis as reported in different human cell systems including cardiomyocytes (Hsu *et al* 2005; Lee *et al* 2005; Nguyen *et al* 2004). Our results demonstrated the involvement of ERK1/2 in SGG-mediated attenuation of apoptosis.

Conclusion

Overall results reveal that ischemia and I/R induces inflammation and apoptosis in H9c2 cells and SGG protects the H9c2 cells from apoptosis by reducing the release of inflammatory cytokines and reduces the cell death by decreasing the expression of Bax proteins and regulating the mRNA expression of genes involved in apoptosis. The study

partly confirms that the protective effect of SGG is mediated through the upregulation of phosphorylated ERK1/2 *via* MAPK kinase signaling pathway.

References

1. Adams JM, Cory S (1998) The Bcl-2 protein family: arbiters of cell survival. *Science* 281: 1322-1326.
2. Buerke M, Murohara T, Skurk C, Nuss C, Tomaselli K, Lefer AM (1995) Cardioprotective effect of insulin-like growth factor I in myocardial ischemia followed by reperfusion. *Proc Natl Acad Sci USA* 92: 8031-8035.
3. Cain BS, Harken AH, and Meldrum DR (1999) Therapeutic strategies to reduce TNF-alpha mediated cardiac contractile depression following ischemia and reperfusion. *J Mol Cell Cardiol* 31: 931-947.
4. Chao DT, Korsmeyer SJ (1998) Bcl-2 family: regulators of cell death. *Annu Rev Immunol* 16: 395-419.
5. Cleveland JL, Troppmair J, Packham G, Askew DS, Lloyd P, Gonzalez-Garcia M, Nunez G, Ihle JN, Rapp UR (1994) v-raf suppresses apoptosis and promotes growth of interleukin-3-dependent myeloid cells. *Oncogene* 9: 2217-2226.
6. Davani EY, Brumme Z, Singhera GK, Cote HCF, Harrigan PR, Dorscheid DR (2003) Insulin-like growth factor-1 protects ischemic murine myocardium from ischemia/reperfusion associated injury. *Crit Care* 7: R176-R183.
7. Dhalla NS, Elmoselhi AB, Hata T, Makino N (2000) Status of myocardial antioxidants in ischemia–reperfusion injury. *Cardiovasc Res* 47: 446-456.
8. Ding R, Gao W, Ostrodci DH, He Z, Song Y, Ma L, Liang C, Wu Z (2013) Effect of interleukin-2 level and genetic variants on coronary artery disease. *Inflammation* 36: 1225-1231.
9. Engelbrecht AM, Niesler C, Page C, Lochner (2004) A p38 and JNK have distinct regulatory functions on the development of apoptosis during simulated ischaemia and reperfusion in neonatal cardiomyocytes. *Basic Res Cardiol* 99: 338-350.
10. Erhardt P, Schremser EJ, Cooper GM (1999) B-Raf inhibits programmed cell death downstream of cytochrome *c* release from mitochondria by activating the MEK/ERK pathway *Mol Cell Biol* 19: 5308-5315.
11. Ferrari R (1999) The role of TNF in cardiovascular disease. *Pharmacol Res* 40: 97-105.
12. Fryer RM, Pratt PF, Hsu AK, Gross GJ (2001) Differential activation of extracellular signal-regulated kinase isoforms in preconditioning and opioid-

induced cardioprotection. *J Pharmacol Exp Ther* 296: 642-649.

13. Garcia-Bermudez M, Lopez-Mejıas R, Gonzalez-Juanatey C, Corrales A, Robledo G, Castaneda S, Miranda-Filloy JA, Blanco R, Fernandez-Gutierrez B, Balsa A, Gonzalez-Alvaro I, Gomez-Vaquero C, Llorca J, Martın J, Gonzalez-Gay MA (2012) Analysis of the interferon gamma (rs2430561, +874T/A) functional gene variant in relation to the presence of cardiovascular events in rheumatoid arthritis. *PLoS ONE* 7(10): e47166. doi:10.1371/journal.pone.0047166.
14. Granger DN (1988) Role of xanthine oxidase and granulocytes in ischemia–reperfusion injury. *Am J Physiol* 255: H1269-H1275.
15. Hamdy NM (2011) Relationship between pro-anti-inflammatory cytokines, T-cell activation and CA 125 in obese patients with heart failure. *Med Sci Monit* 17: CR174-CR179.
16. Hansson GK, Libby P (2006) The immune response in atherosclerosis: a double edged sword. *Nat Rev Immunol* 6: 508-519.
17. Haudek SB, Taffet GE, Schneider MD, Mann DL (2007) TNF provokes cardiomyocyte apoptosis and cardiac remodeling through activation of multiple cell death pathways. *J Clin Invest* 117: 2692-2701.
18. Hausenloy DJ, Tsang A, Mocanu MM, Yellon DM (2005) Ischemic preconditioning protects by activating prosurvival kinases at reperfusion. *Am J Physiol Heart Circ Physiol* 288: H971-H976.
19. Hausenloy DJ, Yellon DM (2004) New directions for protecting the heart against ischaemia-reperfusion injury: targeting the reperfusion injury salvage kinase (RISK)-pathway. *Cardiovasc Res* 61: 448-460.
20. Hsu YL, Kuo PL, Lin LT, Lin CC (2005) Asiatic acid, a triterpene, induces apoptosis and cell cycle arrest through activation of extracellular signal-regulated kinase and p38 mitogen-activated protein kinase pathways in human breast cancer cells. *J Pharmacol Exp Ther* 313: 333-344.
21. Jayachandran M, Brunn GJ, Karnicki K, Miller RS, Owen WG, Miller VM (2007) In vivo effects of lipopolysaccharide and TLR4 on platelet production and activity: implications for thrombotic risk. *J Appl Physiol* 102:429-433.
22. Khaled AR, Kim K, Hofmeister R, Muegge K, Durum S (1999) Withdrawal of IL-

7 induces Bax translocation from cytosol to mitochondria through a rise in intracellular pH. *Proc Natl Acad Sci U S A* 96: 14476-14481.

23. Kim IY, Stadtman TC (1997) Inhibition of NF-kappaB DNA binding and nitric oxide induction in human T cell and lung adenocarcinoma cells by selenite treatment. *Proc Natl Acad Sci U S A* 94: 12904-12907.
24. Kukielka GL, Smith W, Manning AM, Youker KA, Michael LH, Entman ML (1995) Induction of interleukin-6 synthesis in the myocardium: potential role in post reperfusion inflammatory injury. *Circulation* 92: 1866-1875.
25. Lai ZF (2009) TNNI3K could be a novel molecular target for the treatment of cardiac diseases. *Recent Pat on Cardiovasc Drug Discov* 4: 203-210.
26. Lai ZF, Chen YZ, Feng LP, Meng XM, Ding JF, Wang LY, Ye J, Li P, Cheng XS, Kitamoto Y, Monzen K, Komuro I, Sakaguchi N, Kim-Mitsuyama S (2008) Overexpression of TNNI3K, a cardiac-specific MAP kinase, promotes P19CL6-derived cardiac myogenesis and prevents myocardial infarction-induced injury. *Am J Physiol Heart Circ Physiol* 295: H708-H716.
27. Le Gall M, Chambard JC, Breittmayer JP, Grall D, Pouyssegur J, Van Obberghen-Schilling E (2000) The p42/p44 MAP kinase pathway prevents apoptosis induced by anchorage and serum removal. *Mol Biol Cell* 11: 1103-1112.
28. Lee ER, Kang YJ, Kim JH, Lee HT, Cho SG (2005) Modulation of apoptosis in HaCaT keratinocytes via differential regulation of ERK signaling pathway by flavonoids. *J Biol Chem* 280: 31498-31507.
29. Li C, Gao Y, Tian J, Shen J, Xing Y, Liu Z (2011) Sophocarpine administration preserves myocardial function from ischemia-reperfusion in rats via NF-kappaB inactivation. *J Ethnopharmacol* 135: 620-625.
30. Libby P, Maroko PR, Bloor CM, Sobel BE, Braunwald E (1973) Reduction of experimental myocardial infarct size by corticosteroid administration. *J Clin Invest* 52: 599-607.
31. Liu HR, Gao F, Tao L, Yan WL, Gao E, Christopher TA, Lopez BL, Hu A, Ma XL (2004) Antiapoptotic mechanisms of benidipine in the ischemic/reperfused heart. *Br J Pharmacol* 142: 627-634.
32. Liu H, Lu Q, Huang K (2010) Selenium suppressed hydrogen peroxide induced vascular smooth muscle cells calcification through inhibiting oxidative stress and

ERK activation. *J Cell Biochem* 111: 1556-1564.

33. Long X, Boluyt MO, Hipolito ML, Lundberg MS, Zheng JS, O'Neill L, Cirielli C, Lakatta EG, Crow MT (1997) p53 and hypoxia-induced apoptosis of cultured neonatal cardiomyocytes. *J Clin Invest* 99: 2635-2643.
34. Ma XL, Kumar S, Gao F, Louden CS, Lopez BL, Christopher TA, Wang C, Lee JC, Feuerstein GZ, Yue TL (1999) Inhibition of p38 mitogen-activated protein kinase decreases cardiomyocyte apoptosis and improves cardiac function after myocardial ischemia and reperfusion. *Circulation* 99: 1685-1691.
35. Makropoulos V, Bruning T, Schulze-Osthoff K (1996) Selenium-mediated inhibition of transcription factor NF-kappa B and HIV-1 LTR promoter activity. *Arch Toxicol* 70: 277-283.
36. Marchant DJ, Boyd JH, Lin DC, Granville DJ, Garmaroudi FS, McManus BM (2012) Inflammation in myocardial diseases. *Circ Res* 110: 126-144.
37. Meldrum DR, Cleveland JC Jr, Cain BS, Meng X, Harken AH (1998a) Increased myocardial tumor necrosis factor-alpha in a crystalloid-perfused model of cardiac ischemia-reperfusion injury. *Ann Thorac Surg* 65: 439-43.
38. Meldrum DR, Meng X, Dinarello CA, Ayala A, Cain BS, Shames BD, Ao L, Banerjee A, Harken AH (1998b) Human myocardial tissue TNF alpha expression following acute global ischemia in vivo. *J Mol Cell Cardiol* 30: 1683-1689.
39. Mizia-Stec K, Mandecki T, Zahorska-Markiewicz B, Janowska J, Szulc A, Jastrzebska-Maj E, Szymanski L, Majewski T (2002) Selected cytokines and soluble forms of cytokine receptors in coronary artery disease. *Eur J Intern Med* 13: 115-122.
40. Murphy KM, Streips UN, Lock RB (1999) Bax membrane insertion during Fas (CD95)-induced apoptosis precedes cytochrome c release and is inhibited by Bcl-2. *Oncogene* 18: 5991-5999.
41. Nguyen TT, Tran E, Nguyen TH, Do PT, Huynh TH, Huynh H (2004) The role of activated MEK-ERK pathway in quercetin-induced growth inhibition and apoptosis in A549 lung cancer cells. *Carcinogenesis* 25: 647-659.
42. Okada T, Otani H, Wu Y, Kyoi S, Enoki C, Fujiwara H, Sumida T, Hattori R, Imamura H (2005) Role of F-actin organization in p38 MAP kinase-mediated apoptosis and necrosis in neonatal rat cardiomyocytes subjected to simulated

ischemia and reoxygenation. *Am J Physiol Heart Circ Physiol* 289: H2310-H2318.

43. Oltvai ZN, Milliman CL, Korsmeyer SJ (1993) Bcl-2 heterodimerizes in vivo with a consered homolog, Bax, that accelerates programmed cell death. *Cell* 74: 609-619.
44. Pahl HL (1999) Activators and target genes of Rel/NF-kappaB transcription factors. *Oncogene* 18: 6853-6866.
45. Putcha GV, Deshmukl M, Johnson EM (1999) BAX translocation is a critical event in neuronal apoptosis: Regulation by neuroprotectants Bcl-2 and caspases. *J Neurosci* 19: 7476 -7485.
46. Saurin AT, Martin JL, Heads RJ, Foley C, Mockridge JW, Wright MJ, Wang Y, Marber MS (2000) The role of differential activation of p38-mitogen-activated protein kinase in preconditioned ventricular myocytes. *FASEB J* 14: 2237-2246.
47. Schroecksnadel K, Frick B, Winkler C, Fuchs D (2006) Crucial role of interferon-gamma and stimulated macrophages in cardiovascular disease. *Curr Vasc Pharmacol* 4: 205-213.
48. Shames BD, Barton HH, Reznikov LL, Cairns CB, Banerjee A, Harken AH, Meng X. (2002) Ischemia alone is sufficient to induce TNF-alpha mRNA and peptide in the myocardium. *Shock* 17: 114-119.
49. Shanu A, Groebler L, Kim HB, Wood S, Weekley CM, Aitken JB, Harris HH, Witting PK (2013) Selenium inhibits renal oxidation and inflammation but not acute kidney injury in an animal model of rhabdomyolysis. *Antioxid Redox Signal* 18: 756-769.
50. Strohm C, Barancik T, Bruhl ML, Kilian SA, Schaper W (2000) Inhibition of the ER-kinase cascade by PD98059 and U0126 counteracts ischemic preconditioning in pig myocardium. *J Cardiovasc Pharmacol* 36: 218-229.
51. Sun J, Sun G, Meng X, Wang H, Wang M, Qin M, Ma B, Luo Y, Yu Y, Chen R, Ai Q, Sun X (2013) Ginsenoside RK3 prevents hypoxia-reoxygenation induced apoptosis in H9c2 cardiomyocytes via AKT and MAPK pathway. doi.org/10.1155/2013/690190.
52. Wachtel M, Frei K, Ehler E, Bauer C, Gassmann M, Gloor SM (2002)

Extracellular signal-regulated protein kinase activation during reoxygenation is required to restore ischaemia-induced endothelial barrier failure. *Biochem J* 367: 873-879.

53. Wang L, Wang H, Ye J, Xu RX, Song L, Shi N, Zhang YW, Chen X, Meng XM (2011) Adenovirus-mediated overexpression of cardiac troponin I-interacting kinase promotes cardiomyocyte hypertrophy. *Clin Exp Pharmacol Physiol* 38: 278-284.
54. Wolter KG, Hsu Y, Smith CL, Nechushtan A, Xi X, Youle RJ (1997) Movement of Bax from the cytosol to mitochondria during apoptosis. *J Cell Biol* 139: 1281-1292.
55. Xia Z, Dickens M, Raingeaud J, Davis R J, Greenberg ME (1995) Opposing effects of ERK and JNK-p38 MAP kinases on apoptosis. *Science* 270: 1326-1331.
56. Xu T, Li D, Jiang D (2012) Targeting cell signaling and apoptotic pathways by luteolin: cardioprotective role in rat cardiomyocytes following ischemia/reperfusion. Nutrients 4: 2008-2019.
57. Yamamura T, Otani H, Nakao Y, Hattori R, Osako M, Imamura H (2001) IGF-I differentially regulates Bcl-xL and Bax and confers myocardial protection in the rat heart. *Am J Physiol Heart Circ Physiol* 280: H1191-H1200.
58. Yamauchi-Takihara K, Ihara Y, Ogata A, Yshizaki K, Azuma J, Kishimoto T (1995) Hypoxic stress induces cardiac myocyte–derived interleukin-6. *Circulation* 91: 1520-1524.
59. Younce CW, Wang K, Kolattukudy PE (2010) Hyperglycaemia-induced cardiomyocyte death is mediated via MCP-1 production and induction of a novel zinc-finger protein MCPIP. *Cardiovasc Res* 87: 665-674.
60. Youssefi RF, Arnaudeau S, Borner C, Kelley WL, Tschoppi J, Lew DP, Demaurex N, Krause KH (2000) Bcl-2 decreases the free Ca^{2+} concentration within the endoplasmic reticulum. *Proc Natl Acad Sci USA* 97:5723-5728.
61. Yue TL, Ma XL, Wang X, Romanic AM, Liu GL, Louden C, Gu JL, Kumar S, Poste G, Ruffolo RR Jr, Feuerstein GZ (1998) Possible involvement of stress-activated protein kinase signaling pathway and Fas receptor expression in prevention of ischemia/reperfusion-induced cardiomyocyte apoptosis by carvedilol. *Circ Res* 82: 166-174.

62. Yue TL, Wang C, Gu JL, Ma XL, Kumar S, Lee JC, Feuerstein GZ, Thomas H, Maleeff B, Ohlstein EH (2000) Inhibition of extracellular signal-regulated kinase enhances ischemia/reoxygenation-induced apoptosis in cultured cardiac myocytes and exaggerates reperfusion injury in isolated perfused heart. *Circ Res* 86: 692-699.
63. Zhang M, Xu YJ, Saini HK, Turan B, Liu PP, Dhalla NS (2005) TNF-alpha as a potential mediator of cardiac dysfunction due to intracellular Ca^{2+}-overload. *Biochem Biophys Res Commun* 327: 57-63.
64. Zhang M, Zhang HQ, Xue SB (2000) Effect of Bcl-2 and caspase-3 on calcium distribution in apoptosis of HL-60 cell. *Cell Res* 10: 213-20.
65. Zhao Y, Meng XM, Wei YJ, Zhao XW, Liu DQ, Cao HQ, Liew CC, Ding JF (2003) Cloning and characterization of a novel cardiac-specific kinase that interacts specifically with cardiac troponin I. *J Mol Med (Berl)* 81: 297-304.
66. Zhong X, Li X, Qian L, Xu Y, Lu Y, Zhang J, Li N, Zhu X, Ben J, Yang Q, Chen Q (2012) Glycine attenuates myocardial ischemia-reperfusion injury by inhibiting myocardial apoptosis in rats. *J Biomed Res* 26: 346-354.

Summary and Conclusion

Over the past two decades nanoparticles-based therapeutics have been introduced for the treatment of cancer, diabetes, allergy, neurodegenerative diseases, cardiovascular disease, infections and inflammation. Nanoparticles are widely used because of its advantage, which include protection from premature degradation of drugs, the capability to deliver poorly water soluble drugs alone or in combination with soluble drugs, controlled drug release, improved bio-distribution and pharmacokinetics and better intracellular penetration. In drug delivery size, shape and surface characterization of nanoparticles plays a very important role. The materials used for preparing nanoparticles should be biocompatible and biodegradable, well characterized and easily functionalized. Polysaccharides successfully fulfil all of these requirements and are therefore widely used as the building blocks for the preparation of nanoparticles.

Polysaccharides are polymers of monosaccharide and posses many favourable characteristics such as low toxicity, biocompatibility, stability, low cost, hydrophilic nature and availability of reactive sites for chemical modifications. In this study guar gum, a water soluble polysaccharide extracted from the seeds of *Cyamopsis tetragonoloba* was used. The guar gum nanoparticles and selenium incorporated guar gum nanoparticles were prepared by nanoprecipitation method. Little information is available in the open literature for the possibility of using guar gum based nanosized materials as a drug carrier.

Cardiovascular diseases account for high morbidity and mortality all over the world. In the developing countries, cardiovascular diseases lead to an increasing proportion of the non-communicable diseases. The primary conditions that lead to cardiovascular diseases include dyslipidemia, atherosclerosis and hypertension. Treatments for cardiovascular diseases include non-invasive therapy such as prescription medication and lifestyle alterations, or surgical therapy such as coronary artery bypass grafting and angioplasty. Treatments with drugs were effective to lower blood pressure or cholesterol, prevent or dissolve blood clots, relieve and prevent angina symptoms or improve the strength or rhythm of the heart's contractions. Angiotensin- converting enzyme inhibitors, angiotensin receptor blockers, anti-clotting drugs and beta blockers are the examples of drug classes which are commonly used in cardiovascular diseases. Up to date, these drugs are mostly introduced into the market in conventional formulations such as tablets or capsules. Application of

nanotechnology includes nanomedicine in monitoring, diagnosing, preventing, repairing or curing diseases and damaged tissues in biological systems and it is gaining importance for the treatment of cardiovascular diseases. The overall goal of nanomedicine is to diagnose as precisely and early as possible, to treat as effectively as possible with minimal side effects, and to evaluate the efficacy of treatment noninvasively.

Ischemic heart disease is an important clinical problem associated with the reflow of blood to minimize the damage to the heart during some surgical and therapeutic interventions. During the ischemic reperfusion cycle reactive oxygen species are generated mainly along the mitochondrial respiratory chain and they trigger lipid peroxidation, protein oxidation, enzyme inactivation, and the DNA strand breaks, as well as impair physiological functions, e.g., blocking of ion channels, restricting glycolysis, and promoting mitochondrial calcium release etc. In this condition the innate antioxidant status is altered and cause generations of more free radicals and its activates various pathways involved in apoptosis leading to cell death.

Selenium is an essential trace element. It is a structural component of several active site of enzymes which mainly include glutathione peroxidase and has an important role in preventing oxidative stress generated during various diseases like cardiovascular disease, cancers, diabetics etc. Depending on the concentration, selenium plays duel role i.e. it has nutritional functions as well as toxic. Therefore, how to provide efficient and safe application of dietary selenite supplementation has become a challenge topic in recent years. Here in guar gum was selected as carrier and selenium was the therapeutic agent. The physicochemical properties of the nanoparticles were characterized by particle size analyzer, TEM and XRD. In order to see the interaction of SGG with cells we systematically investigated the effect of nanoparticle on H9c2 cells by analyzing various parameters like cell viability, apoptosis, DNA protection, reactive oxygen species generation, mitochondrial transmembrane potential change and alteration in cytoskeleton.

Physical characterization of nanoparticle showed that the size of nanoparticles increased up to ~ 69–173 nm upon selenium incorporation from ~ 41-132 nm. Then the effect of nanoparticle on H9c2 cells was checked. In this regard, various vital parameters of H9c2 cells were studied. Parameters like cell viability, uptake of selenium incorporated guar gum nanoparticle by the cells, effect of SGG on DNA integrity, apoptosis, reactive oxygen species generation, alteration in transmembrane potential of mitochondria and cytoskeleton integrity

had been investigated to check whether the prepared nanoparticle causes any toxicity to the cells. Viability results showed that up to 25 nM of SGG was safe (10.31%) but beyond that it induces cytotoxicity. Cellular uptake of selenium showed that cell permeability for SGG is significantly high compared to normal selenium. There was no apoptosis with SGG and also it protects DNA from hydroxyl radical induced breakage. Likewise no adverse effect on mitochondria was observed for 25 nM of SGG. After that the nanoparticles were screened for antioxidant potential (metal chelation, total reducing power and hydroxyl radical scavenging activity) and showed high antioxidant potential compared with standard.

The prepared selenium incorporated guar gum nanoparticles were evaluated against the cell line based cardiac ischemia/reperfusion model using H9c2 cardiomyoblast with special emphasis on oxidative stress and calcium homeostasis. Results from the study clearly revealed that there was a significant alteration ($P \leq 0.05$) in the innate antioxidant status (glutathione, glutathione peroxidase, thioredoxin reductase, superoxide dismutase, catalase, lipid peroxidation, protein carbonyl, xanthine oxidase, calcium ATPase and intracellular calcium) during ischemia and ischemia reperfusion. For comparative evaluation, selenium (Se), guar gum nanoparticles (GGN) and selenium incorporated guar gum nanoparticles (SGG) were evaluated for their protective properties against ischemia/reperfusion. The study revealed that selenium incorporated guar gum nanoparticles were better at protecting the cells from ischemia/reperfusion compared to selenium and guar gum nanoparticles. The potent antioxidant capability shown by the sample in *in vitro* assays may be the biochemical basis of its better biological activity. Further, the nanodimensions of the particle may be the additional factor responsible for its better effect.

Mitochondrial dysfunction plays a very important role in heart failure. So it is considered as an important target in ischemic heart diseases. In the present study selenium incorporated guar gum nanoparticles was used aganist the mitochondrial dysfunction induced by ischemia and ischemia reperfusion. Ischemia was induced in H9c2 cardiomyoblast and the mitochondrial dysfunction was evaluated. There was a significant alterations in mitochondrial parameters like mitochondrial membrane potential, mitochondrial permeability transition pore opening, mitochondrial superoxide, mitochondrial enzyme complexes like complex I, II, III and IV, oxygen consumption and ATP determination, alteration in stress protein HSP 60, aconitase activity, HIF-1 α level and ANP level in ischemia and in I/R. The activities of mitochondrial respiratory enzymes, oxygen consumption, ATP and aconitase activity were

decreased in ischemia and I/R cells and the activities were increased in selenium incorporated guar gum nanoparticles treated cells.

Ischemia-reperfusion of cardiac tissues may lead to a prominent damage of the myocyte through either necrosis or apoptosis that seems to be the predominant modes of death. NF-$_K$B has an important role in inflammation i.e. many genes encoding cytokines activate the NF-$_K$B which in turn activate the proinflammatory cytokines. In the present study SGG prevents apoptosis in cardiomyocytes subjected to ischemia and I/R by inhibiting TNF-α, IL-6, IL-2, MCP-1 and INF-γ. The mechanism appears to involve inhibition of apoptosis by decreasing caspases 3 activity as well as Bax/Bcl-2 ratio. The protective effect of SGG was mediated via upregulation of ERK1/2 phosphorylation. However, the causal relationship between upregulation of ERK1/2 phosphorylation and SGG activity requires further investigation. In the present study NF-$_K$B nuclear migration and TNF-α secretion was increased in ischemia and ischemia reperfused H9c2 cells (observed via ELISA method). SGG inhibited NF-$_K$B activation and further reduced TNF-α expression and also the expression of other inflammatory cytokines. We also investigated the mRNA expression of genes involved in apoptosis like ERK-1 and 2, IGF-1 and Raf-1. Protein expression studies showed that SGG inhibit the apoptosis by upregulating the expression of ERK. We also checked TNNI3K level in ischemia and ischemia reperfused cells. Here also SGG shows better protective effect and there by upregulating the ERK pathway for preventing apoptosis. Overall results reveal that SGG was superior in activity compared to other test materials in reversing most of the ischemia related changes in H9c2 cells.

List of Publications

1. **Soumya RS,** Vineetha VP, Reshma PL, Raghu KG (2013) Preparation and characterization of selenium incorporated guar gum nanoparticle and its interaction with H9c2 Cells. PLoS ONE 8(9): e74411. doi:10.1371/journal.pone.0074411.
2. **Soumya RS**, Reshmi R, Sebastian J, Antu KA, Riya MP, Raghu KG (2014) Synthesis, characterization and evaluation of antioxidant potential of vanadium encapsulated guar gum nanoparticles. Food and Function 5: 535-544.
3. **Soumya RS**, Vineetha VP, Raj SP, Raghu KG (2014) Beneficial properties of selenium incorporated guar gum nanoparticles against ischemia/reperfusion in cardiomyoblasts (H9c2). Metallomics 6: 2134-2147.
4. Vineetha VP, Prathapan A, **Soumya RS**, Raghu KG (2013) Arsenic trioxide toxicity in H9c2 myoblasts-damage to cell organelles and possible amelioration with *Boerhavia diffusa*. Cardiovascular Toxicology 13: 123-137.
5. Vineetha VP, Girija S, **Soumya RS,** Raghu KG (2014) Polyphenol rich apple (*Malus domestica L.*) peel extract attenuate arsenic trioxide induced cardiotoxicity in H9c2 cells via its antioxidant activity. Food and Function 5: 502-511.
6. Vineetha VP, **Soumya RS**, Raghu KG (2014) Mitochondrial dysfunction by arsenic trioxide in H9c2 is mediated by alterations in membrane permeability and inefficiency of ETC and its possible amelioration with phloretin. European Journal of Pharmacology (Under Review).
7. Vandana Sankar, Salin Raj P, Athira Raj, **Soumya RS**, Raghu KG (2014) Cerium nanoparticles synthesized using aqueous extract of *Centella asiatica*: characterization, determination of free radical scavenging activity and evaluation of efficacy against cardiomyoblast hypertrophy. RSC Advances (Under Review).
8. **Soumya RS**, Raghu KG Mitochondrial alteration during ischemia/reperfusion injury in H9c2 is attenuated by selenium incorporated guar gum nanoparticles. Mitochondrion (Under Preparation).
9. **Soumya RS**, Salin Raj, Raghu KG Ischemia/reperfusion injury induced apoptosis in H9c2 is ameliorated by selenium incorporated guar gum nanoparticles. European Journal of Pharmacology (Under Preparation).

Oral Presentations

1. **Soumya R.S** and Raghu K.G. Encapsulation of selenium in guar gum nanoparticles improves selenium availability and protects cardiomyoblast from ischemia. Oral presentation at International conference on Bioactive Phytochemicals and Therapeutics- 2013. Annamalai University, Chidhamparam, 5-7 April, 2013. (Travel Grant Award).
2. **Soumya R.S** and Raghu K.G. Selenium incorporated guar gum nanoparticles protect H9c2 cardiomyoblasts from ischemia. Oral presentation at 26th annual symposium of Indian society of Atherosclerosis Research. Amala Cancer Center Thrissur, 22-23 November, 2013.

Poster Presentations

3. **Soumya R.S** and Raghu K.G. Evaluation of guar gum nanoparticle incorporated selenium against cardiac ischemia: an *in vitro* cell line based approach. Poster presented at International conference on New Horizons in Biotechnology. Trivandrum, 21-24 November, 2011.
4. Attended state level seminar on New risk factors of Coronary Artey Diseases. N.S.S College Pandalam, 16-17 February, 2012.
5. Attended 25th Kerala Science Congress on 29th Jan- 1st Feb, 2013 at Technopark, Trivandrum.